

Dynamic Optimization, State Estimation and Control of Electric Arc Furnace Operation

Dynamic Optimization, State Estimation and Control of Electric Arc Furnace Operation

by

Smriti Shyamal, B.Tech.

A Thesis
Submitted to the School of Graduate Studies
in Partial Fulfillment of the Requirements
for the Degree of
Doctor of Philosophy

McMaster University

DOCTOR OF PHILOSOPHY (2018)
(Chemical Engineering)

McMaster University
Hamilton, Ontario, Canada

TITLE: Dynamic Optimization, State Estimation and Control
of Electric Arc Furnace Operation
AUTHOR: Smriti Shyamal, B.Tech.
Indian Institute of Technology, Bombay (IIT Bombay), India
SUPERVISOR: Dr. Christopher L.E. Swartz
NUMBER OF PAGESxiv, 168

Abstract

Electric arc furnaces (EAFs) are commonly used in the steel industry for production of steel by melting down the scrap metal and altering its chemistry. The highly energy intensive steelmaking operation is a complex batch process, and involves limited automation. The main aim of this research is to develop a mathematical model and computational framework for on-line optimization-based decision support and control of EAF operation. A dynamic model of the EAF process is implemented and used within an optimization framework to determine the optimal input trajectories. Industrial implementation of the model-based optimization systems is envisaged to generate significant savings through reduced consumption of electric power, natural gas, oxygen, carbon and fluxes such as limestone and dolomite.

In the first part of the study, we present the advances made through this research toward implementing an economic optimization of EAF operations. The three key building blocks for a real-time implementation are discussed: a dynamic model, dynamic simulation and dynamic optimization. We also present the simulation and optimization deployments for the industrial members of the McMaster Steel Research Centre (SRC) through which users can interact with the model.

In the second part of the study, state estimation is investigated through implementing multi-rate Moving Horizon Estimation (MHE) for real-time model calibration. A parameter estimation based multi-rate MHE framework is developed to handle measurements with different sampling rates. The MHE application is further extended for the full batch time with the use of a simultaneous solution approach. A novel MHE initialization scheme is also proposed to reduce the numerical computation time. The estimator showed strong performance in tracking the internal states in the presence of plant-model mismatch and measurement noise, improving from poor initial guesses of the states. The multi-rate MHE is then coupled with an economics-based dynamic optimizer to form an online decision support tool.

In the third part of the study, an energy management approach is introduced that effectively curtails the energy cost in real-time through the implementation of economically optimal operating decisions. An economics-oriented shrinking horizon nonlinear model predictive control (NMPC) algorithm that exploits time-varying electricity prices is coupled with a multi-rate MHE to form an integrated decision-making framework. A novel initialization scheme is also developed for obtaining fast on-line solutions of the economic NMPC and multi-rate MHE dynamic optimization problems. The energy usage optimization results indicated a significant reduction in the operating cost and peak electricity demand compared to the case where the electricity price profile is not updated.

In the fourth part of the study, a real-time dynamic optimization-based advisory system that employs a first-principles EAF model is introduced to support the operator decision making in real-time. Economically optimal process operation is achieved by employing the first-principles dynamic EAF model in the optimization formulation. A dynamic optimization calculation can be triggered by the operator at any point in the batch, an action that can be repeated multiple times during the batch. The advisory system incorporates a multi-rate MHE that continually computes estimates of the process states utilizing current and past inputs and measurements. End-point constraints and potential extension of the batch duration are handled through a multi-tiered optimization algorithm. Our case studies demonstrate a major economic improvement when the dynamic optimization-based advisory system is used.

Acknowledgments

I would like to thank my supervisor Dr. Christopher L.E. Swartz for providing his support and guidance throughout the research duration. His expert mentorship and leadership helped me to develop myself as a professional researcher. The research work would not have been possible without his direction, inputs and insights.

I would like to thank the supervisory committee members Dr. Thomas A. Adams and Dr. Bartosz Protas for their helpful inputs and discussions which gave proper direction to the research project.

I would like to acknowledge support provided by the McMaster Steel Research Center (SRC), the McMaster Advanced Control Consortium (MACC) and the Ontario Graduate Scholarship (OGS) for this work. Special thanks go to Dr. Gordon Irons, Dr. Ken Coley, Dr. Neslihan Dogan and John Thomson of SRC for getting involved with the research project.

I would also like to thank my graduate course instructors at McMaster University, Dr. Prashant Mhaskar, Dr. Elkafi Hassini, Dr. Chris Swartz, Dr. Sanzheng Qiao, Dr. Jim Reilly, Dr. Kai Huang and Dr. Simon Haykin for equipping me with all the valuable knowledge.

I would also like to thank my colleagues and alumni of McMaster Advanced Control Consortium for providing their help and support. Also, support from my family and friends is gratefully appreciated.

Table of Contents

1	Introduction	1
1.1	Motivation and Goals	1
1.2	Background	3
1.2.1	Dynamic Optimization	4
1.2.2	Nonlinear Model Predictive Control (NMPC)	6
1.3	Main Contributions	9
1.4	Thesis Outline	10
	References	11
2	Modeling, Simulation and Optimization of EAF Operation	14
2.1	Introduction	16
2.2	Dynamic Modeling	16
2.2.1	Model reformulation	18
2.3	Dynamic Simulation	20
2.3.1	Deployment: Off-line Application using a Simulation User Interface	22
2.4	Dynamic Optimization	24
2.5	Conclusion	26
	References	26
3	Moving Horizon Estimation	29

3.1	A Multi-rate Moving Horizon Estimation Framework for Electric Arc Furnace Operation	31
3.1.1	Introduction	31
3.1.2	EAF model	34
3.1.3	Moving horizon estimation	35
	Multi-rate MHE problem formulation	36
	Parameter estimation framework	38
	Implementation	40
3.1.4	Case study	41
	Computational results	43
3.1.5	Section summary	45
3.2	Multi-Rate Moving Horizon Estimation using different optimization paradigms	46
3.2.1	Sequential approach	47
3.2.2	Simultaneous approach	49
	Novel initialization scheme for MHE	51
3.2.3	Case Study	53
3.3	Optimization-based Online Decision Support Tool for Electric Arc Furnace Operation	55
3.3.1	Introduction	55
3.3.2	EAF model overview	57
3.3.3	Dynamic Optimization and MHE based on-line Decision Support Tool	57
	Shrinking Horizon Dynamic Optimization	59
	Multi-rate MHE	60
	DST Implementation	62
3.3.4	Case study	63
	Computational results	66
3.3.5	Conclusion	67
3.A	Derivation of $W'_i(t, w_k)$ based on hyperbolic tangent functions	68
	References	69

4 Real-time Energy Management	74
4.1 Introduction	76
4.2 Electric arc furnace model	79
4.3 Formulation and solution strategy	82
4.3.1 Shrinking Horizon Economic Model Predictive Control	83
4.3.2 Multi-rate Moving Horizon Estimation	85
4.3.3 Novel initialization scheme for MHE and NMPC	89
4.3.4 Implementation	91
4.4 Case studies	93
4.4.1 Actual and predicted electricity prices	95
4.4.2 Case study 1: Price peak decrease with price change at 25 th min	97
4.4.3 Case study 2: Price peak increase with price change at 25 th min	99
4.4.4 Case study 3: Price decrease with a price change at 40 th min	103
4.4.5 Case study 4: Price decrease with a price change at 15 th min	103
4.4.6 Multi-rate MHE performance	105
4.4.7 Computational results	105
4.5 Conclusions and future work	107
References	109
5 Real-time Dynamic Optimization-based Advisory System	116
5.1 Introduction	118
5.2 Electric arc furnace model	123
5.3 Dynamic optimization problem	125
5.3.1 Model formulation	125
5.3.2 Model contraction	126
5.3.3 Optimization formulation	127
5.4 Multi-tiered Optimization	129
5.4.1 Tier 1: Direct optimization	129
5.4.2 Tier 2: Feasibility through horizon extension	130
5.4.3 Tier 3: End-point constraint relaxation	131
5.4.4 EAF Implementation	132

Tier 1: Direct Optimization	134
5.5 Multi-rate Moving Horizon Estimation	135
5.5.1 Model for State Estimation	136
5.5.2 Constrained Least-Squares Formulation	137
5.5.3 Arrival Cost Update	139
5.5.4 Disturbance handling	141
5.6 Real-time Advisory System	141
5.6.1 Algorithm operation	142
5.6.2 Multi-tiered initialization strategy	143
5.6.3 Implementation	145
5.7 Case studies	147
5.7.1 Problem Setup	147
5.7.2 Case Study Descriptions and Results	150
Case study 1: Economic benefit of real-time advisory system execution	150
Case study 2: Feasibility through multi-tiered optimization strategy	153
5.7.3 Moving Horizon Estimation Results	154
5.7.4 Computational Results	156
5.8 Conclusion	157
References	157
6 Conclusion	165
6.1 Summary and Key Contributions	165
6.2 Recommendations for Future Work	168

List of Figures

1.1	Electric arc furnace Operation	3
1.2	Dynamic optimization solution methods.	7
1.3	MPC graphical representation	8
2.1	Schematic of EAF model with zones, inputs and components within zones indicated.	17
2.2	Translating model from gPROMS to CasADI.	20
2.3	Backend of the simulation interface for McMaster Steel Centre industrial members.	22
2.4	Simulation interface for McMaster Steel Centre industrial members. . .	23
2.5	Optimal power and oxygen input trajectories for different electricity prices.	25
2.6	Simulation interface for McMaster Steel Centre industrial members. .	26
3.1	Schematic of EAF model. [14]	35
3.2	A continuous, differentiable approximation $W'_i(t, w_k)$ to the piecewise constant process noise function $W_i(t, w_k)$	39
3.3	Normalized nominal input profiles.	42
3.4	A selection of normalized state estimates compared with the real trajectory of the states. The MHE tracking ability is demonstrated in the presence of plant-model mismatch and erroneous initial conditions of the states.	44

3.5	Dynamic optimization solution methods.	46
3.6	MHE implementation for sequential approach using gO:RUN and MATLAB.	48
3.7	Implementation of MHE using both the dynamic optimization approaches.	48
3.8	Novel initialization scheme for MHE.	51
3.9	State estimates for the case study with respect to time (in minutes). sm_C: Carbon in slag-metal zone, ss_mass: Solid scrap mass, mm_C: Carbon in molten metal zone, mm_T: Temperature of molten metal, gs_C: Carbon in gas zone, gs_T: Temperature of gas.	53
3.10	Solution times for MHE problems with horizons of N = 6 time steps using the sequential approach.	54
3.11	Solution times for MHE problems with horizons of N = 6 time steps using the simultaneous approach. The solve time denoted by 'fast' rep- resents computational time when the proposed initialization scheme is used. 'Nominal' represents the MHE solves carried out without the use of the proposed initialization scheme.	54
3.12	Online decision support tool for EAF operation	58
3.13	State estimates with respect to time (in minutes).	65
3.14	Case Study: DST input profiles compared to nominal inputs.	66
3.15	Solution times for MHE problem with horizons of N = 6 time steps. . .	67
4.1	Schematic of the EAF model [39] employed showing inputs, outputs and material flow between the four zones.	80
4.2	Real-time energy management control framework.	82
4.3	Initialization for Moving Horizon Estimation	91
4.4	Dynamic optimization implementation framework.	92
4.5	Hourly Ontario (Canada) electricity price (actual and predicted) for 15-21 March 2017.	95
4.6	Price forecast error analysis for 2016 for the Ontario electricity whole- sale market.	96

4.7	Electricity price profiles for the four case studies. The electricity price variation is for a 1 hour electricity price market.	98
4.8	Case study 1: Input variable profiles.	100
4.9	Case study 1: Off-gas profiles, scaled to within their maximum and minimum ranges.	101
4.10	Case study 2: Input variable profiles.	102
4.11	Case study 4: Input variable profiles.	104
4.12	State estimates for case study 1 with respect to time (in minutes). sm_C: Carbon in slag-metal zone, ss_mass: Solid scrap mass, mm_C: Carbon in molten metal zone, mm_T: Temperature of molten metal, gs_C: Carbon in gas zone, gs_T: Temperature of gas, T_wall: Furnace wall temperature, sm_Mn: Manganese in slag-metal zone, sm_d: Disturbance state in slag-metal zone.	106
4.13	Solution times for MHE problems with horizons of N = 6 time steps. The solve time denoted by ‘fast’ represents computational time when the proposed initialization scheme is used. ‘Nominal’ represents the MHE solves carried out without the use of the proposed initialization scheme.	106
4.14	Solution times for shrinking horizon NMPC problems. The solve time denoted by ‘fast’ represents computational time when the proposed initialization scheme is used. ‘Nominal’ represents the NMPC solves carried out without the use of the proposed initialization scheme. . . .	107
5.1	Schematic of the EAF model [7, 13] used in the study showing the 4 zones and associated inputs, outputs and material flows.	124
5.2	Multi-tiered optimization strategy.	133
5.3	Real-time advisory system.	142
5.4	Input profiles for case study 1.	152

5.5	State estimate profiles and corresponding estimation error (variable name appended with 'e_') varying with respect to time (in minutes) for case study 3. T_roof (temperature of furnace roof), T_wall (temperature of furnace wall), sm_cao_f (floating carbon content in slag-metal zone), mm_C (Moles of Carbon in molten-metal zone), ss_mass (mass of solid scrap) and sm_d2 (Disturbance state for ss_mass).	155
5.6	Solution times for multi-rate MHE problems (horizon length is 6 minutes) for case study 3. 'Fast' represents solution times when the multi-tiered initialization scheme is used. 'Nominal' denotes solutions times when the proposed initialization scheme is not utilized.	156

List of Tables

3.1	Multi-rate measurement structure for the case study.	42
3.2	State, measurement and model noise covariance values for the case study.	43
3.3	Result comparison for the case study.	64
3.4	Measurements for the case study.	64
3.5	Multi-rate measurement structure for the case study.	64
3.6	Solution time for shrinking horizon optimization problem.	67
4.1	Multi-rate measurement structure for the case study.	94
4.2	Measurement availability in the case study.	94
4.3	Summary of the case studies comparing NMPC ^{nom} with NMPC ^{up} . Wherever % is shown, the values are with respect to NMPC ^{nom} . The time of electricity price change is the time instant during the batch process of length 60 minutes.	97
5.1	Multi-rate measurement structure for the EAF process.	148
5.2	Measurement availability for the EAF process.	148
5.3	Results for Case study 2.	151
5.4	Solution times for the multi-tiered dynamic optimization problems of case study 3.	156

Chapter 1

Introduction

1.1	Motivation and Goals	1
1.2	Background.	3
1.3	Main Contributions	9
1.4	Thesis Outline.	10
	References	11

In this chapter, we present the motivation for the research project and the key research goals associated with it. In the next subsection we give a brief description on dynamic optimization and Nonlinear Model Predictive Control (NMPC). We then discuss the main research contributions. Finally, the thesis outline is presented.

1.1 Motivation and Goals

Electric arc furnaces (EAFs) are widely used in steel industries to produce molten steel from scrap metal and account for approximately one-quarter of world crude steel

production [1]. EAFs also account for more than 40% of steelmaking production in North America [1]. This is a highly energy intensive complex batch process. The high energy consumption (approximately 400 kWh/ton of steel [2]) by EAFs motivates this project to develop optimization and control strategies for the EAF operation to reduce the cost of production and also maintaining the quantity of steel produced.

The EAF we are studying in this project is of capacity approximately 100 tons and runs on AC power. The operation of EAF is illustrated in Fig. 1.1. The scrap is charged into the furnace and electrical energy is transferred through the electrodes. Burners are used to inject natural gas (CH_4) and oxygen (O_2), which provide chemical energy via combustion to the scrap. When there is enough space in furnace due to the scrap melting (approximately at the end of 25 minutes), another batch of scrap is typically added. The melting continues and a flat bath of molten steel is formed at the end of batch (duration of approximately 60 minutes). The oxygen reacts with metals to form their oxides which forms the slag layer floating on top of the molten steel. Slag chemistry can be varied by direct addition of carbon, lime and dolomite through the roof of the furnace and by adjusting oxygen and carbon lancing. The online data used in this project were obtained from our industrial partner ArcelorMittal Contrecoeur Ouest in Quebec, Canada.

The EAF operation involves a very low level of automation and almost all decisions are made by the operator using past experience. As with most industrial processes, operator experience is invaluable for the operation of the process. However, this experience can be limited due to the complex interactions and relationships that may not be immediately obvious. The steel industry can potentially save a significant amount of money by optimizing the amount and timing of additions of scrap, arc power, fluxes, methane, carbon and oxygen. This research aims to develop off-line and on-line decision support tools for the operators to determine economically optimal policies. This involves using a detailed first-principles dynamic model of the EAF operation in an optimization and control framework to determine the optimal

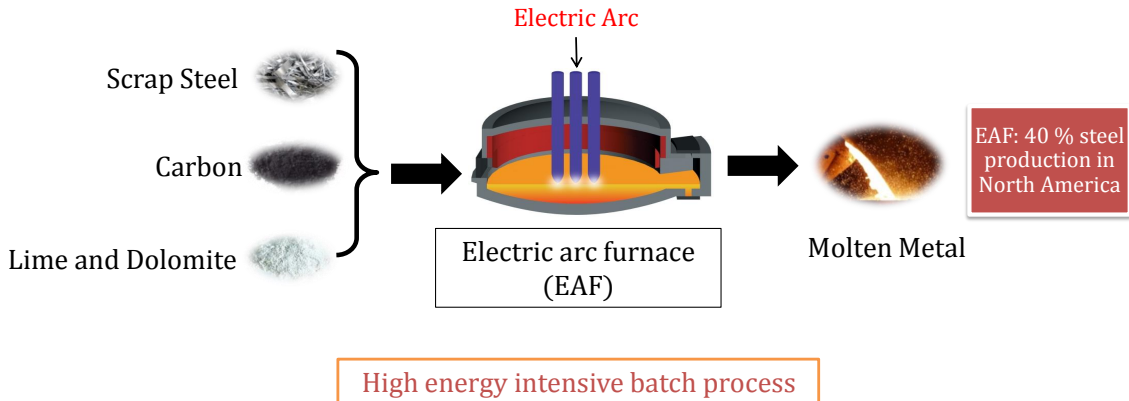


Figure 1.1: Electric arc furnace Operation

inputs.

For the model to be used for real-time applications, state knowledge is necessary due to model uncertainty and disturbances. The ability of Moving Horizon Estimation (MHE) to estimate the current states is investigated. In addition, we seek to develop an energy management strategy that effectively curtails the energy cost in real-time through the implementation of economically optimal operating decisions. The application of such an energy management procedure can generate additional profit through optimal utilization of electric power (in response to electricity price change) and other inputs. Finally we aim to develop a real-time dynamic optimization-based advisory system that could be used by the operator at any point during the batch to identify the optimized trajectories of the control variables until end of the batch.

1.2 Background

In this section we first describe dynamic optimization and the solution methods very briefly. Then, we discuss Nonlinear Model Predictive Control (MPC).

1.2.1 Dynamic Optimization

When provided with a dynamic process, dynamic optimization aims to find the optimal profile of control input variables for the full time horizon. The problem formulation involves utilization of a mathematical model of the system to capture the relationship between variables, and deciding on a performance criterion and constraints. The optimization cost function consists of any performance or economic objective, which is maximized or minimized subject to a set of specified constraints. The equations of the mathematical model (usually a differential algebraic equation (DAE) system) for the system act as equality constraints that need to be satisfied while there are other physical inequality or equality constraints. Different nonlinear programming (NLP) techniques are widely used to solve the optimization problems as they are very efficient in solving optimal control problems.

The cost function for the dynamic optimization specifies the performance criterion to be maximized or minimized which can be expressed as a sum of an integral cost and a terminal cost. The constraints which are commonly imposed in the problem formulation are point constraints and path constraints. Point constraints specify a function of the state variable or the state variable itself to be within certain bounds at a specific instant of time. Path constraints define the range of values a mixed function of state and control variable can take over a specified time interval. Generally this occurs as a restriction on the control variables.

Direct solution methods discretize the control profile (or trajectory) and then apply NLP techniques to the finite dimensional search space. The strategy is also called "control vector parameterization"[3]. The control (or input) variables \mathbf{u} are generally discretized as piecewise constant for a constant sampling time over the optimization horizon, $\mathbf{u}(t) = \mathbf{u}_i$ for time $t \in [t_i, t_{i+1}]$. In summary, the general form for the

optimization of a DAE system is shown as [4]:

$$\min_{\mathbf{u}(t), t_f} \phi(t_f, \mathbf{x}(t_f), \mathbf{z}(t_f), \mathbf{u}(t_f), \mathbf{v}, \theta) \quad (1.1)$$

$$\text{subject to } \dot{\mathbf{x}}(t) = \mathbf{f}(t, \mathbf{x}(t), \mathbf{z}(t), \mathbf{u}(t), \mathbf{v}, \theta); \mathbf{x}(t_0) = \mathbf{x}_0 \quad (1.2)$$

$$\mathbf{0} = \mathbf{h}(t, \mathbf{x}(t), \mathbf{z}(t), \mathbf{u}(t), \mathbf{v}, \theta) \quad (1.3)$$

$$\mathbf{0} \geq \mathbf{g}(t, \mathbf{x}(t), \mathbf{z}(t), \mathbf{u}(t), \mathbf{v}, \theta) \quad (1.4)$$

$$\mathbf{x}^L \leq \mathbf{x}(t) \leq \mathbf{x}^U \quad (1.5)$$

$$\mathbf{z}^L \leq \mathbf{z}(t) \leq \mathbf{z}^U \quad (1.6)$$

$$\mathbf{u}^L \leq \mathbf{u}(t) \leq \mathbf{u}^U \quad (1.7)$$

in which $\mathbf{z}(t)$ represents the algebraic variables, $\mathbf{x}(t)$ is the vector consisting of the differential state variables and the vector \mathbf{v} comprises time invariant design variables. θ represents the parameters for the system which remain unchanged with respect to time. The cost function for the dynamic optimization is represented as ϕ , which is a function of variable values at final time t_f . The initial condition for the DAE system is $\mathbf{x}(t_0) = \mathbf{x}_0$. \mathbf{f} , \mathbf{h} and \mathbf{g} represent the differential equation constraints, equality constraints and inequality constraints respectively. Bounds on the variables are defined through equations (1.5), (1.6) and (1.7). The two most common methods for solving dynamic optimization problems are: the sequential approach and the simultaneous approach [5]. Only the input vector is discretized in the sequential approach for dynamic optimization [6] whereas both state and input profiles are discretized in the simultaneous approach [7]. The third approach known as the multiple shooting method also parameterizes the input variables while enforcing the state continuity at the solution of the optimization problem; during the optimization iterates, discontinuities are allowed [8].

The sequential approach is a two-layered strategy, where nonlinear optimization and DAE integration steps are performed separately. The DAE model still holds and the optimization is carried out in the decision variables space only [9]. DAE

integration is carried out by a DAE solver using a set of initial conditions for the state variables and a starting control profile. The evaluated objective function value and sensitivity information obtained from the system by the DAE integrator is then passed to optimizer which tries to find new control actions to improve the objective function value. The iterative process between the optimizer and integrator continues until the optimal control profiles are reached satisfying a termination criterion. The disadvantage of this method is the computational effort required for integrating a DAE system and every single NLP iteration [10].

The simultaneous method (also known as “full discretization”) discretizes the DAE system to form a large-scale algebraic equation system [11]. The state variables are discretized and approximated through a set of polynomials. A popular method for full discretization is orthogonal collocation on finite elements (OCFE) [12]. This reduces the dynamic optimization problem to a very sparse finite NLP problem. The optimization in this case is carried in the full space of the discretized variables using specialized solution strategies[13]. The method is also referred to as the infeasible path approach [14], because the differential equations are satisfied at the converged solution of the NLP only. The solution of the model and the optimization is carried out simultaneously. Key advantages of this method are: path constraints are handled naturally within the optimization formulation and as the DAE system is only solved once, unstable or nonexistent intermediate solutions are bypassed[13]. Both the dynamic optimization approaches and the advantages of the simultaneous approach are shown in Fig. 1.2.

1.2.2 Nonlinear Model Predictive Control (NMPC)

Model Predictive Control (MPC) is one of the most popular advanced control strategies [15]. MPC uses a given model in a dynamic optimization framework to solve an optimal control problem (OCP). The optimization problem becomes nonlinear for nonlinear systems, which gives rise to Nonlinear MPC. A key advantage of NMPC

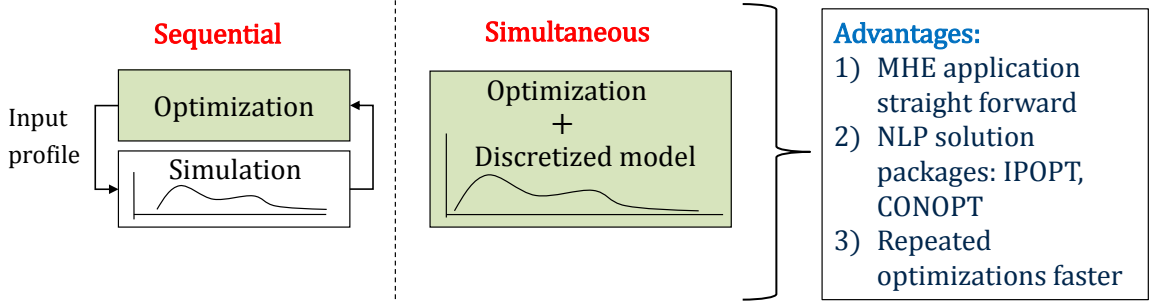


Figure 1.2: Dynamic optimization solution methods.

is that it handles constraints and the dynamic system directly. Current plant states or estimated states are taken as inputs in an NMPC controller and it then solves a NLP problem to generate the values for the manipulated variables to be implemented on the plant. NMPC solves moving horizon OCPs online for the nonlinear process model given as

$$\mathbf{x}_{k+1} = \mathbf{f}(\mathbf{x}_k, \mathbf{u}_k) \quad (1.8)$$

$$\mathbf{y}_k = \mathbf{g}(\mathbf{x}_k). \quad (1.9)$$

With knowledge of the current plant state or its estimate $\mathbf{x}(k)$, NMPC uses the model

$$\mathbf{z}(l+1) = \mathbf{f}(\mathbf{z}_l, \mathbf{v}_l), \mathbf{z}_0 = \mathbf{x}(k), l = 0, \dots, N \quad (1.10)$$

to find a sequence of computed control inputs $\{\mathbf{v}_0, \mathbf{v}_1, \dots, \mathbf{v}_{N-1}\}$ and predicted state variables $\{\mathbf{z}_0, \mathbf{z}_1, \dots, \mathbf{z}_N\}$ as shown in Fig. 1.3. The following dynamic optimization problem is generally solved to obtain the inputs and state variables (other different objective functions can also be chosen to meet a variety of process objectives [16])

$$\min_{\mathbf{z}_l, \mathbf{v}_l} \sum_{l=0}^N (||\mathbf{z}_l - \mathbf{z}_{ref}||_Q^2 + ||\mathbf{v}_l - \mathbf{v}_{ref}||_R^2) \quad (1.11)$$

$$\text{s.t. } \mathbf{z}_{l+1} = \mathbf{f}(\mathbf{z}_l, \mathbf{v}_l), \quad l = 0, \dots, N-1 \quad (1.12)$$

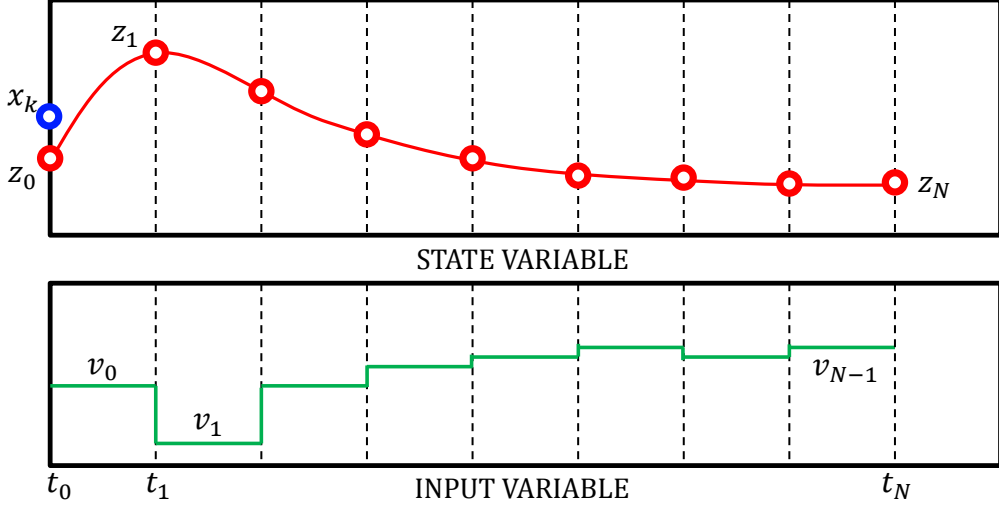


Figure 1.3: MPC graphical representation

$$\mathbf{z}_0 = \mathbf{x}(k) \quad (1.13)$$

$$\mathbf{z}_l \in Z, \mathbf{v}_l \in V \quad (1.14)$$

The objective function in equation (1.11) tries to regulate the states and inputs to a set-point given as \mathbf{z}_{ref} and \mathbf{v}_{ref} for states and inputs respectively, using a quadratic error criterion [17]. Q and R indicate the weighing matrices in vector norms. Constraints on the state and input variables are compactly given in equation (1.14), indicating that state variables must lie in some set Z , similarly for inputs. Of the sequence of computed control inputs $\{\mathbf{v}_0, \mathbf{v}_1, \dots, \mathbf{v}_{N-1}\}$ only the first one $\mathbf{u}(k) = \mathbf{v}_0$ is implemented on the plant. When the new state $\mathbf{x}(k+1)$ is available, the prediction horizon is shifted by one sample time and the parameters of the problem are updated to solve a new optimization problem to find $\mathbf{u}(k+1)$. The feedback law is given as

$$\mathbf{u}(k) = \mathbf{h}(\mathbf{x}(k)). \quad (1.15)$$

The NMPC controller is usually assumed to solve the problem instantaneously. The main issue in closed-loop implementation, as mentioned by [18], occurs if there is a computational delay in finding a solution of the NLP[19]. The plant moves away from its current state while the NLP solution is being found.

1.3 Main Contributions

The key research contributions are:

1. We investigated the simultaneous solution approach for optimizing the EAF operation. For using the simultaneous approach, we adopted Implicit Euler discretization for formulating the optimization problem. The optimization solution time was within 1 minute. Additionally, we have developed simulation and optimization web interfaces in collaboration with the McMaster Steel Research Centre (SRC) for SRC industrial members.
2. We investigated both the sequential and simultaneous approaches for implementing multi-rate moving horizon estimation (MHE). For carrying out the sequential approach, we developed a novel parameter-estimation framework for MHE. CasADi was employed for MHE using the simultaneous approach, and compared to the sequential approach. Furthermore, to solve the MHE problem more quickly, we developed a novel initialization strategy.
3. Our approach proposes an economic nonlinear MPC strategy that utilizes a first-principles dynamic model of an electric arc furnace, coupled with an MHE scheme, to manage the energy utilization in electric arc furnace operation. We also propose novel initialization schemes for the NMPC and MHE optimization problems that significantly reduce the computation time.
4. For real-time dynamic optimization implementation, we introduced a real-time advisory system for EAFs which employs a first-principles EAF model to support the operator decision making in real-time for economically optimal process operation. The advisory system is kept cognizant of the on-line states through use of a multi-rate Moving Horizon Estimator (MHE) that runs in parallel with the plant. Upon an operator's request for a decision support, an economics-based multi-tiered dynamic optimizer is executed to recommend an input sequence for optimal performance. The optimizer effectively handles

end-point constraints on state variables by tackling infeasibilities through a three tier calculation sequence. We also proposed a multi-tiered initialization scheme for solving the large-scale optimal control problems in the advisory system quickly.

1.4 Thesis Outline

We have structured the remainder of the thesis into following chapters.

In Chapter 2, we present a review of research advances toward economic optimization of EAF operations. The remainder of the chapter is organized into three sections covering the key building blocks of a real-time implementation: a dynamic model, dynamic simulation and dynamic optimization. Additionally, we discuss the simulation and optimization web interfaces developed in collaboration with the McMaster Steel Research Centre (SRC) for SRC industrial members.

In Chapter 3, we first develop a rigorous framework for MHE for the EAF process. Multi-rate MHE is posed as a parameter estimation problem where the discrete process noise terms are handled using a continuous function. The reformulation is studied for a first-principles dynamic EAF model developed originally in [20]. The multi-rate MHE is utilized to estimate states for an EAF heat (batch) under flat bath conditions. The performance is thereafter illustrated through application to a case study based on the EAF model. We then extend the MHE application for the full batch time with the use of a simultaneous approach. The multi-rate MHE formulation using the simultaneous approach is coupled with an economics-based dynamic optimizer to form an online decision support tool (DST). A case study is presented which demonstrates the increase in profit through the use of the DST.

In Chapter 4, we describe a real-time energy management strategy for EAF operation. We begin by employing multi-rate MHE to reconstruct the state vector at any

point in the batch duration. We then combine MHE and shrinking horizon economic model predictive control (EMPC) with time-varying cost coefficients into a single real-time energy management framework, utilizing a nonlinear first-principles based EAF model. We cast the NMPC and MHE optimization problems as NLP problems using the simultaneous approach to compute optimal solutions for the state estimates and control actions. Additionally, a novel initialization scheme is introduced for a combined MHE-NMPC implementation to obtain rapid solutions. Finally, the efficacy of the proposed energy demand-curbing strategy is demonstrated under real-time dispatch (RTD) electricity pricing scenarios. We also compare the energy savings obtained with and without a price update.

In Chapter 5, we describe the real-time dynamic optimization-based advisory system for EAF operation. We start with a description of the EAF process model and then introduce the dynamic optimization problem we are trying to solve. We then present the multi-tiered optimization where the working of the three tiers is explained. Next, we describe the algorithmic working of the real-time dynamic optimization-based advisory system. Finally, we describe the application of the advisory system for the electric arc steelmaking process.

In Chapter 6, we provide a brief summary and concluding remarks on the contributions described in the previous chapters. We then identify and present future research directions.

References

- [1] Steel Statistical Yearbook of World Steel Association. <http://www.worldsteel.org/steel-by-topic/statistics/steel-statistical-yearbook-.html>. 2016.
- [2] R. J. Fruehan. *The Making, Shaping, and Treating of Steel: Ironmaking volume*. Vol. 2. AISE Steel Foundation, 1999.
- [3] W. Ray. *Advanced process control*. New York: McGraw-Hill, 1981.
- [4] A. Cervantes and L. T. Biegler. "Optimization strategies for dynamic systems". In: *Encyclopedia of Optimization*. Springer, 2001, pp. 1886–1897.
- [5] Z. Chong. "Dynamic Optimization Formulations for Plant Operation under Partial Shutdown Conditions". PhD thesis. McMaster University, 2012.
- [6] R. Sargent and G. Sullivan. "The development of an efficient optimal control package". In: *Proceedings of the eighth IFIP conference on optimization techniques, part 2*. Ed. by J. Stoer. Springer, 1977.
- [7] L. T. Biegler. "Solution of dynamic optimization problems by successive quadratic programming and orthogonal collocation". In: *Comput. Chem. Eng.* 8 (1984), pp. 243–284.
- [8] H. Bock and K. Plitt. "A multiple shooting algorithm for direct Solution of optimal control problems". In: *Proceedings of the ninth IFAC world congress, Budapest*. Pergamon Press, 1984.
- [9] B. Chachuat. *Intoduction to Direct Solution Methods of Dynamic Optimization*.
- [10] O Abel and W. Marquardt. "Scenario-integrated modeling and optimization of dynamic systems". In: *AIChE Journal* 46.4 (2000), pp. 803–823.
- [11] L. T. Biegler, A. M. Cervantes, and A. Wächter. "Advances in simultaneous strategies for dynamic process optimization". In: *Chemical Engineering Science* 57.4 (2002), pp. 575–593.

- [12] J. E. Cuthrell and L. T. Biegler. "On the optimization of differential-algebraic process systems". In: *AIChE Journal* 33.8 (1987), pp. 1257–1270.
- [13] L. T. Biegler and I. E. Grossmann. "Retrospective on optimization". In: *Computers & Chemical Engineering* 28.8 (2004), pp. 1169–1192.
- [14] V. Vassiliadis, R. Sargent, and C. Pantelides. "Solution of a class of multistage dynamic optimization problems. 1. Problems without path constraints". In: *Industrial & Engineering Chemistry Research* 33.9 (1994), pp. 2111–2122.
- [15] X. Yang and L. T. Biegler. "Advanced-multi-step nonlinear model predictive control". In: *Proc. Int. Symp. Adv. Control of Chemical Processes (ADCHEM)*, Singapore. 2012, pp. 426–431.
- [16] M. A. Henson and D. E. Seborg. *Nonlinear process control*. Prentice-Hall, Inc., 1997.
- [17] J. B. Rawlings and D. Q. Mayne. *Model predictive control: Theory and design*. Nob Hill Pub., 2009.
- [18] H. Pirnay, R. López-Negrete, and L. T. Biegler. "Optimal sensitivity based on IPOPT". In: *Mathematical Programming Computation* 4.4 (2012), pp. 307–331.
- [19] L. O. Santos, P. A. Afonso, J. A. Castro, N. M. Oliveira, and L. T. Biegler. "Online implementation of nonlinear MPC: an experimental case study". In: *Control Engineering Practice* 9.8 (2001), pp. 847–857.
- [20] R. D. MacRosty and C. L. E. Swartz. "Dynamic modeling of an industrial electric arc furnace". In: *Industrial & engineering chemistry research* 44.21 (2005), pp. 8067–8083.

Chapter 2

Modeling, Simulation and Optimization of EAF Operation

2.1	Introduction	16
2.2	Dynamic Modeling	16
2.3	Dynamic Simulation	20
2.4	Dynamic Optimization	24
2.5	Conclusion	26
	References	26

The formulations and results in this chapter have been published, and presented in:

- [1] S. Shyamal and C.L.E. Swartz. "Dynamic Optimization of Electric Arc Furnace Operation with State Estimation as a Decision Support Tool". *64th CSChE Conference* (2014). Niagara Falls, ON, Canada.
- [2] C.L.E. Swartz and S. Shyamal. "Dynamic Optimization, Estimation and Control of Electric Arc Furnace Operation". *Current Advances of Materials and Processes*

(CAMP- ISIJ), 30(2), 174th ISIJ Meeting (2017). Sapporo, Japan.

Online resources produced:

- [1] S. Shyamal, V. Carri, J. Thompson and C.L.E. Swartz. "Online Electric Arc Furnace Model for Optimization". *McMaster Steel Research Centre Website* (2017).
- [2] S. Shyamal, P. Warnick, J. Thompson and C. L. E. Swartz. "Online Electric Arc Furnace Model for Simulation". *McMaster Steel Research Centre Website* (2016).

2.1 Introduction

Electric arc furnaces (EAFs) are widely used in the steel industry to produce steel by melting scrap metal and adjusting the composition through the addition of oxygen, carbon and fluxes. They are highly energy intensive operations, and due to the harsh operating conditions, have limited measurements.

This chapter presents the advances made by the research work toward economic optimization of EAF operations. The remainder of the chapter is organized into three sections covering the key building blocks of a real-time implementation: a dynamic model, dynamic simulation and dynamic optimization.

2.2 Dynamic Modeling

Various modeling paradigms have been applied to EAFs, ranging from very detailed models involving computational fluid dynamics, to purely empirical models. In order to be used in a real-time setting, key considerations are computational speed and reliability. The model should also be dynamic in order to capture the transient nature of a heat (batch), and capture the relationship between the process inputs, response variables, constraints and a suitably defined objective function.

First-principles based dynamic models have been proposed by several researchers. Cameron et al. [1] present an EAF model for dynamic simulation in which the EAF contents are considered as four phases, with mass transfer between phases and chemical equilibrium at phase interfaces. Matson and Ramirez [2] consider two control volumes in which chemical equilibrium is assumed. The scrap is modeled as spheres. Optimal carbon and oxygen additions are determined using iterative dynamic programming. Bekker et al. [3], on the other hand, utilize kinetic relationships in a dynamic EAF model developed for closed-loop simulation. MacRosty and Swartz

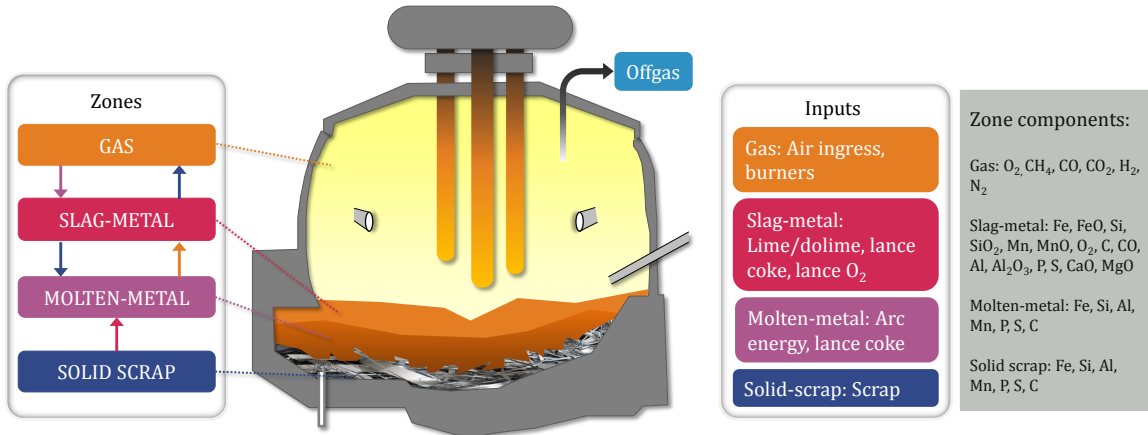


Figure 2.1: Schematic of EAF model with zones, inputs and components within zones indicated.

[4] present a dynamic EAF model comprising four zones, illustrated in Fig. 2.1, with chemical equilibrium considered in the gas and slag-metal zones, and mass transfer across zone interfaces determined by concentration gradients. The model includes material and energy balances, accounts for the addition of a second scrap charge as well as oxygen, carbon and fluxes, includes radiative heat transfer between the arc and exposed surfaces, and accounts for slag depth through empirical relationships. The model takes the form of a differential-algebraic equation (DAE) system with 85 differential and 1050 algebraic state variables. Six parameters are chosen for rigorous parameter estimation based on a sensitivity analysis in which the model response trajectories are matched to industrial data in a weighted least-squares sense, with the model subsequently validated against batch data not used in the estimation. The model was modified and reconfigured by Ghobara [5]. The following two major changes were implemented: addition of three JetBoxes which control the supply of oxygen, and assuming a flat surface geometry for scrap melting unlike the cone-frustum assumed by MacRosty and Swartz [4]. The modified differential-algebraic equation system was modeled in gPROMS [6] and contained 40 differential variables.

2.2.1 Model reformulation

The EAF model of Ghobara [5] was reduced to speed up computation and improve robustness for real-time applications. The initial model reduction strategy applied was to reduce the model dimension through simplifying the physics and kinetics of the process:

1. **Removal of the radiation model:** The base model considered radiation within the furnace and approximated the geometry of each surface to calculate the net radiative heat transfer from each surface to the other. In the literature, the scrap melting geometry has not been clearly established, and as a result several assumptions are required to develop the radiation model. Therefore, the radiation model was removed and the amount of radiation lost to the walls and the roof of the furnace was approximated through an estimated parameter, simplifying the model significantly.
2. Two state variables were removed:
 - State for Nitrogen in slag-metal zone: Since it stayed at a constant value of 0.01, it was removed and replaced with 0.01.
 - State for Magnesium in molten-metal zone: Since the state variable took values which were very small (close to 1.0×10^{-13}), it was removed from the model and replaced with a constant small number.

Next, we performed the changes needed for numerical robustness. The key changes that were incorporated in the model are as follows.

1. Scaling was performed by transforming the units of mass and energy. For example, kg was transformed into tonnes, KW to MW, mol to kmol and kJ to MJ. The units of heat capacity and other physical parameters were scaled as well.
2. We used gPROMS to find out which variables of the model can be pre-calculated [6]. The pre-calculated variables were removed and replaced with their respec-

tive values manually, thus reducing the size of the model. This process is described through the following example.

$$\begin{array}{ccc}
 & \left(\begin{array}{l} a = 2 \\ b = 2 \\ c = a + b \\ d = e + c \end{array} \right) & \rightarrow \left(\begin{array}{l} a = 2 \\ b = 2 \\ d = e + 4 \end{array} \right) \\
 \text{(previous expressions)} & & \text{(new expressions)}
 \end{array} \tag{2.1}$$

Here, a and b are defined as parameters whereas c , d and e are defined as variables. c is the pre-calculated variable which is replaced with the exact value of 4 in the reformulated expression.

Remark: Pre-calculated variables ideally should be defined as a parameter during the model formulation but such a definition is not obvious when a large-scale first-principles model is built. In particular, in the above example, c is a function of two parameters; thus it is clear at the outset that c is also a parameter. However, in the more general case, a variable may be a function of both variables and parameters.

3. To avoid ‘division by zero’ error, we added a small tolerance ϵ value to the denominator of division expressions,

$$\frac{a}{b} \text{ changed to } \frac{a}{b + \epsilon},$$

where a and b are the variables defining the division expression.

The modified DAE model was then explored for simulation and applying simultaneous method for dynamic optimization.

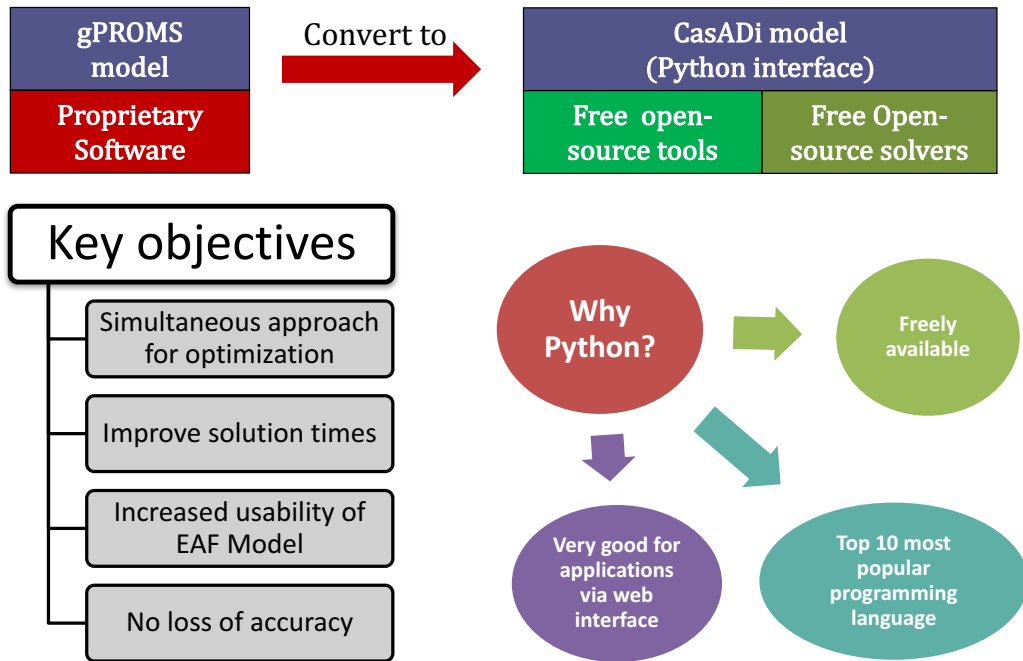


Figure 2.2: Translating model from gPROMS to CasADI.

2.3 Dynamic Simulation

The model developed above was coded in gPROMS (General Process Modeling System)(see [4]) which uses a direct sequential approach for dynamic optimization. Computational time for optimization with the sequential method needs to be compared with a simultaneous approach and reduced to enhance the on-line implementation of the model. Suitable software platforms for carrying out the simultaneous method were explored. An open-source Python framework CasADI [7] was identified as a potential tool and the gPROMS model was translated to be used in CasADI (see Fig. 2.2).

We first transformed the DAE model into an explicit form manually. This was possible due to the representation of the derivatives in the original DAE. The consistent initialization values for the algebraic variables were extracted from gPROMS and transported to CasADI. The DAE model in CasADI after the translation from gPROMS

can be expressed as

$$\dot{\mathbf{x}} = \mathbf{f}_x(\mathbf{x}(t), \mathbf{z}(t), \mathbf{u}(t), t) \quad (2.2)$$

$$\mathbf{0} = \mathbf{f}_z(\mathbf{x}(t), \mathbf{z}(t), \mathbf{u}(t), t) \quad (2.3)$$

$$\mathbf{x}(0) = \mathbf{x}_0. \quad (2.4)$$

For simulating the above DAE system, three different solution approaches in CasADI were studied:

1. **Integrator:** We use the IDA integrator [8] from the SUNDIALS suite for simulation. The integrator method implements a variable order, variable coefficient BDF (Backward differentiation formula). The CasADI implementation provides the facility to extract variable values at any time point of the IDA simulation.
2. **Nonlinear system:** We discretize the continuous time system manually using Implicit Euler Scheme and solve the nonlinear system using Newton iterations. The Implicit Euler discretization was adopted instead of collocation [9] to avoid formulation complexity. The variables for the nonlinear system were initialized using the IDA simulation solution.
3. **Nonlinear Programming Problem (NLP):** The simulation can be expressed as the following optimization problem:

$$\min_{\mathbf{x}(t), \mathbf{z}(t)} 0 \quad (2.5a)$$

$$s.t. \quad \text{Discretized model equations.} \quad (2.5b)$$

We employ IPOPT [10] to solve the NLP problem. The simulated profiles obtained using IDA were used as initial guesses to solve the problem and reliable solution was obtained.

The simulation time in CasADI for the full EAF model was approximately 2 seconds using any of the above three approaches. This gave us the confidence in formulating

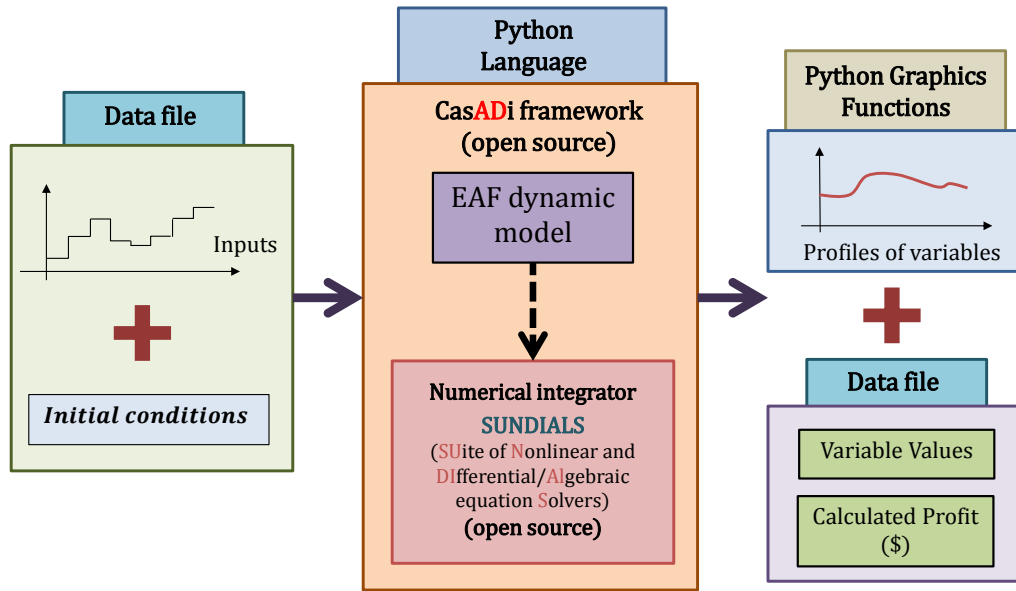


Figure 2.3: Backend of the simulation interface for McMaster Steel Centre industrial members.

the optimization problem in CasADI.

2.3.1 Deployment: Off-line Application using a Simulation User Interface

The objective for deployment was to build a web interface for the industrial members of the McMaster Steel Research Centre (SRC) through which users can interact with the model. As the model is written in Python, attaching it to a front-end webpage was not very difficult. The backend for the online implementation is represented in Fig. 2.3. Key to the implementation of such a backend is to clearly identify and separate the input and output variables. These input variable will take values provided by users through the input webpage (see Fig. 2.4) [11]. The simulation is carried out in the Python background on the SRC server and then results are passed to the output user interface.

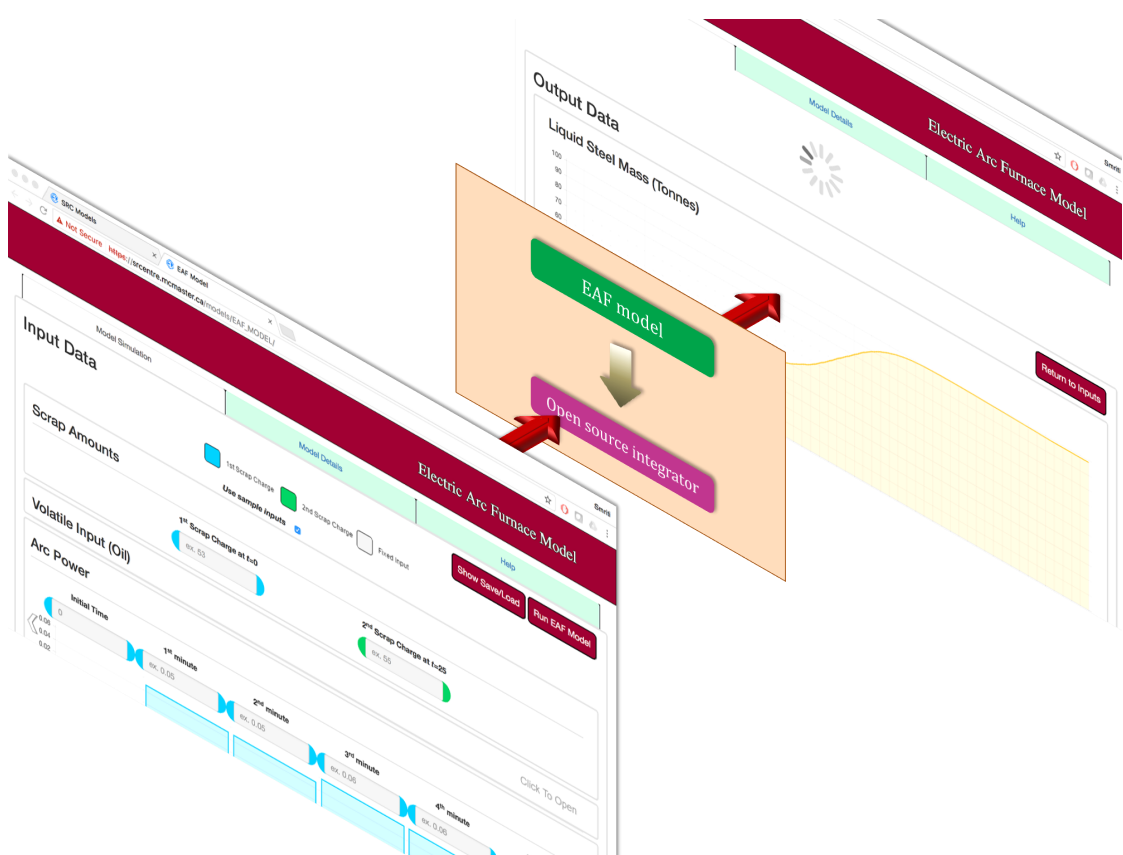


Figure 2.4: Simulation interface for McMaster Steel Centre industrial members.

2.4 Dynamic Optimization

A dynamic optimization problem that maximizes a performance criterion over the duration of the heat can be formulated as

$$\max_{\mathbf{u}(t)} \phi(\mathbf{x}(t), \mathbf{z}(t), \mathbf{u}(t), t_f) \quad (2.6)$$

$$s.t. \quad \mathbf{f}(\dot{\mathbf{x}}(t), \mathbf{x}(t), \mathbf{z}(t), \mathbf{u}(t), t) = \mathbf{0} \quad (2.7)$$

$$\mathbf{g}(\mathbf{x}(t), \mathbf{z}(t), \mathbf{u}(t), t) \geq \mathbf{0} \quad (2.8)$$

$$\mathbf{g}_s(\mathbf{x}(t_s), \mathbf{z}(t_s), \mathbf{u}(t_s), t_s) \geq \mathbf{0} \quad (2.9)$$

where ϕ represents a suitable objective function such as profit, \mathbf{f} represents a set of differential and algebraic equations describing the process, and \mathbf{g} and \mathbf{g}_s represent path and point constraints respectively. \mathbf{x} , \mathbf{z} and \mathbf{u} represent differential state, algebraic state and input variables. MacRosty and Swartz [12] use a profit based objective function given by

$$\begin{aligned} \phi = & c_0 M_{steel}(t_f) - \left(c_1 \int_0^{t_f} P dt + c_2 \int_0^{t_f} (F_{O_2,brnr} + F_{O_2,Inc}) dt + c_3 \int_0^{t_f} F_{CH_4,brnr} dt \right. \\ & \left. + c_4 \int_0^{t_f} F_{C,inj} dt + c_5 \int_0^{t_f} F_{C,chg} dt + c_6 \int_0^{t_f} F_{flux} dt + c_7 \int_0^{t_f} (F_{scrap,1} + F_{scrap,2}) dt \right) \end{aligned}$$

where P represents the electrical power, the F_i are the inputs and the c_i are revenue/cost coefficients.

Parameterization of the inputs by a finite set of parameters, such as through piecewise constant inputs, allows the dynamic optimization problem to be cast as a nonlinear programming (NLP) problem. In a sequential solution approach [13, 14], the optimization and integration of the dynamic equations occur sequentially, with updated input trajectories provided to the DAE integration at each optimization iteration. A simultaneous solution or direct transcription approach [9], on the other hand, involves discretization of the dynamic system over the time horizon under consideration,

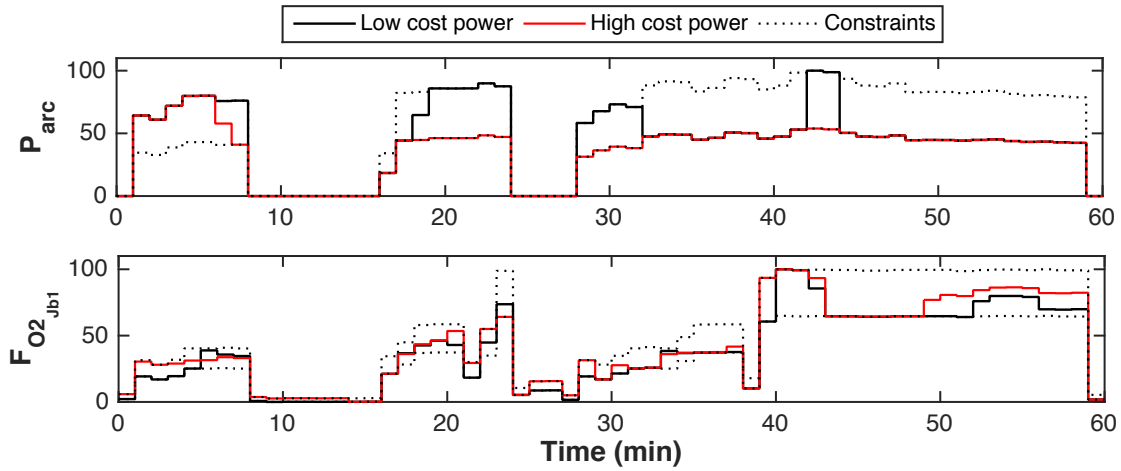


Figure 2.5: Optimal power and oxygen input trajectories for different electricity prices.

and inclusion of the resulting algebraic equations as equality constraints in a single, large-scale optimization problem. MacRosty and Swartz [12] and Ghobara [5] apply a sequential optimization strategy implemented in gPROMS/gOPT to determine the optimal operation of an EAF under various conditions.

In this work, we used simultaneous solution approach for dynamic optimization using CasADI. To further improve the robustness and solution time, CasADI was then employed to eliminate a subset of the algebraic variables and equations (details given in Chapter 5). The optimization solution time using the reduced model was within 1 minute. We used the solutions obtained from solving the feasibility optimization problem (2.5) as initial guesses to solve the economic dynamic optimization problem. Fig. 2.5 shows the economically optimal solution profiles of the power and oxygen inputs to an EAF for using the EAF model as adapted in Shyamal and Swartz [15]. Two optimal profiles for each variable are shown, corresponding to high and low electricity prices respectively. When the electricity cost is high, less power is used over the duration of the heat, with the product end-point and operational constraints enforced over the heat. The complexity of the relationships and interactions between the variables and constraints prohibits the generation of high quality solutions based on operator experience and judgement alone. An interface for optimization was built

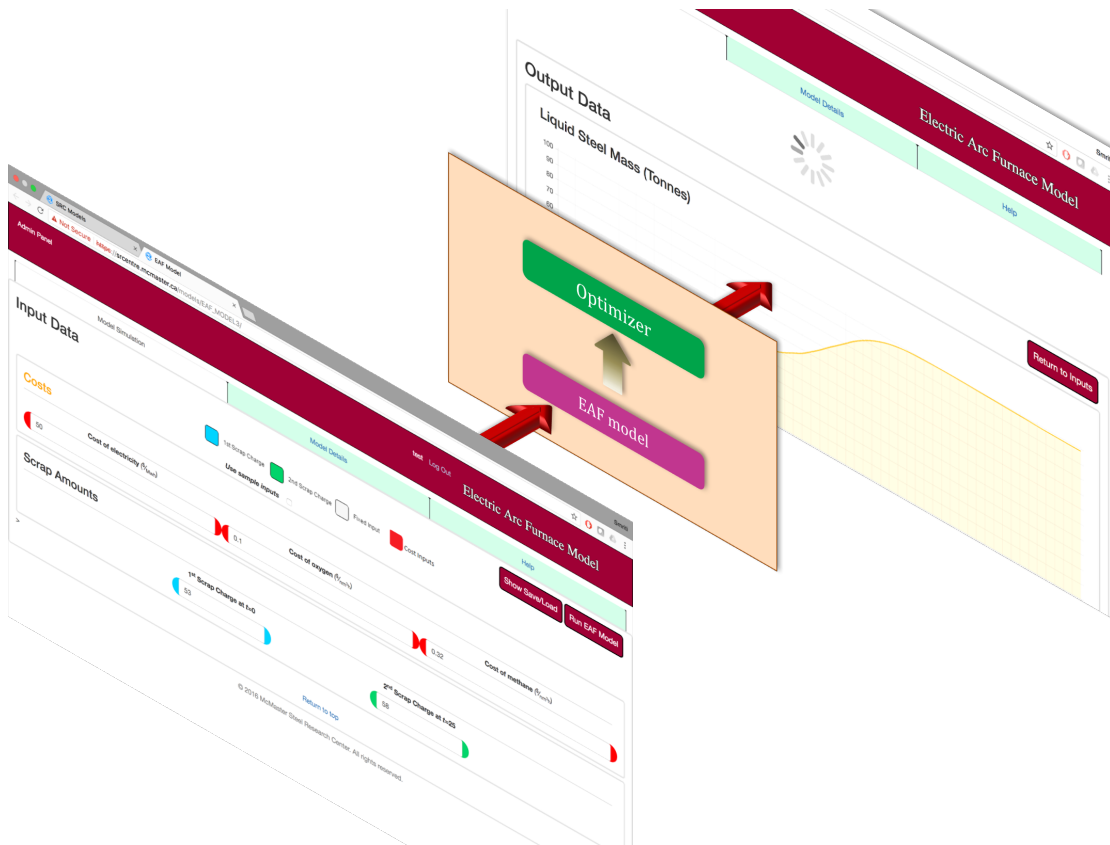


Figure 2.6: Simulation interface for McMaster Steel Centre industrial members.

for SRC industrial members (see Fig. 2.6) [16].

2.5 Conclusion

The high energy consumption of EAFs make them prime candidates for economic optimization. The complexity of the EAF process, multiple constraints, and limited process measurements pose significant challenges for operator-based optimization. In this chapter, the components of a real-time EAF optimization strategy are described. The potential economic benefit of these approaches has been demonstrated through simulation studies, with plant trials constituting a useful next step.

References

- [1] A Cameron, N Saxena, and K Broome. "Optimizing EAF operations by dynamic process simulation". In: *ELECTRIC FURNACE CONFERENCE*. Vol. 56. IRON and STEEL SOCIETY OF AIME. 1998, pp. 689–696.
- [2] S Matson and W. F. Ramirez. "Optimal operation of an electric arc furnace". In: *57 th Electric Furnace Conference*. 1999, pp. 719–730.
- [3] J. G. Bekker, I. K. Craig, and P. C. Pistorius. "Modeling and simulation of an electric arc furnace process". In: *ISIJ international* 39.1 (1999), pp. 23–32.
- [4] R. MacRosty. *Modelling, Optimization and Control of an Electric Arc Furnace*. McMaster University (Canada), 2005.
- [5] E. M. Y. Ghobara. "Modeling, Optimization and Estimation in Electric Arc Furnace (EAF) Operation". PhD thesis. 2013.
- [6] Process Systems Enterprise Ltd. *gPROMS*, www.psenterprise.com/gproms, 1997-2015. 2015.
- [7] J. Andersson, J. Åkesson, and M. Diehl. "CasADI: A symbolic package for automatic differentiation and optimal control". In: *Recent advances in algorithmic differentiation*. Springer, 2012, pp. 297–307.
- [8] A. C. Hindmarsh, P. N. Brown, K. E. Grant, S. L. Lee, R. Serban, D. E. Shumaker, and C. S. Woodward. "SUNDIALS: Suite of nonlinear and differential/algebraic equation solvers". In: *ACM Transactions on Mathematical Software (TOMS)* 31.3 (2005), pp. 363–396.
- [9] L. T. Biegler. "An overview of simultaneous strategies for dynamic optimization". In: *Chemical Engineering and Processing: Process Intensification* 46.11 (2007), pp. 1043–1053.
- [10] A. Wächter and L. T. Biegler. "On the implementation of an interior-point filter line-search algorithm for large-scale nonlinear programming". In: *Mathematical Programming* 106.1 (2006), pp. 25–57.

- [11] S. Shyamal and C. L. E. Swartz. "Optimization and Control of Electric Arc Furnace Operation (Status Update and Online EAF Model)". In: *McMaster Steel Research Centre Meeting*. 2016.
- [12] R. D. MacRosty and C. L. E. Swartz. "Dynamic optimization of electric arc furnace operation". In: *AIChe journal* 53.3 (2007), pp. 640–653.
- [13] V. Vassiliadis, R. Sargent, and C. Pantelides. "Solution of a class of multistage dynamic optimization problems. 1. Problems without path constraints". In: *Industrial & Engineering Chemistry Research* 33.9 (1994), pp. 2111–2122.
- [14] V. Vassiliadis, R. Sargent, and C. Pantelides. "Solution of a class of multistage dynamic optimization problems. 2. Problems with path constraints". In: *Industrial & Engineering Chemistry Research* 33.9 (1994), pp. 2123–2133.
- [15] S. Shyamal and C. L. E. Swartz. "Real-time energy management for electric arc furnace operation". In: *Journal of Process Control* <https://doi.org/10.1016/j.jprocont.2018.03.002> (2018).
- [16] S. Shyamal and C. L. E. Swartz. "Optimization and Control of Electric Arc Furnace Operation (Status Update and Online EAF Model)". In: *McMaster Steel Research Centre Meeting*. 2017.

Chapter 3

Moving Horizon Estimation

3.1	A Multi-rate Moving Horizon Estimation Framework for Electric Arc Furnace Operation.	31
3.2	Multi-Rate Moving Horizon Estimation using different optimization paradigms	
	46	
3.3	Optimization-based Online Decision Support Tool for Electric Arc Furnace Operation	55
3.A	Derivation of $W'_i(t, w_k)$ based on hyperbolic tangent functions.	68
	References	69

The formulations and results in this chapter have been published, and presented in:

- [1] S. Shyamal and C.L.E. Swartz. "A multi-rate moving horizon estimation framework for electric arc furnace operation". *IFAC-PapersOnLine* 49, no. 7, 1175-1180 (2016).
- [2] S. Shyamal and C.L.E. Swartz. "Multi-Rate Moving Horizon Estimation for an Electric Arc Furnace Steelmaking Process". *AICHE Annual Meeting* (2016). San

Francisco, CA, USA.

- [3] S. Shyamal and C.L.E. Swartz. "Optimization-based Online Decision Support Tool for Electric Arc Furnace Operation.". *IFAC-PapersOnLine* 50, no. 1, 10784-10789 (2017).

Sections 1, 2 and 3 describe the research works presented in the three publications respectively.

3.1 A Multi-rate Moving Horizon Estimation Framework for Electric Arc Furnace Operation¹

Electric arc furnaces (EAFs) are widely used in steel industries to produce molten steel from scrap metal. EAF operation, being a highly energy intensive process, is characterized by a limited number of measurements at multiple rates, most of which do not correspond to system states. The ability to estimate the states would enhance the application of control and real-time optimization strategies. In this work, a multi-rate moving horizon estimation (MHE) framework for EAF operation under flat-bath conditions is introduced and implemented. Key features are the restructuring of MHE problem to a parameter estimation problem, multi-rate measurements handling, and use of a nonlinear model. The approach is implemented in the gPROMS (General Process Modeling System) modeling language. The components of the framework are presented, and the method is applied to a case study illustrating its performance.

3.1.1 Introduction

Electric arc furnaces (EAFs) are widely used for production of steel by melting scrap steel and adjusting its chemistry. This is a highly energy intensive, complex batch process involving both electrical and chemical energy to melt scrap. The electrical energy is transferred through electrodes, and burners are used to inject natural gas and oxygen, which provide chemical energy through combustion. The melting continues and a flat bath of molten steel is formed. The flat bath conditions usually last for the last 20 minutes of the batch duration. The oxygen reacts with metals to form oxides which become components of the slag layer floating on top of the molten steel. Slag chemistry is varied by direct addition of carbon, lime and dolomite through the roof of the furnace and by adjusting oxygen and carbon lancing. The high energy consumption motivates the development of estimation and control strategies for

¹S. Shyamal and C.L.E. Swartz. "A multi-rate moving horizon estimation framework for electric arc furnace operation via Sequential Optimization". *IFAC-PapersOnLine* 49, no. 7, 1175-1180 (2016)

EAFs.

Due to the harsh operating conditions, EAFs lack measurements and most of the states are not directly measured. State knowledge is very important in real-time control applications. There are limited applications of state estimation for EAF operation. Billings et al. [1] applied the extended Kalman Filer (EKF) to the refining stage of EAF operation but the model had 4 states, which are insufficient to capture the detailed process dynamics. Wang et al. [2] used an EKF to identify the arc current parameter for obtaining the electrical properties of the EAF load. However, the EAF model only involved the power system. Ghobara [3] implemented a constrained multi-rate EKF to estimate the states of EAF system using plant measurements. The EKF showed acceptable performance in tracking the true states of the process, even in the presence of a parametric plant-model mismatch. Out of the many available tools for state estimation, moving horizon estimation (MHE) is gaining popularity [4] due to the ability to handle constraints and to use computationally efficient numerical optimization algorithms. Although different versions of the Kalman filter such as the EKF, unscented Kalman filter etc. are employed by some researchers, many studies have shown MHE to have superior performance than Kalman filters [5].

The MHE problem consists of solving a nonlinear dynamic optimization problem subject to the nonlinear system under consideration and some other constraints specified by the user. It uses a finite set of past available measurements to reconstruct the full state of the process, thus keeping the optimization problem numerically tractable. The use of a finite size window of measurements by MHE provides a natural framework to include measurements with different sampling rates. López-Negrete and Biegler [6] mention that including the slow measurements for state estimation can improve system observability. They proposed a variable structure multi-rate MHE and illustrated it using two simulation examples.

Direct techniques that can be used for solving the dynamic optimization problem of MHE are sequential (i.e., single shooting), simultaneous (i.e., full transcription), and multiple-shooting methods. Simultaneous and multiple shooting methods have

been extensively explored by researchers for MHE applications incorporating large scale differential-algebraic equation (DAE) systems. The contributions are due to the developments and applications related to tools: AMPL [7] with solver IPOPT [8], ACADO toolkit [9], JModelica.org [10] and MUSCOD II [11]. However, the sequential method has received less attention due to unavailability of mature platforms for MHE implementations. Although gPROMS [12] provides commercial products for model-based chemical engineering and has capabilities for solving dynamic optimization using shooting algorithms, it had not yet been demonstrated that whether MHE can be readily formulated within the gPROMS framework. It transpires that it is relatively straightforward to formulate MHE as a parameter estimation problem in gPROMS [13]. This is intuitive as both MHE and parameter estimation have a similar approach to maximize a joint probability function, given the measurements. However, for MHE it is the joint probability for a trajectory of state values whereas in case of parameter estimation it is for the measurement values being predicted by the mathematical model [12].

In this section, we develop a rigorous framework for MHE for the EAF process. Multi-rate MHE is posed as a parameter estimation problem where the discrete process noise terms are handled using a continuous function. The formulation is particularly suitable for applications in sequential dynamic optimization platforms such as gPROMS/gEST. The reformulation is studied for a first-principles dynamic EAF model developed in [14]. The multi-rate MHE is utilized to estimate states for an EAF heat (batch) under flat bath conditions. The following sections provide an overview of the EAF model and a description of the multi-rate MHE framework developed. The performance is thereafter illustrated through application to a case study based on the EAF model.

3.1.2 EAF model

The first principles EAF model developed by MacRosty and Swartz [14] divided the furnace into 4 zones:

1. the *gas zone*, considers gases in the freeboard volume of the furnace above the scrap material;
2. the *slag-metal interaction zone*, contains all the slag material and the portion of molten steel zone interacting with it;
3. the *molten steel zone*, comprises mainly of the metals in their liquid state excluding the portion included in the slag-metal interaction zone; and,
4. the *solid scrap zone*, represents solid form of the charged scrap.

Fig. 3.1 is a schematic diagram of the process showing inputs, outputs and material exchanges for the zones. The model equations contain dynamic mass and energy balances, chemical equilibrium, and heat transfer relationships. Chemical equilibrium is considered within the slag and gas zones, and calculated by minimizing the Gibbs free energy. The reactions occurring inside the zones are limited by mass transfer between the zones. Radiation within the furnace and slag foaming are also modeled. Parameter estimation was done using real plant data and verified using additional data sets. The model was reconfigured and modified in [15] and [3]. The following two major changes were made: addition of three JetBoxes which control the supply of oxygen and assuming a flat surface geometry for scrap melting unlike the cone-frustum assumed in [14]. The differential-algebraic equation system was modeled in gPROMS and contained 40 differential variables.

This work is built upon the model described in [3]. The radiation model is removed and replaced with a parameter that divides the energy lost from the arc power through radiation between the roof, the walls, the scrap and the molten metal. The modified model was validated using parameter estimation and matching profiles

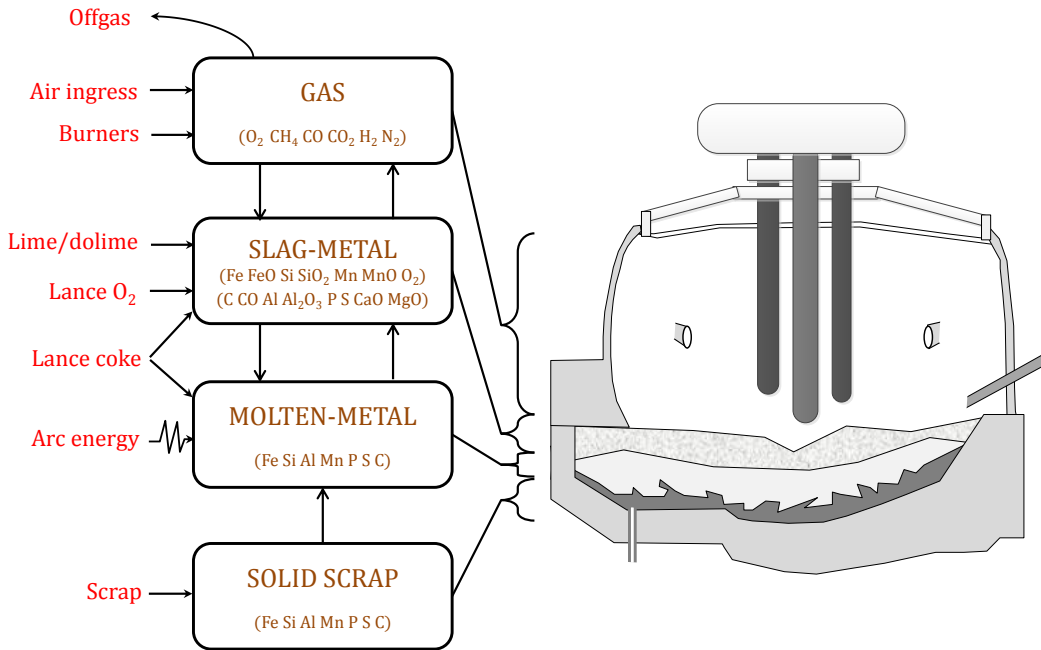


Figure 3.1: Schematic of EAF model. [14]

were obtained between the plant and the model data in a weighted least-squares sense. This provided confidence in carrying forward with using such an assumption that removes a lot of nonlinearity in the system. It has been assumed that all the oxides are present in the slag-metal zone, and therefore the oxide states in the molten metal zone were always negligible. Those states were removed from the molten metal, except oxygen which is usually required if lancing occurs. The modified EAF model in consideration has 29 differential states and 518 algebraic variables. Flat bath conditions are assumed wherein all the scrap has melted.

3.1.3 Moving horizon estimation

Real-time applications of the EAF model require the states to be known at the time in consideration. The state observer needs to estimate the internal states of the EAF system with the limited availability of measurements and various plant-model mismatch scenarios. This would enable the operators to implement effective control

strategies during the batch operation. In this section, we present a novel multi-rate MHE framework for EAF operation under flat bath conditions.

The EAF process is very complex to model and there are fluctuations due to frequent addition of materials to the furnace. As with any first principles model, there exists plant-model mismatch and modeling errors. There are also unknown disturbances during the batch operation. The proposed estimation strategy handles the uncertainties through process noise terms. Another issue arises due to the measurements being taken at different sampling rates. The off-gas compositions viz. the concentration of carbon monoxide (CO), carbon dioxide (CO₂), oxygen (O₂) and hydrogen (H₂), as well as the roof and walls temperatures, are measured every 1 minute. On the other hand, only one sample is taken to measure the composition of iron II oxide (FeO), aluminum oxide (Al₂O₃), silicon dioxide (SiO₂), magnesium oxide (MgO) and calcium oxide (CaO) in the slag. Two samples are taken for the molten metal temperature and carbon content in molten metal. The multi-rate nature of the measurements is handled naturally by placing the slow measurements in their proper locations in the measurement history.

Multi-rate MHE problem formulation

Suppose the EAF model is at time instant t_i where i is the current sampling index and we have a history of past inputs and measurements. The multi-rate MHE includes measurements with various sampling rates. The slower measurements related to slag and molten metal zones can easily be placed in their appropriate locations in the moving horizon frame of length N time intervals. Assuming the slow measurements are positioned at the sampling times of the fast measurements, the vector of fast measurements is defined as \mathbf{y}_k^F and the vector containing both the slow and fast measurements is defined as \mathbf{y}_k^{SF} . The measurement distribution can be given as, for example, $\mathbf{Y}_i = \{\mathbf{y}_{i-N}^F, \mathbf{y}_{i-N+1}^{SF}, \mathbf{y}_{i-N+2}^F, \dots, \mathbf{y}_i^F\}$; where the measurement set at time t_{i-N+1} contains the slow measurements. However, different structures of \mathbf{Y}_i are

possible. As time moves forward, when a new measurement becomes available it is appended to the horizon window, and the first measurement is dropped.

Consider the multi-rate MHE problem for a nonlinear system which is observable along the state trajectories in the following general form:

$$\begin{aligned} \min_{\mathbf{x}_{i-N}, \mathbf{w}_k} & \sum_{k=i-N}^{i-1} \|\mathbf{w}_k\|_Q^{-2} + \sum_{\substack{k=i-N \\ k \in \mathbb{I}_F}}^i \|\mathbf{y}_k^F - \mathbf{h}^F(\mathbf{x}_k)\|_{(R^F)^{-1}}^2 \\ & + \sum_{\substack{k=i-N \\ k \in \mathbb{I}_{SF}}}^i \|\mathbf{y}_k^{SF} - \mathbf{h}^{SF}(\mathbf{x}_k)\|_{(R^{SF})^{-1}}^2 + \|\mathbf{x}_{i-N} - \hat{\mathbf{x}}_{i-N}\|_{S_i^{-1}}^2 \end{aligned} \quad (3.1)$$

$$\text{s.t. } \mathbf{x}_{k+1} = \mathbf{f}(\mathbf{x}_k, \mathbf{u}_k) + \mathbf{w}_k, \quad k = i-N, \dots, i-1 \quad (3.2)$$

$$\mathbf{x}^{LB} \leq \mathbf{x}_k \leq \mathbf{x}^{UB}, \quad k = i-N, \dots, i \quad (3.3)$$

where \mathbf{x}_k is the system state vector, \mathbf{u}_k is the control input, \mathbf{w}_k is a noise term introduced to model the model uncertainty (i.e. the process noise), $\hat{\mathbf{x}}_{i-N}$ is an estimate for the state at the beginning of the horizon, \mathbf{f} integrates the model, given the state \mathbf{x}_k , control input \mathbf{u}_k and process noise \mathbf{w}_k , over one sampling interval, and $\{\mathbf{h}^F, \mathbf{h}^{SF}\}$ are the measurement functions that map the system state to \mathbf{y}_k^F and \mathbf{y}_k^{SF} respectively. Q , R^F , R^{SF} and S_i are the covariance matrices (of appropriate dimensions) for the model noise, measurement noise and for the arrival cost respectively. \mathbf{x}^{LB} and \mathbf{x}^{UB} represent lower and upper bounds respectively on the state variables.

The cost function (3.1) comprises four terms of which the first three are weighted minimization of errors over a time horizon. The fourth term of (3.1), the arrival cost, summarizes the previous measurement data not considered in the moving horizon frame. The weighing matrix S_i is updated to S_{i+1} for the next MHE run using the solution of the currently solved MHE optimization problem. An EKF update is used in general [16],

$$S_{i+1} = Q + A_i [S_i - S_i C_i^T (R + C_i S_i C_i^T)^{-1} C_i S_i] A_i^T \quad (3.4)$$

where $A_i = \nabla_{\mathbf{x}} \mathbf{f}(\mathbf{x}_{i-N}^*, \mathbf{u}_{i-N}, \mathbf{w}_{i-N}^*)$ and $C_i = \nabla_{\mathbf{y}} \mathbf{h}(\mathbf{x}_{i-N}^*)$. \mathbf{x}_{i-N}^* and \mathbf{w}_{i-N}^* represent solution of MHE optimization problem (3.1).

Parameter estimation framework

To transform the multi-rate MHE formulation into a parameter estimation problem, the decision variables of (3.1) need to be parameters rather than variables. The discrete values of process noise term $\{w_{i-N}, w_{i-N+1}, \dots, w_{i-1}\}$ for a state can be expressed as a discontinuous piecewise constant function $W_i(t, w_k)$. $W_i(t, w_k)$ is replaced by a continuous function $W'_i(t, w_k)$ which treats $\{w_{i-N}, w_{i-N+1}, \dots, w_{i-1}\}$ as parameters. An approximation based on hyperbolic tangent functions is given as [13],

$$\begin{aligned} W'_i(t, w_k) = & \frac{1}{2} (w_{i-N} + w_{i-1}) \\ & + \sum_{k=i-N}^{i-2} (w_{k+1} - w_k) \tanh \frac{\alpha}{\delta t} (t - t_k), \end{aligned} \quad (3.5)$$

where, α is a positive constant that is used to adjust the quality of the approximation, δt is time interval duration, and t_k is the time boundary between interval k and $k + 1$ (i.e. in the case of intervals of equal length $t_k = k\delta t$). The derivation for this expression is given in the appendix 3.A. The division by δt inside the tanh is used for scaling purposes. Now, $W'_i(t, w_k)$ is treated as an artificial measured variable, measured to be 0 at the mid-points of the time intervals. With the approximation for all the process noise terms, the term $\sum_{k=i-N}^{i-1} \|\mathbf{W}_i(t_{k+\frac{\delta t}{2}})\|_{Q^{-1}}^2$ is introduced in the MHE objective function. Fig. 3.2 illustrates the model noise approximation and the measurement points discussed above.

Remark: It is to be noted that with the EKF update (3.4), S_i is expected to become a dense matrix instead of a diagonal matrix. To implement this in gPROMS, the term 4 of MHE objective function is defined in the gPROMS model itself using a new variable $J(t) = \sqrt{\|\mathbf{x}_{i-N} - \hat{\mathbf{x}}_{i-N}\|_{S^{-1}}^2}$ and J is treated as a measured variable. We then consider only one measurement of J being 0 at time $t = 0$ and the standard deviation as 1. This

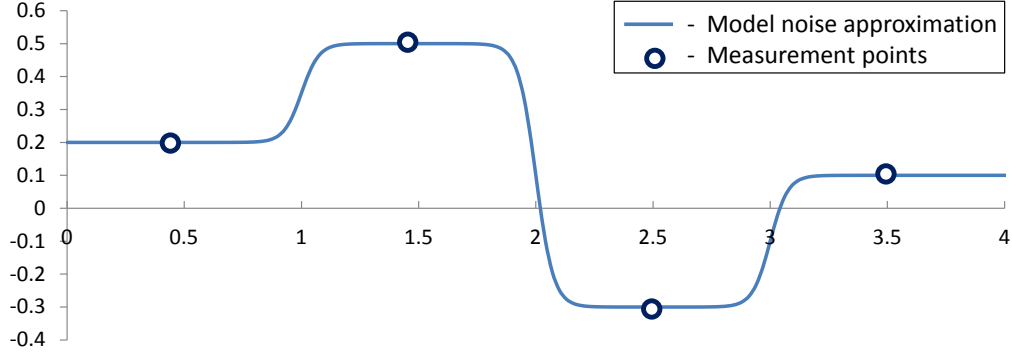


Figure 3.2: A continuous, differentiable approximation $W'_i(t, w_k)$ to the piecewise constant process noise function $W_i(t, w_k)$.

indirectly includes the original arrival cost term in the MHE objective function.

Using the above reformulations we propose the following multi-rate MHE framework for the EAF model in a DAE form,

$$\begin{aligned}
 & \min_{\mathbf{x}_0, \mathbf{w}_k} \sum_{k=i-N}^{i-1} \|\mathbf{W}'_i(t_{k+\frac{\delta t}{2}})\|_{Q^{-1}}^2 \\
 & + \sum_{\substack{k=i-N \\ k \in \mathbb{I}_F}}^i \|\bar{\mathbf{y}}_k^F - \mathbf{y}^F(t_k)\|_{(R^F)^{-1}}^2 \\
 & + \sum_{\substack{k=i-N \\ k \in \mathbb{I}_{SF}}}^i \|\bar{\mathbf{y}}_k^{SF} - \mathbf{y}^{SF}(t_k)\|_{(R^{SF})^{-1}}^2 + J(t_{i-N})^2
 \end{aligned} \tag{3.6}$$

$$\text{s.t. } \dot{\mathbf{x}}(t) = \mathbf{f}(\mathbf{x}(t), \mathbf{z}(t), \mathbf{y}(t), \mathbf{u}_k) + \mathbf{W}'_i(t) \tag{3.7}$$

$$\mathbf{0} = \mathbf{h}(\mathbf{x}(t), \mathbf{z}(t), \mathbf{y}(t), \mathbf{u}_k), \tag{3.8}$$

$$k = i - N, \dots, i - 1$$

$$\begin{aligned}
 \mathbf{W}'_i(t) = & \frac{1}{2} (\mathbf{w}_{i-N} + \mathbf{w}_{i-1} \\
 & + \sum_{k=i-N}^{i-2} (\mathbf{w}_{k+1} - \mathbf{w}_k) \tanh \frac{\alpha}{\delta t} (t - t_k))
 \end{aligned} \tag{3.9}$$

$$\mathbf{x}_{dy}(t) = \mathbf{x}(t) - \mathbf{x}\mathbf{0}_i \tag{3.10}$$

$$\mathbf{x}_{\mathbf{dy}}(0) = 0 \quad (3.11)$$

$$J(t) = \sqrt{\|\mathbf{x0}_i - \hat{\mathbf{x}}_{i-N}\|_{S_i^{-1}}^2} \quad (3.12)$$

$$\mathbf{x0}_i \in X, \mathbf{w}_{i-N} \dots \mathbf{w}_{i-1} \in Y \quad (3.13)$$

where i is the current time index at which the MHE problem is solved, $\mathbf{x0}_i$ is a vector of parameters specifying the initial conditions of the DAE system represented by \mathbf{f} and \mathbf{h} functions, \mathbf{g} represents any path constraints, $J(t)$ represents the arrival cost term, $\{\bar{\mathbf{y}}_k^F, \bar{\mathbf{y}}_k^{SF}\}$ are the measurement vectors, $\mathbf{z}(t)$ are the algebraic variables which are not measured, $\mathbf{y}(t)$ are the measured algebraic variables (both slow and fast) and $\mathbf{x}_{\mathbf{dy}}(t)$ are the artificial variables introduced to express the initial conditions of the state variables as parameters $\mathbf{x0}$. $\{\mathbf{x0}, \mathbf{w}_{i-N}, \dots, \mathbf{w}_{i-1}\}$ are the parameters to be estimated by the parameter estimation problem. Any constraints on the initial states or the model noise parameters are given by (3.13). The above multi-rate MHE formulation can be solved using any of the three direct dynamic optimization approaches. It is to be noted that uniform time intervals are used in our application. However, the methodology applies to non-uniform time intervals with a slight modification of notation regarding the interval length.

Implementation

The multi-rate MHE framework is implemented by using the following software packages: MATLAB [17], gPROMS and Microsoft Excel. The modeling and parameter estimation optimization are carried out using gPROMS/gEST. The maximum likelihood objective function of gPROMS parameter estimation is reduced to a weighted least squares problem by choosing the *constant variance* model for the measured variables. The single shooting approach is used for solving the dynamic optimization problem. The gPROMS ModelBuilder [12] environment is used to run and represent the perturbed model of the process used by MHE. Before each MHE iteration i , the input data required for the model to run are modified in gPROMS Modelbuilder man-

ually with the appropriate measurement data, the controls, guesses of the initial states and their respective bounds. The solution of an optimization run is stored in Microsoft Excel for plotting.

The linearization of the perturbed model is carried out using gLINEARIZE [12] to get the A_i and C_i matrices for the arrival cost update (3.4). Subsequently, the matrix S is updated in an input file by MATLAB. The input file is injected into the model using the *Data input Foreign Object* included in gPROMS 4.1.0. The hot-starting capability of optimisation-based activities, added to gPROMS 4.1.0 release, is used to approximate the initial Hessian matrix. A solver option in gPROMS enables storage of the Hessian at the termination of an optimization run, which is used in the subsequent run. To reduce the computational time for MHE optimization, the results from the previous MHE run are provided as initial guesses for the next run.

3.1.4 Case study

In this section, the performance of the proposed multi-rate MHE framework for the EAF model is analyzed. We demonstrate the tracking ability of the MHE estimator in the presence of poor initial guesses of the states and a plant-model mismatch. Finally, the computational performance of the strategy is discussed.

The EAF model is considered under flat bath conditions wherein almost all the scrap charge is in melt form. The conditions typically last for last 20 minutes in a batch of duration 60 minutes. In this case study we consider the first 9 minutes out of the full 20 minutes. The measurement values and the *true* states are obtained from a simulation of the original EAF model using a set of nominal inputs represented in Fig. 3.3. Table 3.1 shows the number of measured variables at different sampling times. The original DAE model is then perturbed with a parametric mismatch to generate a model to be used in the multi-rate MHE framework. The parameter names with their respective mismatches are the power factor (k_p) (+5%), the base mass transfer coefficient (k_m) (-5%) and the oxygen injection factor in the slag-metal zone

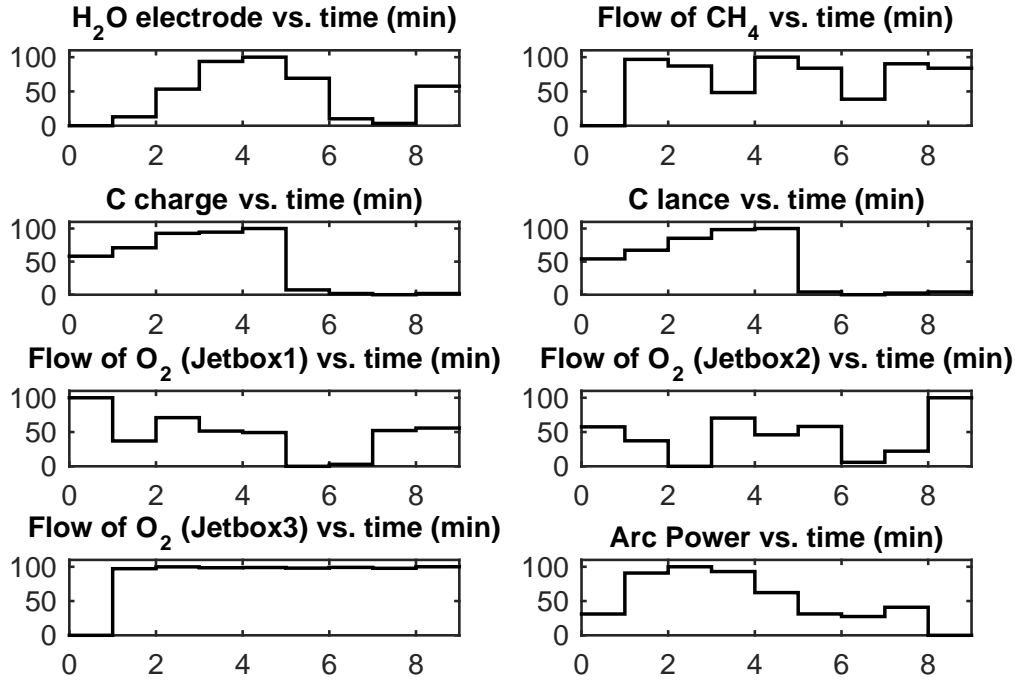


Figure 3.3: Normalized nominal input profiles.

Table 3.1: Multi-rate measurement structure for the case study.

Time (min)	0	1	2	3	4	5	6	7	8	9
Number of measured variables	6	6	6	13	6	6	6	8	6	6

$(Bias_{O_2} SM) (+5\%)$. The model equations effected by the mismatch can be found in [3].

An observability test is important before carrying out state estimation. Observability indicates the ability to fully reconstruct the internal states of the system through using the inputs and outputs of the system. For the case study, local linear observability is tested for the nonlinear model by linearizing the model using gLINEARIZE at the operating point. The Obsvf command in the Control System Toolbox of MATLAB is then used to extract the observable states [17]. By carrying out the above test, the system is found to be fully observable.

Table 3.2: State, measurement and model noise covariance values for the case study.

Q	diag(36, ..., 36)	R^{SF}	diag(9, ..., 9)
R^F	diag(9, ..., 9)	S_0	diag(16, ..., 16)

The estimator model does not know the exact initial conditions and the initial guesses of the states are generated by perturbing the *true* values by -10% . This scenario is very critical, since it reflects what happens in the real plant, where the exact initial conditions are always unknown. The temperatures of furnace roof and wall, being measured states, are fixed to their measured values. The bounds on the initial states are chosen as $\pm 30\%$ of the *true* values. The parameter α which is used to adjust quality of the model noise approximation is taken as 20. The model noise parameters are bounded as ± 1 . The values for the MHE covariance matrices (Q , R^{SF} and R^F) as well as the initial value of the arrival cost covariance (S_0) are provided in Table 3.2. The values were determined by trial and error which involved performance analysis of multiple simulations. A moving estimation horizon of 6 minutes and a total estimation horizon of 9 time steps are used. The estimates for a selection of states are compared to the actual plant values in Fig. 3.4. For EAF control applications, the molten metal temperature (MM.T) needs to be estimated accurately as it determines the tap time which is the time when the molten metal is poured out of the furnace. It is observed that the MHE is showing very good performance in tracking the *true* states and is recovering from erroneous initial states very quickly. Offsets of small magnitudes occurred for a few state variables due to the small total estimation horizon length. However, the corresponding estimated state trajectories show the general trend of convergence towards the *true* profiles.

Computational results

The MHE dynamic optimization problem consists of 935 variables and 736 equations. We used Intel® Core™ i7-3770 processor with 4 CPU cores running Windows at 3.40 GHz to perform the numerical calculations. The solution time history (in CPU

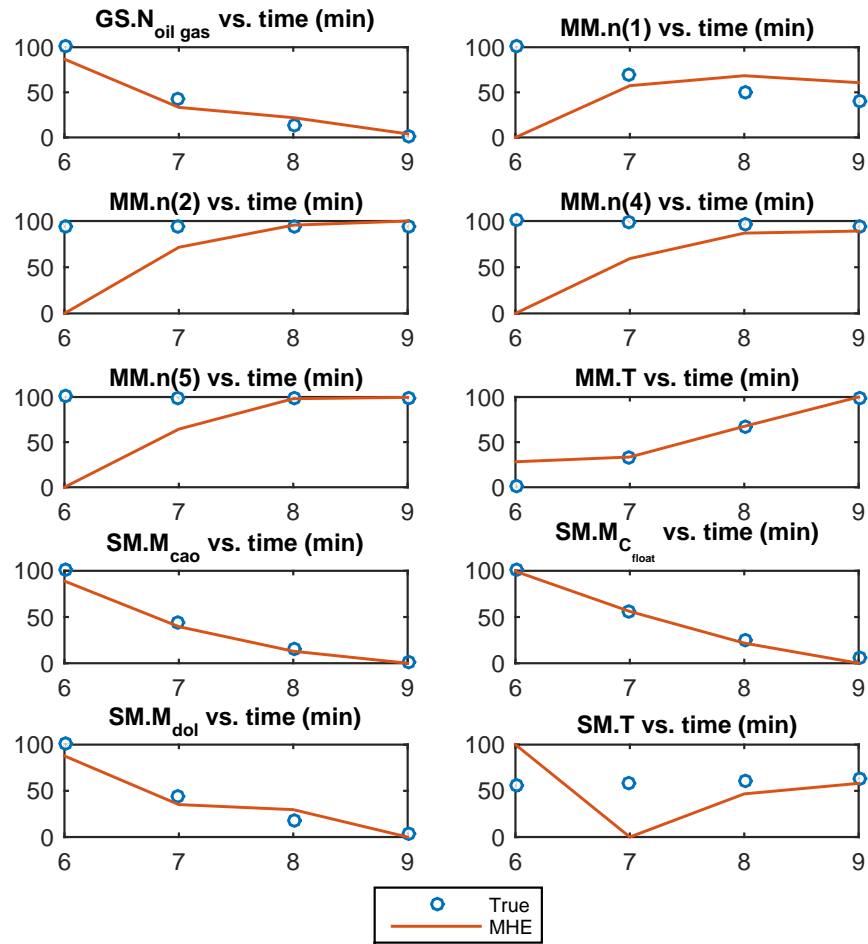


Figure 3.4: A selection of normalized state estimates compared with the real trajectory of the states. The MHE tracking ability is demonstrated in the presence of plant-model mismatch and erroneous initial conditions of the states.

seconds) of the 4 MHE runs using the default gEST solver tolerances is: 48.2, 70.1, 151 and 51. On the average the MHE problem is solved in 80 CPU seconds. This shows the MHE framework is computationally feasible.

3.1.5 Section summary

In this section, we have presented a parameter estimation based multi-rate MHE strategy that is implemented for the EAF operation. The strategy involves approximation of process noise terms with a continuous function. In addition, as MHE considers a past batch of measurements for estimation, both slow and fast measurements typically encountered in an EAF process can be included in a straightforward manner. The state estimation framework developed for the detailed first principles EAF model is suitable for applications related to large scale DAE models. We have used the very-well established sequential strategy for dynamic optimization to solve the multi-rate MHE problem. The estimator showed strong performance in tracking the internal states of the EAF model, in the presence of plant-model mismatch, improving from poor initial guesses of the states.

In the next section, we test the proposed multi-rate MHE for cases when the measurements are corrupted with Gaussian noise. The estimation framework is evaluated for the entire duration of the EAF batch. For real time applications of the framework, reducing the MHE solve time will help in the on-line implementation of the model. In the next section, we compare the simultaneous and the sequential approaches for solving the MHE optimization problems.

3.2 Multi-Rate Moving Horizon Estimation using different optimization paradigms²

The MHE problem described in the previous section can be solved using any of the three dynamic optimization approaches viz. the simultaneous approach, the sequential approach and the multiple shooting approach. In this section, we compare investigation of two DAE optimization paradigms viz. sequential and simultaneous approaches of dynamic optimization, in the solution of the MHE optimization problem (see Fig. 3.5).

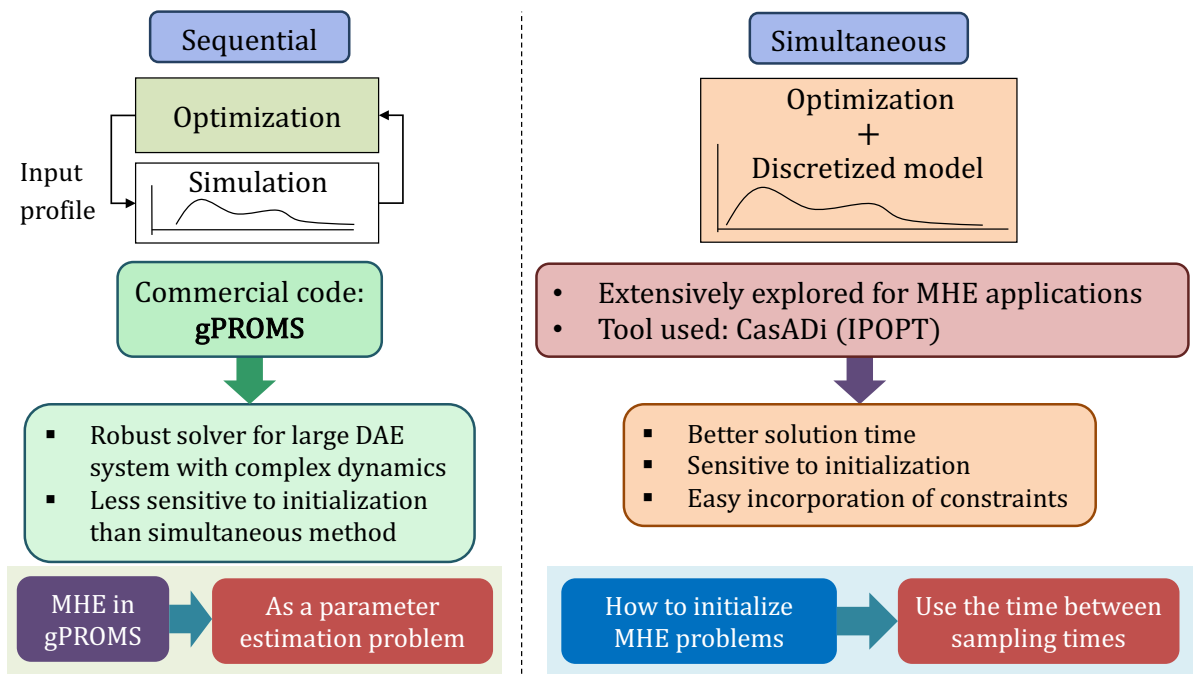


Figure 3.5: Dynamic optimization solution methods.

Key objectives of this study are, (1) to compare the two implementation strategies, and (2) to develop implementation/computation enhancement strategies to decrease online solve time for the MHE optimization problem. We present two rigorous multi-

²S. Shyamal and C.L.E. Swartz. "Multi-Rate Moving Horizon Estimation for an Electric Arc Furnace Steelmaking Process". *AICHE Annual Meeting* (2016). San Francisco, CA, USA.

rate MHE solution strategies for the EAF process based on different DAE optimization paradigms. We also provide an initialization scheme for solving the online MHE problem.

We again consider the EAF model presented in section 1 of this chapter which contained 29 differential states and 518 algebraic variables. As the 29th state in the prior model took values which were very small (close to 1.0×10^{-13}), it was removed from the model and replaced with a constant small number.

3.2.1 Sequential approach

A novel approach to do moving horizon state estimation (MHE) using the sequential method of dynamic optimization was proposed in the previous section. A key feature of this approach involves continuous approximation of discrete process noise terms. The implementation using the gPROMS modeling language is adopted here for studying the sequential approach. Instead of carrying out the MHE optimizations manually, a new framework was developed using MATLAB and gO:RUN (see Fig. (3.6)). Two models are used in the state estimation implementation. Both models are built in gPROMS. The original model (plant model) mimics the plant and another model (estimator model) with perturbed parameters is used for estimation. The plant model runs in parallel with the estimator model. The plant model is integrated using gO:Run (with gSIM_5 add-on) to provide the measurements to the estimator. MHE calculates the state estimates, using the gPROMS model with perturbed parameters, in the gO:Run (with gEST_5 add-on) environment. The states estimates are then obtained and stored for plotting. The data flow and calling of gO:RUN instances are carried using MATLAB scripts. The implementation for sequential approach is summarized in the left-hand block in Fig. 3.7.

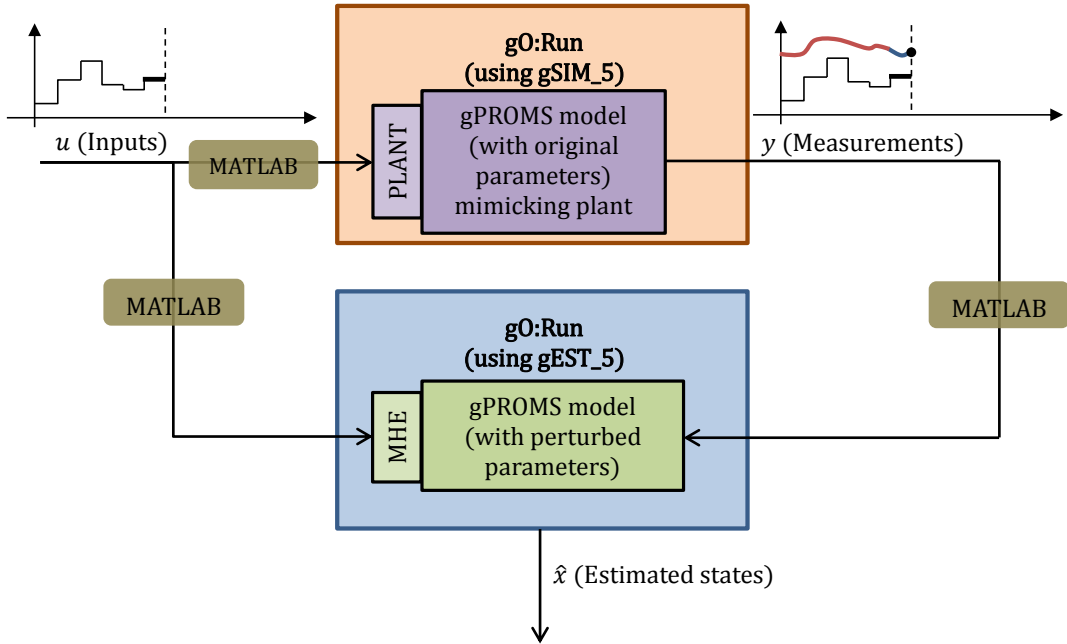


Figure 3.6: MHE implementation for sequential approach using gO:RUN and MATLAB.

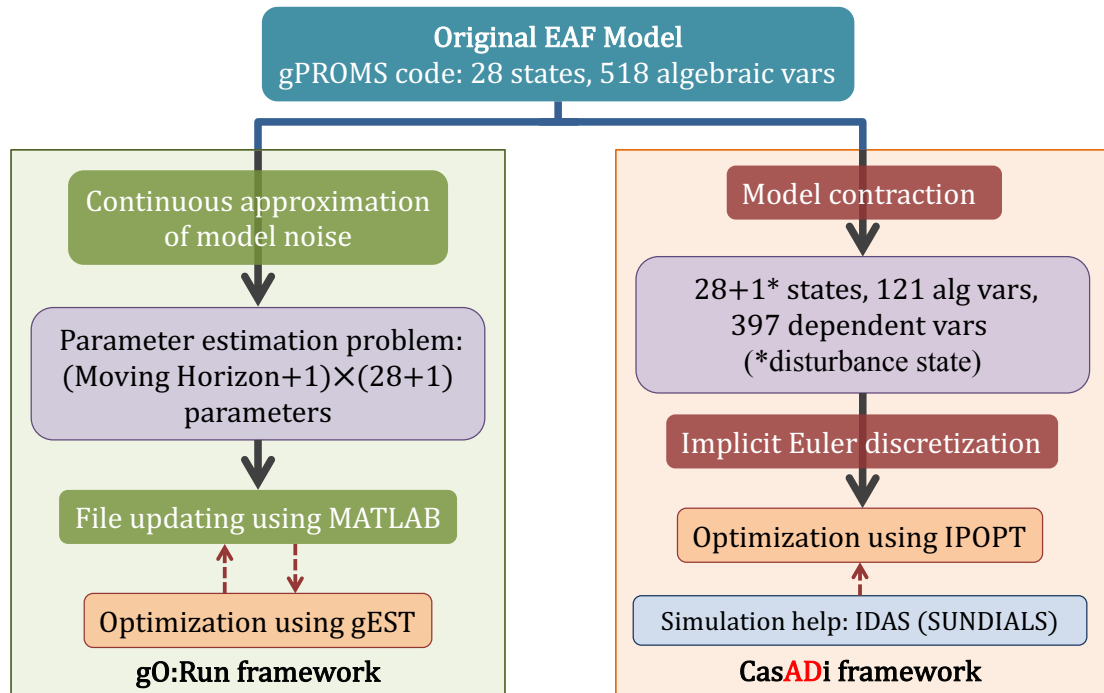


Figure 3.7: Implementation of MHE using both the dynamic optimization approaches.

3.2.2 Simultaneous approach

The multi-rate MHE optimization problem for a discrete-time nonlinear system observable for the state profile is given as:

$$\begin{aligned} \min_{\mathbf{x}_{i-N}, \mathbf{w}_k} & \sum_{k=i-N}^{i-1} \|\mathbf{w}_k\|_{Q^{-1}}^2 + \sum_{\substack{k=i-N \\ k \in \mathbb{I}_F}}^i \|\mathbf{v}_k^F\|_{(R^F)^{-1}}^2 \\ & + \sum_{\substack{k=i-N \\ k \in \mathbb{I}_{SF}}}^i \|\mathbf{v}_k^{SF}\|_{(R^{SF})^{-1}}^2 + \|\mathbf{x}_{i-N} - \hat{\mathbf{x}}_{i-N}\|_{S_i^{-1}}^2 \end{aligned} \quad (3.14)$$

$$\text{s.t. } \mathbf{x}_{k+1} = \mathbf{f}_k(\mathbf{x}_k, \mathbf{u}_k) + \mathbf{w}_k, \quad k = i-N, \dots, i-1 \quad (3.15)$$

$$\mathbf{y}_k^F = \mathbf{h}_k^F(\mathbf{x}_k) + \mathbf{v}_k^F, \quad k \in \mathbb{I}_F \quad (3.16)$$

$$\mathbf{y}_k^{SF} = \mathbf{h}_k^{SF}(\mathbf{x}_k) + \mathbf{v}_k^{SF}, \quad k \in \mathbb{I}_{SF} \quad (3.17)$$

$$\mathbf{x}^{LB} \leq \mathbf{x}_k \leq \mathbf{x}^{UB}, \quad (3.18)$$

$$\mathbf{w}^{LB} \leq \mathbf{w}_k \leq \mathbf{w}^{UB}. \quad (3.19)$$

Here, \mathbf{w}_k is included to represent the process noise (i.e. the model uncertainty). $\hat{\mathbf{x}}_{i-N}$ is the *a priori* estimate of the state at the starting point of the moving window. Given the states \mathbf{x}_k and the known inputs \mathbf{u}_k , $\mathbf{f}_k(\cdot)$ integrates the process model forward over one sample time. The measurement functions $\mathbf{h}_k^F(\cdot)$ and $\mathbf{h}_k^{SF}(\cdot)$ map the state variables \mathbf{x}_k to the measurements \mathbf{y}_k^F and \mathbf{y}_k^{SF} respectively. The measurement noise terms corresponding to \mathbf{y}_k^F and \mathbf{y}_k^{SF} are represented respectively as \mathbf{v}_k^F and \mathbf{v}_k^{SF} . Equation (3.15) represents a discretized form of the EAF process model. We note here that (3.15) represents a closed form solution of the DAE system which is not always possible to get. Here we view it only in an abstract form and thus the algebraic variables/equations are eliminated [18]. The covariance matrices of appropriate dimensions for the model noise, measurement noise and for the arrival cost are represented here as Q , R^F , R^{SF} and S_i . The state constraints are provided by the lower bound \mathbf{x}^{LB} and the upper bound \mathbf{x}^{UB} . The model noise \mathbf{w}_k is allowed to move between lower and upper bounds

of \mathbf{w}^{LB} and \mathbf{w}^{UB} respectively. The estimate of current states \mathbf{x}_i are obtained from the solution of optimization problem stated above.

The least-squares objective function of the multi-rate MHE scheme (3.14) comprises four terms. The first three terms are a weighted minimization of model and measurement errors over a moving time horizon of length N . The fourth term in (3.14) is the arrival cost that represents the measurement information not included in the moving window. The covariance S_i is generally updated when the next MHE problem is formulated, to S_{i+1} using the current solution. However, the covariance update is not necessary when the system is strongly observable [19]. An extended Kalman filter covariance propagation equation is commonly used [16],

$$S_{i+1} = Q + A_i [S_i - S_i C_i^T (R + C_i S_i C_i^T)^{-1} C_i S_i] A_i^{-1} \quad (3.20)$$

where A_i and C_i are matrices in the linearized model,

$$\begin{aligned} \mathbf{x}_{i+1} &= A_i \mathbf{x}_i + B_i \mathbf{u}_i \\ \mathbf{y}_i &= C_i \mathbf{x}_i + D_i \mathbf{u}_i. \end{aligned} \quad (3.21)$$

We have suppressed the superscripts ‘F’ and ‘SF’ for R and \mathbf{y} in (3.20) for ease of readability. However, appropriate dimensions for R and correct measurement functions ($\mathbf{h}_k^F(\cdot)$ or $\mathbf{h}_k^{SF}(\cdot)$) are to be considered when carrying out EKF update (3.20). The solutions of the current MHE optimization problem (3.14) are represented as \mathbf{x}_{i-N}^* and \mathbf{w}_{i-N}^* . The covariance S_{i+1} can be computed using other filters as well, such as the unscented Kalman filter [20] and constrained particle filter [21]. Note that for time steps t_i with $i \leq N$, new measurements are added to the past history in consideration without dropping the oldest one, and also the initial state covariance is not changed.

Novel initialization scheme for MHE

To carry out MHE using the simultaneous approach, we developed a novel initialization scheme for MHE. The scheme is based on a background solves to improve solution time.

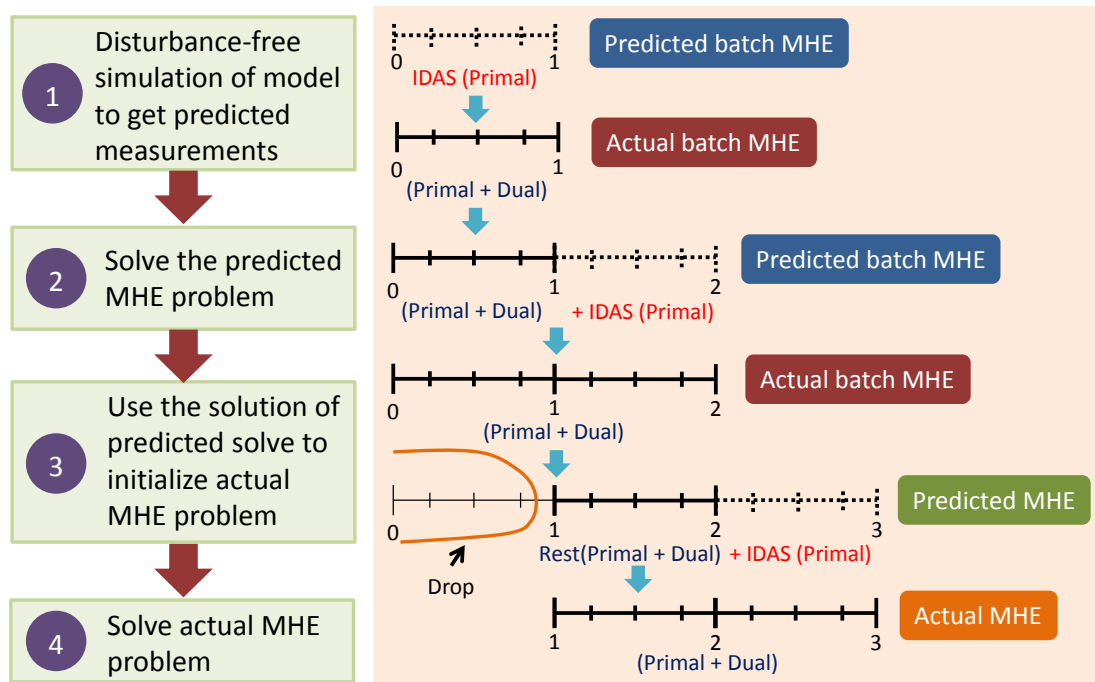


Figure 3.8: Novel initialization scheme for MHE.

Suppose at time instant t_k , we have the following information: the current state estimate \mathbf{x}_k and input \mathbf{u}_k . We have suppressed the superscripts used for representing slow and fast measurements for ease of readability. We refer to the time gap between consecutive sampling times of frequent measurements as 'background' time. We introduce an initialization scheme using the given information at time t_k for obtaining fast optimal solutions of MHE problems:

In background mode, between t_k and t_{k+1} :

- **Step 1:** Use \mathbf{x}_k and \mathbf{u}_k to generate the predicted future measurements $\bar{\mathbf{y}}_{k+1}$

though a disturbance-free ($\mathbf{w}_k = 0$) model simulation $\bar{\mathbf{x}}_{k+1} = \mathbf{f}(\mathbf{x}_k, \mathbf{u}_k)$ and $\bar{\mathbf{y}}_{k+1} = \mathbf{h}(\bar{\mathbf{x}}_{k+1})$. We employ IDAS (part of the SUNDIALS [22] suite of solvers) for carrying out the simulation. The forward simulation provides the initial guesses for the primal values associated with the new terminal stage.

- **Step 2:** Construct and solve the predicted MHE problem using $\bar{\mathbf{y}}_{k+1}$ to get predicted state estimates $\tilde{\mathbf{x}}_{k+1}$. Retain the problem solution \tilde{s}_k^{mhe} (both primal and dual).

On-line, at t_{k+1} :

- **Step 3:** Receive the *true* measurements y_{k+1} from the plant and initialize the *true* MHE optimization problem by employing \tilde{s}_k^{mhe} as initial guesses.
- **Step 4:** Solve the actual MHE optimization problem to compute true state estimates \mathbf{x}_{k+1} .

The initialization scheme is illustrated in Fig. 3.8 for MHE solves starting at time $t=0$. The MHE horizon is considered as 2 in the figure for illustration. The MHE initialization strategy is particularly suitable for applications incorporating large-scale differential-algebraic equation (DAE) systems.

MHE is implemented for a discretized model using the Python front end of CasADi (see Fig. 3.7). The variable space of the EAF model written in gPROMS is first reduced in CasADi to get a reduced DAE system. CasADi was then employed to eliminate a subset of the algebraic variables and equations by transforming them into dependent variables defined by explicit expressions containing only the differential and algebraic variables. The model reduction exercise, which removed a significant amount of complexity, reduced the variable count to 28 states and 121 algebraic variables. Next, the dynamic optimization problems are solved by employing the simultaneous solution approach. We set 7 finite elements per control stage to carry out time discretization for MHE. Using the simultaneous approach, the optimal control problems are expressed

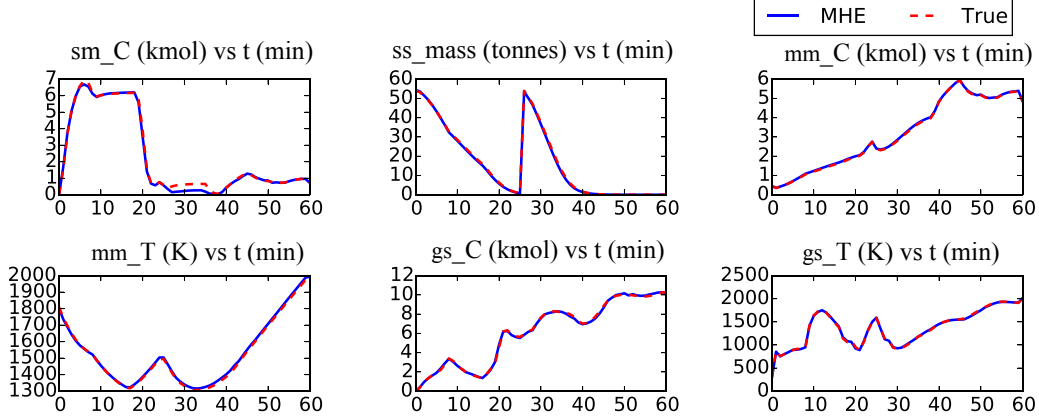


Figure 3.9: State estimates for the case study with respect to time (in minutes). sm_C: Carbon in slag-metal zone, ss_mass: Solid scrap mass, mm_C: Carbon in molten metal zone, mm_T: Temperature of molten metal, gs_C: Carbon in gas zone, gs_T: Temperature of gas.

as large-scale sparse NLP problems, which are then solved with the interior-point solver IPOPT [23] using the linear solver MA27.

3.2.3 Case Study

The case study is conducted using a first-principles dynamic EAF model developed in the previous section, in which the EAF is partitioned into four zones (gas, solid scrap, slag-metal and molten metal). The measurements, their variances and its multi-rate structure are given in Table 3.4 and 3.5. In the case study, the true initial conditions are perturbed by adding Gaussian noise with 1% relative variance. A subset of the *true* and estimated state variables is plotted with respect to time in Fig. 3.9.

The computational performance of the MHE using two different optimization strategies is illustrated here. An Intel Core i7-3770 processor with 4 CPU cores running Windows 7 at 3.40 GHz was used for all the numerical computations. The computation times for solving the MHE problems using the sequential method with g0:Run/gEST is shown in Fig. 3.10. The average CPU time required is 39 seconds. The CPU times required to solve the multi-rate MHE problems when the simultaneous

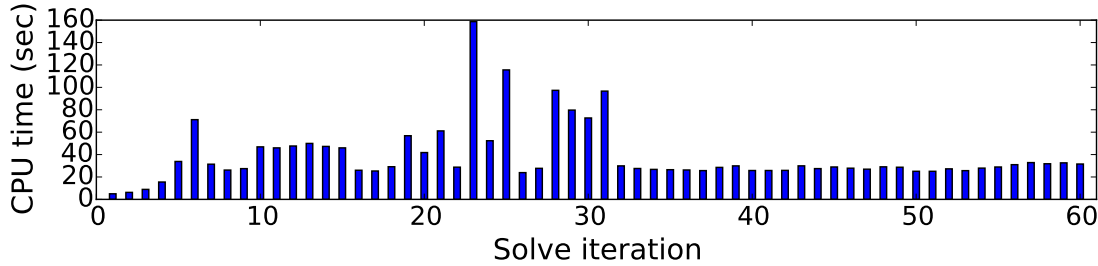


Figure 3.10: Solution times for MHE problems with horizons of $N = 6$ time steps using the sequential approach.

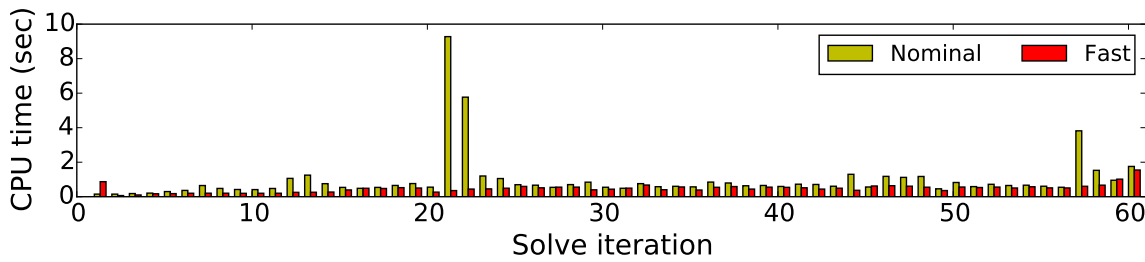


Figure 3.11: Solution times for MHE problems with horizons of $N = 6$ time steps using the simultaneous approach. The solve time denoted by ‘fast’ represents computational time when the proposed initialization scheme is used. ‘Nominal’ represents the MHE solves carried out without the use of the proposed initialization scheme.

method is employed, using the proposed initialization (fMHE) and without using the scheme (nMHE), is shown in Fig. 3.11. We observe that the initialization scheme is able to reduce the computation time for the MHE significantly. The average CPU time required to solve the fMHE and nMHE problems are 1 and 0.5 seconds respectively. There is 50% decrease in MHE on-line CPU solve time when the proposed initialization scheme is used. Furthermore, computational times required for background MHE solves are well within 1 minute. On comparing the simultaneous to the sequential implementation, the simultaneous approach (using the novel initialization scheme) takes 98.7% less time to solve the MHE problem. In the next section, we describe the MHE-based decision support tool for the operators of EAFs.

3.3 Optimization-based Online Decision Support Tool for Electric Arc Furnace Operation³

The EAF steelmaking batch process is highly energy intensive and involves a low level of automation. The decisions associated with the amount and timing of injected inputs depend heavily on the EAF operators. Although the operators' practical experience is crucial in running the EAF, the important multivariable interactions and subtle relationships are easily overlooked. In this section, a multi-rate moving horizon estimator (MHE) is coupled with an economics-based dynamic optimizer to form an online decision support tool (DST). The tool is able to reconstruct the states and provide optimal decisions to operators in less than 18 CPU seconds on average despite the use of a highly nonlinear large-scale EAF model. This framework is developed using entirely open source tools to have a high appeal to industrial practitioners. A case study is presented which demonstrates a 2.4 % increase in profit through the use of the DST.

3.3.1 Introduction

EAFs are typically operated with a low level of automation and a lot of operator involvement. Although the experience-based knowledge of operators is useful for the EAF operation, this understanding can be limited due to the multivariable nature of the complex process and underlying relationships which may be overlooked. Subsequently, process operating procedures are based upon what has worked well in the past in most situations. Research efforts have been directed towards developing a detailed dynamic mathematical model to describe the melting process, chemical changes and account for reagent and energy additions. The model can then be used within a mathematical optimization procedure to determine the optimal trajectories for the process inputs. However, a characteristic of this process that makes the online

³S. Shyamal and C.L.E. Swartz. "Optimization-based Online Decision Support Tool for Electric Arc Furnace Operation." . *IFAC-PapersOnLine* 50, no. 1, 10784-10789 (2017).

application of optimization more complex, is the small number of online process measurements from which it is difficult to infer the current state of the process. Billings et al. [1] applied the extended Kalman filter (EKF) to reconstruct the states for the refining stage of EAF operation but the application model contained 4 states, which is too few to capture the detailed process dynamics. Ghobara [3] implemented a multi-rate version of EKF to handle varying sampling rates of the measurements taken during a typical heat.

Of the many reported tools for state estimation, moving horizon estimation (MHE) has become quite popular [4] due to its constraint handling ability and the use of computationally efficient numerical optimization algorithms. MHE involves solving a nonlinear dynamic optimization problem subject to the nonlinear system under consideration and some other relevant constraints. The use of a finite set of past available measurements by MHE to reconstruct the full state vector keeps the optimization problem numerically tractable. Although for batch processes, an expanding horizon for MHE would minimize loss of information due to clipping, it would increase the on-line computational burden leading to a delayed feedback action. The finite size window of measurements also provides a natural framework to include measurements with different sampling rates. Shyamal and Swartz [24] demonstrated a parameter estimation based multi-rate MHE strategy for a short simulation horizon of an EAF heat. The MHE application was then implemented for the entire duration of the EAF batch by Shyamal and Swartz [25].

In this work, we extend the results of [25] by developing an online decision support tool (DST) which uses the multi-rate MHE to provide the state knowledge to an economics-based optimizer for improved performance. Objectives other than economics have also been reported in the literature, such as minimizing power [26], model predictive control's (MPC) set-point tracking objective function [27] to determine optimal inputs, and a weighted function to minimize the offgas CO content, the final FeO and the final time [28]. MacRosty and Swartz [29] showed that a dynamic

optimization procedure can effectively maximize the profit while considering the trade-offs between the process inputs and processing time. To solve the optimization problem, they employed a sequential approach which can be time-consuming particularly when repeated optimizations need to be carried out involving a large-scale differential-algebraic equation (DAE) model [30]. On the other hand, the simultaneous approach for dynamic optimization can become quite useful for real time applications such as an online DST. The simultaneous approach using Implicit Euler discretization is employed in this work for both the estimator and the shrinking horizon optimizer to achieve a reasonable CPU solve time. The first-principles based dynamic model developed in MacRosty and Swartz [14] is utilized to develop the online DST for the EAF operators. The DST framework involves the state estimator running in parallel with the plant while the shrinking horizon optimizer can be called multiple times during the batch duration as desired by the operators. The potential economic improvement achieved though the use of the DST is illustrated through an application to a case study.

3.3.2 EAF model overview

We consider the EAF model presented in the previous section of this chapter which contained 28 states and 518 algebraic variables. In this section, we are using the same model of Section 3.2 to carry out the case study presented in the last subsection.

3.3.3 Dynamic Optimization and MHE based on-line Decision Support Tool

In this section, we describe the proposed on-line DST for EAF operation. A key feature of the DST involves a real-time dynamic optimization implementation wherein the model runs in parallel with the plant as shown in Fig. 3.12. The model states at any point in the heat reflect the actual plant inputs up to that point. The state

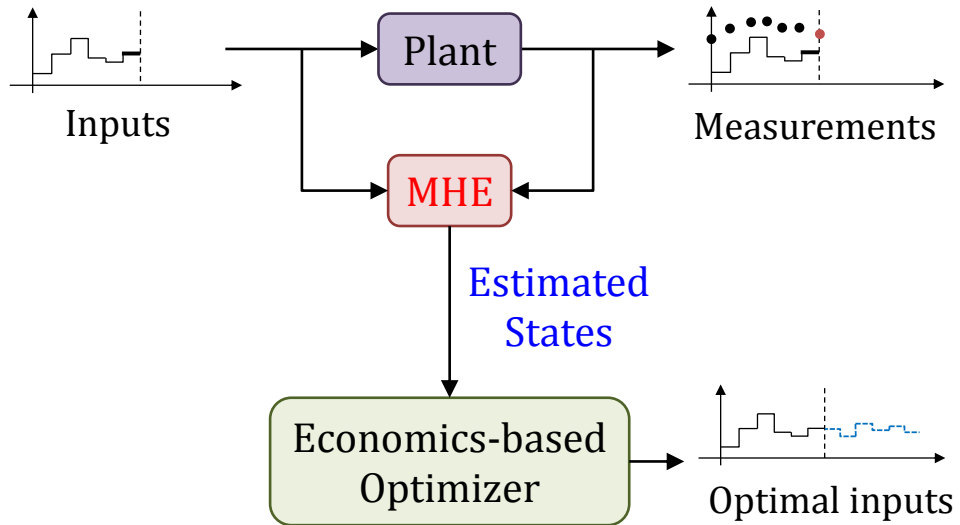


Figure 3.12: Online decision support tool for EAF operation

variables are inferred on the basis of plant measurements using state estimation. The reason for using a state estimator is to ensure that the unknown initial conditions and disturbances during the batch operation are handled by the model in real-time. Once the state estimates are obtained from MHE, they are sent to a shrinking horizon optimizer which calculates an economically optimal sequence of control variables. The EAF operators can execute the optimizer during the heat whenever they need a recommendation with regard to the optimal input. However, the MHE will automatically be running every 1 minute to calculate the state estimates by minimizing the differences between model predictions and measurements. Furthermore, the operators will access only the final computed optimal inputs, with the other internals of the DST hidden from them.

The optimization procedure in the DST is computationally challenging because real-time solutions of the dynamic optimization problems are needed to avoid delays in passing decision support to the operators. Faster running of the models is achieved through the use of full discretization approach to solve the infinite dimensional problems. The approach converts the problem into a general nonlinear program (NLP) in

purely algebraic form. Quick solutions of the NLP problems are obtained by initializing both the primal and dual variables and using an interior-point solver. The details of formulation and solution strategy are presented in the subsequent subsections.

Shrinking Horizon Dynamic Optimization

The EAF dynamic optimization problem considered here maximizes the profit per batch, in dollars. Based on the state estimates received from the multi-rate MHE (discussed in next subsection), a shrinking horizon problem with t_f as the fixed final duration of the heat, is formulated. The DAE model equations $\mathbf{h}(\cdot)$ appear in a discretized form as equality constraints. At the current time t_i , the optimization problem under consideration is given by,

$$\begin{aligned} \max_{u(t)} \quad & c_0 M_{steel}(t_f) - \left(c_1 \int_{t_i}^{t_f} P dt + c_2 \int_{t_i}^{t_f} F_{CH_4,brnr} dt \right. \\ & \left. + c_3 \int_{t_i}^{t_f} (F_{O_2,Jetbox1} + F_{O_2,Jetbox2} + F_{O_2,Jetbox3}) dt \right) \end{aligned} \quad (3.22)$$

subject to

Model equations:

$$\mathbf{0} = \mathbf{h}(\dot{\mathbf{x}}(t), \mathbf{x}(t), \mathbf{u}(t), \mathbf{y}(t), t) \quad (3.23)$$

Input constraints:

$$P^{min}(t) \leq P \leq P^{max}(t) \quad (3.24)$$

$$F_k^{min}(t) \leq F_k \leq F_k^{max}(t) \quad (3.25)$$

where P is the electrical arc power, $F_{CH_4,brnr}$ is the flow rate of natural gas from the burner, and $F_{O_2,Jetbox1}$, $F_{O_2,Jetbox2}$ and $F_{O_2,Jetbox3}$ are oxygen flow rates from Jetboxes 1,2, and 3 respectively. $M_{steel}(t_f)$ is the mass of liquid steel at the end of the batch and c_k ($k = 0, 1, 2, 3$) is the associated unit cost of each component. The decision variables

$\mathbf{u}(t)$ for the optimization problem , consisting of P , $F_{CH_4,brnr}$, $F_{O_2,Jetbox1}$, $F_{O_2,Jetbox2}$, and $F_{O_2,Jetbox3}$, are taken as piecewise constants. \mathbf{x} and \mathbf{y} are the differential and algebraic variables of the process model respectively. The four flow rates are represented as F_k in concise form. The input constraints bound the control variables between upper (P^{max}, F_k^{max}) and lower bounds (P^{min}, F_k^{min}) to ensure that the power addition and the flows are allowed to move within realistic bounds. The optimal sequence of the inputs calculated from the above problem provides the decision support to the operators.

Multi-rate MHE

EAF process operation is significantly complex, and subject to fluctuations due to frequent material additions to the furnace. As a first principles model constitutes an approximation to reality, plant-model mismatch and modeling errors are inevitably present. There are some unknown disturbances as well during the batch operation. The estimation strategy introduced here uses process noise terms to account for uncertainties. Further issues that need to be addressed are the limited availability of measurements, and their availability at different rates. The multi-rate MHE formulation is adopted here to take advantage of both fast and slow measurements.

Consider as a reference point time instant t_i , where i is the current sampling index and a past sequence of inputs and measurements is available. The multi-rate MHE formulation includes measurements with multiple sampling rates. The infrequent measurements related to the molten metal and slag zones are simply introduced in their appropriate locations in the moving horizon window of length N time intervals. Assuming the slow measurements are placed at the sampling times of the fast measurements without any delays, the vector of only fast measurements is defined as \mathbf{y}_k^F and the vector containing both the slow and fast measurements is defined as \mathbf{y}_k^{SF} . The measurement distribution in a moving window can be given as, for example, $\mathbf{Y}_i = \{\mathbf{y}_{i-N}^F, \mathbf{y}_{i-N+1}^{SF}, \mathbf{y}_{i-N+2}^F, \dots, \mathbf{y}_i^F\}$, where the measurement set at time t_{i-N+1} contains both the slow and fast measurements. The example can be adapted for different

structures of \mathbf{Y}_i . At the next sampling time, when a new measurement arrives it is included in the horizon window, and the oldest measurement is dropped.

The multi-rate MHE problem for a nonlinear system which is observable along the state trajectories takes the following general form:

$$\begin{aligned} \min_{\mathbf{x}_{i-N}, \mathbf{w}_k} & \sum_{k=i-N}^{i-1} \|\mathbf{w}_k\|_Q^{-1} + \sum_{\substack{k=i-N \\ k \in \mathbb{I}_F}}^i \|\mathbf{v}_k^F\|_{(R^F)^{-1}}^2 \\ & + \sum_{\substack{k=i-N \\ k \in \mathbb{I}_{SF}}}^i \|\mathbf{v}_k^{SF}\|_{(R^{SF})^{-1}}^2 + \|\mathbf{x}_{i-N} - \hat{\mathbf{x}}_{i-N}\|_{S_i^{-1}}^2 \end{aligned} \quad (3.26)$$

$$\text{s.t. } \mathbf{x}_{k+1} = \mathbf{f}(\mathbf{x}_k, \mathbf{u}_k) + \mathbf{w}_k, \quad k = i-N, \dots, i-1 \quad (3.27)$$

$$\mathbf{y}_k^F = \mathbf{h}^F(\mathbf{x}_k) + \mathbf{v}_k^F, \quad k \in \mathbb{I}_F \quad (3.28)$$

$$\mathbf{y}_k^{SF} = \mathbf{h}^{SF}(\mathbf{x}_k) + \mathbf{v}_k^{SF}, \quad k \in \mathbb{I}_{SF} \quad (3.29)$$

$$\mathbf{x}^{LB} \leq \mathbf{x}_k \leq \mathbf{x}^{UB}, \quad (3.30)$$

where \mathbf{w}_k is a piecewise constant noise term introduced to model the process noise (i.e. the model uncertainty) and $\hat{\mathbf{x}}_{i-N}$ is an estimate for the state at the beginning of the horizon. \mathbf{f} is the system function, \mathbf{x}_k denotes the state vector and the control input is represented as \mathbf{u}_k . $\{\mathbf{h}^F, \mathbf{h}^{SF}\}$ are the measurement functions that map the system state to \mathbf{y}_k^F and \mathbf{y}_k^{SF} respectively. \mathbf{v}_k^F and \mathbf{v}_k^{SF} are the measurement noise terms. The implicit Euler method is employed to generate the discretized form of model (3.27) from the DAE model. Q , R^F , R^{SF} and S_i are the covariance matrices (of appropriate dimensions) for the model noise, measurement noise and for the arrival cost respectively. \mathbf{x}^{LB} and \mathbf{x}^{UB} represent lower and upper bounds respectively on the state variables.

The cost function (3.26) contains four terms of which the first three are weighted minimization of errors over a time horizon N . The fourth term of (3.26), the arrival

cost, summarizes the previous measurement data not considered in the moving horizon window. The weighing matrix S_i is updated to S_{i+1} for the next MHE run using the solution of the currently solved MHE optimization problem. An EKF update is used in general [16],

$$S_{i+1} = Q + A_i[S_i - S_i C_i^T(R + C_i S_i C_i^T)^{-1} C_i S_i] A_i^{-1} \quad (3.31)$$

where $A_i = \nabla_x \mathbf{f}(\mathbf{x}_{i-N}^*, \mathbf{u}_{i-N}, \mathbf{w}_{i-N}^*)$ and $C_i = \nabla_y \mathbf{h}(\mathbf{x}_{i-N}^*)$. \mathbf{x}_{i-N}^* and \mathbf{w}_{i-N}^* are solution vectors of the MHE optimization problem (3.26). It is to be noted that for time step $t_i \leq N$, a constant initial state covariance matrix is used, and the past window of measurements is allowed to grow without dropping any measurements.

DST Implementation

The DST is implemented for a discretized model in CasADi using the Python interface. For time discretization we choose 7 and 4 finite elements per time step (1 minute for our case), with the backward Euler scheme, for the multi-rate MHE and the shrinking horizon dynamic optimization respectively. IPOPT [23] using the linear solver MA27 is employed to solve the sparse NLP problem thus obtained. The optimal sequence of inputs computed by the DST is applied on the plant model to get measurements until the shrinking horizon optimizer is called again. Plant and model simulations, required for measurement generation and forward integration, are performed with IDAS (part of the SUNDIALS [22] suite of solvers). To find a good starting point to solve the MHE and the shrinking horizon optimization problem, the primal and the dual variable values are extracted from the respective previous optimization solves. The set of values is truncated by dropping the first time interval values in the case of MHE. A forward simulation is also carried out to obtain an initial guess for the MHE primal variables associated with the new terminal interval. For the shrinking horizon optimizer, the appropriate number of the values is removed for time intervals starting from the first one.

The implementation involves a plant-model mismatch created by decreasing a power factor parameter k_p by 10% in the model. This mismatch significantly decreases the amount of energy delivered to the scrap charge due to the arc power input. The model equations where k_p appears can be found in [3]. The impact of unmeasured disturbances on the model due to the mismatch is mitigated by augmenting the system state with an integrated disturbance \mathbf{d}_k , driven by white noise \mathbf{w}_{dk} . We implement the state estimator using the augmented system model

$$\begin{aligned}\mathbf{x}_{k+1} &= \mathbf{f}(\mathbf{x}_k, \mathbf{u}_k) + \mathbf{B}_d \mathbf{d}_k + \mathbf{w}_k \\ \mathbf{y}_k &= \mathbf{h}(\mathbf{x}_k) + \mathbf{v}_k \\ \mathbf{d}_{k+1} &= \mathbf{d}_k + \mathbf{w}_{dk}, \quad \mathbf{w}_{dk} \sim \mathcal{N}(0, \mathbf{Q}_d)\end{aligned}\tag{3.32}$$

where \mathbf{B}_d is used to adjust the effect of disturbance state on the system and \mathbf{Q}_d is the covariance of \mathbf{w}_{dk} . For the case study conducted, the disturbance state is implemented on the state variable representing moles of manganese in the slag zone model.

3.3.4 Case study

In this section, a case study is presented to demonstrate the economic benefit due to the DST implementation in the presence of plant-model mismatch. The tracking ability of the multi-rate MHE is also analyzed. Finally, the computational performance of the DST is discussed.

The EAF heat considered here is of duration 60 minutes with 2 scrap charges. The economics based optimization for the plant gives an objective function value of 100 (normalized \$profit/batch). The value is represented as the *theoretical* best in Table 3.3. The optimization is then conducted for the model with perfect initial state knowledge and the solution is implemented on the plant to obtain an objective function value of 95.39. The *nominal* solution of 95.39 is expected because less percentage of arc power

Table 3.3: Result comparison for the case study.

	Theoretical	Nominal	Using DST
Profit [\$/batch]	100	95.39	97.67

Table 3.4: Measurements for the case study.

Measurement	Sampling Time	Variance
Off-gas compositions (CO, CO ₂ , O ₂ , H ₂)	Every 1 min	0.01
T _{roof} , T _{wall}	Every 1 min	3
Slag compositions (FeO, Al ₂ O ₃ , SiO ₂ , MgO, CaO)	43rd min	0.1
Molten-metal temperature	43rd & 47th min	5
Molten-metal carbon content	43rd & 47th min	0.01

is used, in melting the scrap charge, due to the plant-model mismatch. To carry out the analysis for DST, the measurement values are corrupted with Gaussian zero mean noise. The measurements considered for the estimation and their corresponding variance values are given in Table 3.4. Table 3.5 shows the number of measured variables at different sampling times. Observability of the system is analyzed by checking the observability metric value, as defined in [31], at every time step. The system is found to be full observable with the lowest metric value as 7.0×10^{-7} . The multi-rate MHE is set up using perfect initial state knowledge and a estimation horizon of 6 minutes. The covariances S_0 and Q are determined by trial and error which involved analysis of multiple simulations. Lower and upper bounds are imposed for the states, the algebraic variables and the model noise. The estimated and true profiles for a selection of states is presented in Fig. 3.13. It is observed that the MHE is showing very good performance in estimating the true states despite the adverse effects of plant-model mismatch and measurement noise. The strong convergence property of the MHE is reflected directly on the profit calculated using the DST. This is attributed to the fact

Table 3.5: Multi-rate measurement structure for the case study.

Time (min)	0 ... 42	43	44 ... 46	47	48 ... 60
Number of measured variables	6	13	6	8	6

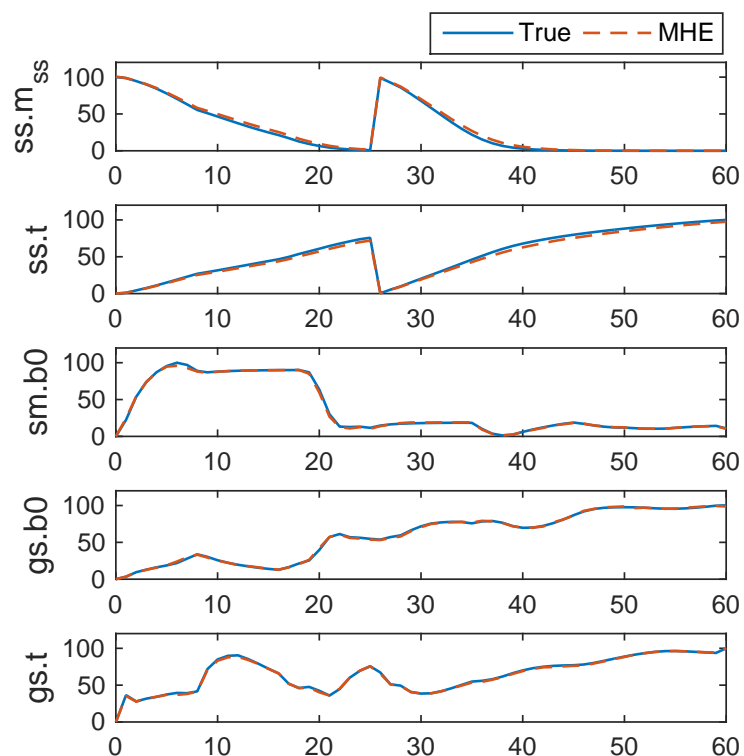


Figure 3.13: State estimates with respect to time (in minutes).

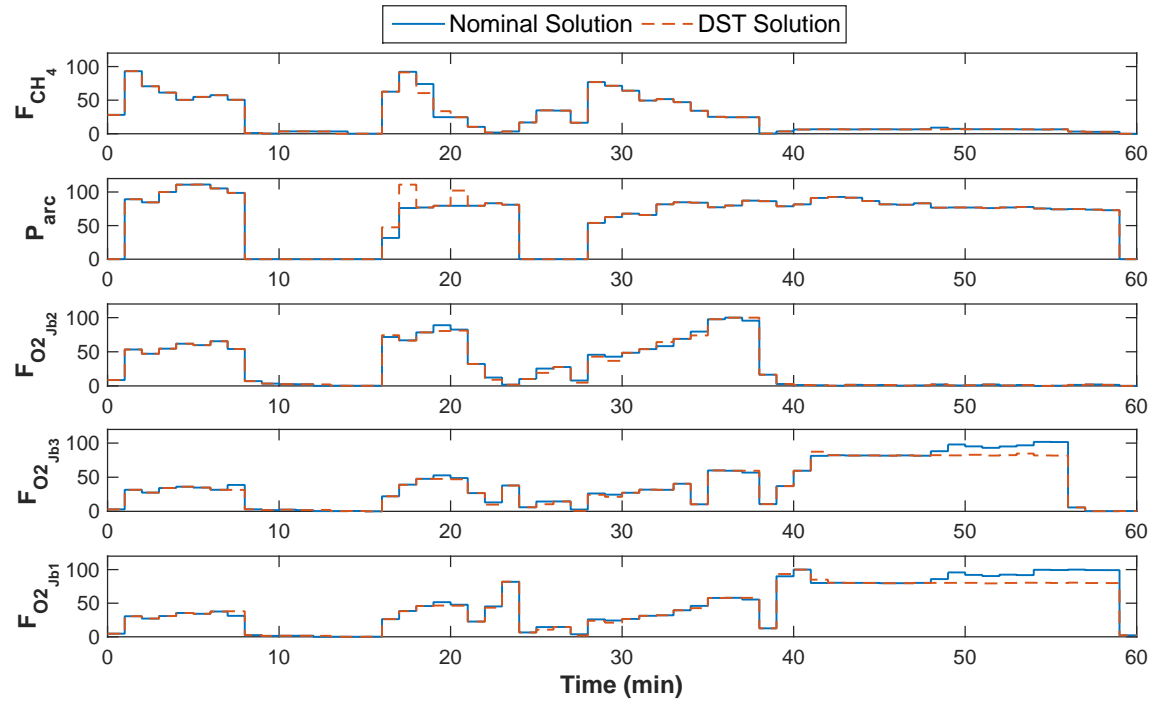


Figure 3.14: Case Study: DST input profiles compared to nominal inputs.

that a state estimation procedure acts as a pathway for the plant information to flow into the model. Fig. 3.14 shows the comparison between the DST and the nominal inputs. An objective value of 97.67 is achieved with 5 on-line re-optimizations carried out at 10th, 20th, 30th, 40th and 50th minute. The 2.4% increase in objective value due to the application of the DST would translate to a significant annual increase in profit. The economic improvement points to the need for on-line corrections and output feedback when using a first principles model for real-time applications.

Computational results

We performed the numerical computations on an Intel® Core™ i7-3770 processor with 4 CPU cores running Windows 7 at 3.40 GHz. The solution time history (in CPU seconds) of the MHE runs is shown in Fig. 3.15. The MHE solve is very fast with a remarkably small average solve time of 0.69 s. The solution times for the shrinking horizon optimization is presented in Table 3.6. On average, the economic

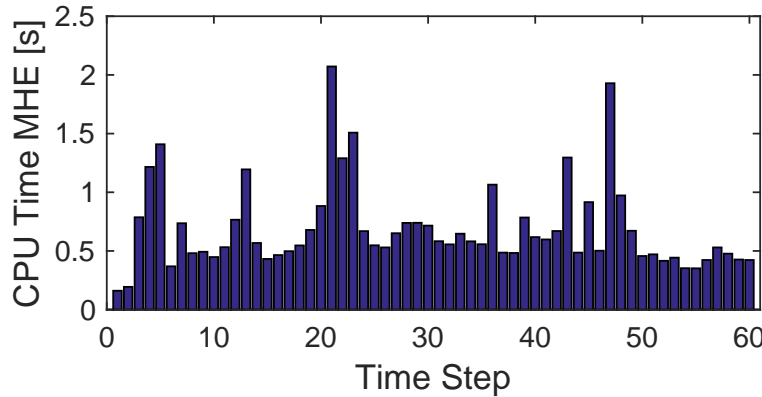
Figure 3.15: Solution times for MHE problem with horizons of $N = 6$ time steps.

Table 3.6: Solution time for shrinking horizon optimization problem.

Time where DST is called by Operator (min)	10	20	30	40	50
CPU Time (s)	42.4	28.6	9.8	5.2	1.2

optimization problem is solved in 17.4 s. This is well below the sampling time of 1 minute.

3.3.5 Conclusion

In this section, we propose an on-line DST based on multi-rate MHE for the EAF steel-making process. The DST combines the MHE with the shrinking horizon optimizer to provide economically optimal input trajectories based on the current state of the system. The full discretization approach is used to solve the optimization problems. The proposed DST takes advantage of a detailed EAF model and can be used in real-time by EAF operators. As a subsequent work, effect of uncertainties other than the parametric one will be investigated. We also intend to study the economic impact of an increase in optimizer execution frequency in the DST. Additionally, a closed-loop economic model predictive controller coupled with MHE would be a useful avenue of investigation for application for EAFs. Finally, an interesting research direction is to explore the effects of increased frequency of slow measurements and quantifying

the quality of the state estimates thus obtained.

3.A Derivation of $W'_i(t, w_k)$ based on hyperbolic tangent functions

Consider a general hyperbolic tangent function described as $y = f(x) = d + a \tanh b(x - c)$, where x and y are the independent and dependent variables respectively. The constants a and b define the function's amplitude and slope respectively. The constants d and c are used to shift the function curve along the y-axis and x-axis respectively. The function can be considered as a continuous approximation of a discontinuous function given as

$$y' = f'(x) = \begin{cases} d - a & x \in (-\infty, c) \\ d & x = c \\ d + a & x \in (c, \infty) \end{cases}. \quad (3.33)$$

Using the above, the continuous approximation for the first 2 consecutive constant pieces of the discontinuous piecewise constant function $W_i(t, w_k)$ is approximated as

$$\begin{aligned} W'_i(t, w_{i-N}, w_{i-N+1}) &= \frac{w_{i-N} + w_{i-N+1}}{2} \\ &+ \frac{w_{i-N+1} - w_{i-N}}{2} \tanh b(t - t_{i-N}). \end{aligned} \quad (3.34)$$

The above approximation can be extended for the first 3 consecutive pieces as

$$\begin{aligned} W'_i(t, w_{i-N}, w_{i-N+1}, w_{i-N+2}) &= W'_i(t, w_{i-N}, w_{i-N+1}) + \frac{w_{i-N+1} + w_{i-N+2}}{2} \\ &+ \frac{w_{i-N+2} - w_{i-N+1}}{2} \tanh b(t - t_{i-N+1}) \\ &- w_{i-N+1}. \end{aligned} \quad (3.35)$$

Extending the above for the full MHE time horizon, we have

$$\begin{aligned}
 W'_i(t, w_k) &= W'_i(t, w_{i-N}, w_{i-N+1}) \\
 &\quad + W'_i(t, w_{i-N+1}, w_{i-N+2}) \\
 &\quad + \cdots + W'_i(t, w_{i-2}, w_{i-1}) - \sum_{k=i-N+1}^{i-2} w_k.
 \end{aligned} \tag{3.36}$$

Simplifying the above expression and substituting $b = \frac{\alpha}{\delta t}$ gives (3.5).

References

- [1] S. Billings, F. Boland, and H Nicholson. "Electric arc furnace modelling and control". In: *Automatica* 15.2 (1979), pp. 137–148.
- [2] F. Wang, Z. Jin, Z. Zhu, and X. Wang. "Application of extended Kalman filter to the modeling of electric arc furnace for power quality issues". In: *Neural Networks and Brain, 2005. ICNN&B'05. International Conference on*. Vol. 2. IEEE. 2005, pp. 991–996.
- [3] Y. Ghobara. "Modeling, Optimization and Estimation in Electric Arc Furnace (EAF) Operation". MA thesis. McMaster University, 2013, p. 8166.
- [4] F. Allgöwer, T. A. Badgwell, J. S. Qin, J. B. Rawlings, and S. J. Wright. "Nonlinear predictive control and moving horizon estimation - an introductory overview". In: *Advances in Control*. Springer, 1999, pp. 391–449.
- [5] F. V. Lima and J. B. Rawlings. "Nonlinear stochastic modeling to improve state estimation in process monitoring and control". In: *AIChE Journal* 57.4 (2011), pp. 996–1007.
- [6] R. López-Negrete and L. T. Biegler. "A moving horizon estimator for processes with multi-rate measurements: A nonlinear programming sensitivity approach". In: *Journal of Process Control* 22.4 (2012), pp. 677–688.
- [7] R. Fourer, D. M. Gay, and B. W. Kernighan. "A modeling language for mathematical programming". In: *Management Science* 36.5 (1990), pp. 519–554.
- [8] V. M. Zavala and L. T. Biegler. "Optimization-based strategies for the operation of low-density polyethylene tubular reactors: Moving horizon estimation". In: *Computers & Chemical Engineering* 33.1 (2009), pp. 379–390.
- [9] B. Houska, H. J. Ferreau, and M. Diehl. "ACADO toolkit - An open-source framework for automatic control and dynamic optimization". In: *Optimal Control Applications and Methods* 32.3 (2011), pp. 298–312.

- [10] J. Åkesson, K.-E. Årzén, M. Gäfvert, T. Bergdahl, and H. Tummescheit. "Modeling and optimization with Optimica and JModelica.org - Languages and tools for solving large-scale dynamic optimization problems". In: *Computers & Chemical Engineering* 34.11 (2010), pp. 1737–1749.
- [11] T. Kraus, P. Kuhl, L. Wirsching, H. G. Bock, and M. Diehl. "A moving horizon state estimation algorithm applied to the Tennessee Eastman benchmark process". In: *Multisensor Fusion and Integration for Intelligent Systems, 2006 IEEE International Conference on*. IEEE. 2006, pp. 377–382.
- [12] Process Systems Enterprise Ltd. *gPROMS*, www.psenterprise.com/gproms, 1997-2015. 2015.
- [13] C. Pantelides. *Personal communication*. 2015.
- [14] R. D. M. MacRosty and C. L. E. Swartz. "Dynamic modeling of an industrial electric arc furnace". In: *Industrial & Engineering Chemistry Research* 44 (2005), pp. 8067–8083.
- [15] T. Sheikhzeinoddin. "Modeling, Optimization and Estimation in Electric Arc Furnace (EAF) Operation". In: *McMaster Steel Research Centre Meeting*. 2011.
- [16] C. V. Rao, J. B. Rawlings, and D. Q. Mayne. "Constrained state estimation for nonlinear discrete-time systems: Stability and moving horizon approximations". In: *IEEE Transactions on Automatic Control* 48.2 (2003), pp. 246–258.
- [17] MATLAB. *version 8.4.0 (R2014b)*. Natick, Massachusetts: The MathWorks Inc., 2014.
- [18] C. V. Rao and J. B. Rawlings. "Constrained process monitoring: Moving-horizon approach". In: *AIChE journal* 48.1 (2002), pp. 97–109.
- [19] A. Alessandri, M. Baglietto, and G. Battistelli. "Moving-horizon state estimation for nonlinear discrete-time systems: New stability results and approximation schemes". In: *Automatica* 44.7 (2008), pp. 1753–1765.

- [20] C. C. Qu and J. Hahn. "Computation of arrival cost for moving horizon estimation via unscented Kalman filtering". In: *Journal of Process Control* 19.2 (2009), pp. 358–363.
- [21] R. Lopez-Negrete, S. C. Patwardhan, and L. T. Biegler. "Constrained particle filter approach to approximate the arrival cost in moving horizon estimation". In: *Journal of Process Control* 21.6 (2011), pp. 909–919.
- [22] A. C. Hindmarsh, P. N. Brown, K. E. Grant, S. L. Lee, R. Serban, D. E. Shumaker, and C. S. Woodward. "SUNDIALS: Suite of nonlinear and differential/algebraic equation solvers". In: *ACM Transactions on Mathematical Software (TOMS)* 31.3 (2005), pp. 363–396.
- [23] A. Wächter and L. T. Biegler. "On the implementation of an interior-point filter line-search algorithm for large-scale nonlinear programming". In: *Mathematical Programming* 106.1 (2006), pp. 25–57.
- [24] S. Shyamal and C. L. E. Swartz. "A Multi-rate Moving Horizon Estimation Framework for Electric Arc Furnace Operation". In: *IFAC-PapersOnLine* 49.7 (2016), pp. 1175–1180.
- [25] S. Shyamal and C. L. E. Swartz. "Multi-Rate Moving Horizon Estimation for an Electric Arc Furnace Steelmaking Process". In: *2016 AIChE Annual Meeting* (2016).
- [26] C Woodside, B Pagurek, J. Pauksens, and A Ogale. "Singular arcs occurring in optimal electric steel refining". In: *IEEE transactions on automatic control* 15.5 (1970), pp. 549–556.
- [27] D. Oosthuizen, I. Craig, and P. Pistorius. "Model predictive control of an electric arc furnace off-gas procedure combined with temperature control". In: *Africon*. Vol. 1. IEEE. 1999, pp. 415–420.
- [28] S Matson and W. F. Ramirez. "Optimal operation of an electric arc furnace". In: *57 th Electric Furnace Conference*. 1999, pp. 719–730.

- [29] R. D. M. MacRosty and C. L. E. Swartz. "Dynamic optimization of electric arc furnace operation". In: *AICHE Journal* 53 (2007), pp. 640–653.
- [30] L. T. Biegler. "An overview of simultaneous strategies for dynamic optimization". In: *Chemical Engineering and Processing: Process Intensification* 46.11 (2007), pp. 1043–1053.
- [31] L. Ji and J. B. Rawlings. "Application of MHE to large-scale nonlinear processes with delayed lab measurements". In: *Computers & Chemical Engineering* 80 (2015), pp. 63–72.

Chapter 4

Real-time Energy Management

4.1	Introduction	76
4.2	Electric arc furnace model	79
4.3	Formulation and solution strategy	82
4.4	Case studies	93
4.5	Conclusions and future work	107
	References	109

The formulations and results in this chapter have been published, and presented in:

- [1] S. Shyamal and C.L.E. Swartz. "Real-time Energy Management for Electric Arc Furnace Operation". *Journal of Process Control* (2018),
<https://doi.org/10.1016/j.jprocont.2018.03.002>.
- [2] S. Shyamal and C.L.E. Swartz. "Real-time Energy Management for Electric Arc Furnace Operation". *AICHE Annual Meeting* (2017). Minneapolis, Minnesota, USA.

Electric arc furnaces are used extensively in the steel industry for steel production.

Development of energy savings strategies for the highly energy-intensive batch process is extremely challenging due to the complexity of the process and lack of measurements due to the harsh operating conditions. Here we introduce a new energy management approach that effectively curtails the energy cost in real-time through the implementation of economically optimal operating decisions. An economics-oriented shrinking horizon nonlinear model predictive control (NMPC) algorithm that exploits time-varying electricity prices is coupled with a multi-rate moving horizon estimator (MHE) to form an integrated decision-making framework. With a detailed first-principles dynamic model functioning at the core, the multi-variable interactions and plant variations are successfully incorporated into the control strategy to achieve reliable performance. We also present a novel initialization scheme for obtaining fast on-line solutions of the economic NMPC and multi-rate MHE dynamic optimization problems. Using this initialization algorithm, we show that the optimal input decisions are obtained with sufficient computational speed for real-time implementation. The energy usage optimization results indicate a significant reduction in the operating cost and peak electricity demand compared to the case where the electricity price profile is not updated.

4.1 Introduction

EAF steelmaking contributes more than 25% of the world's total crude steel production [1]. The highly energy intensive batch operation consumes approximately 400 kilowatt-hours/ton [2] of steel produced. Electrical power is transferred to solid scrap by multiple electrodes whereas chemical energy is added through the combustion of injected natural gas and oxygen. As the batch (heat) progresses, the scrap steel melts and forms a flat bath of molten steel at the bottom of furnace. The metal also reacts with oxygen present to give metal oxides which float on top of the molten metal as slag. During the heat, reactions occurring in the slag are controlled by oxygen and carbon lancing, and with some direct lime, carbon and dolomite additions. EAFs have limited measurements due to the harsh operating conditions, with low levels of automation, and rely heavily on the operator's involvement in the decision making process. Although operator's experience is crucial for EAF operation, the complexity of interactions poses a challenge for consistent and optimal operation. Advanced EAF control and optimization strategies can take advantage of more complex relationships to find a cost optimal balance of the energy contributions from chemical reactions and electrical power. The implementation of such an energy management procedure is envisaged to result in significant savings through an optimal utilization of electrical power, natural gas, oxygen, carbon and fluxes such as limestone and dolomite in response to electricity price change.

Electrical energy fulfills approximately 60% of an EAF's total energy requirement [2]. The high dependence on modern power grids to provide the required electricity presents a challenging problem in developing efficient energy management strategies in response to external variations. Power grid operation has recently shifted from a centralized electricity provider to a deregulated approach [3]. Deregulation of electricity allows a competitive market and active consumer participation. Wholesale electricity markets in North America [3, 4, 5] generally provide either or all of the following time varying electricity price policies for consumers: day-ahead market

(DAM) with price changing every 1-hour, fifteen minute market (FMM), and real-time dispatch (RTD) market with a change every 5-minutes or 1-hour. Electricity cost depends on the time of use and thus there is a high economic incentive for industries to adjust their energy demand according to the volatile market. Companies shifting their high electricity consuming operations from on-peak times to non-peak times of electricity price are generating considerable savings [4]. Another part of the electricity bill is due to the coincidence peak (CP) pricing. Depending on the company's demand contribution in the top specified number of demand peaks over a certain time period (generally 1 year or 4 months), the company is proportionally charged. Thus, there is a great incentive for large-scale consumers to watch for peak demand occurrences and avoid using electricity during the peak time duration. Additionally, such smart plant operation reduces the overall burden on the energy generation side by keeping the real time demand stable with fewer and lower load peaks. A comprehensive real-time energy management strategy with demand response (DR) as a major component within it can be an excellent tool for energy management of EAFs.

Complex industrial facilities typically have a hierarchical decision making structure to compensate for disturbances across multiple time scales and maximize process performance. The hierarchy is composed of planning, scheduling, real-time optimization (RTO), multi-variable control and single-loop regulatory control layers, or a subset thereof. The challenge is to make use of the time-varying electricity price information in all the layers to improve profit. Research efforts directed towards incorporating electricity demand side management into planning and scheduling layers have made significant progress [6]. Low order dynamic models can also be integrated into the scheduling decision making to take advantage of the fast-changing electricity price [7]. Reported research on economic based control of EAFs, suitable for DR operation, is sparse. Control strategies for handling the EAF electrode system have been proposed [8, 9, 10, 11, 12], with linear MPC for off-gas control reported in [13, 14]. It is only recently that NMPC was proposed using a detailed first principles model of the EAF process [15]. However, full state measurement was assumed and a sequential approach for dynamic optimization was used.

Replacement of the traditional set-point tracking objective in MPC with an economic objective is at the core of recently advanced economic MPC (EMPC) schemes [16, 17]. Time varying stage costs have been considered in [18, 19], and provide a straightforward way to incorporate a real-time electricity price profile in an economic NMPC formulation. Economic MPC applications considering real-time electricity pricing for continuous processes such as air conditioning (HVAC) systems [20] and a chemical processing plant [21], have been shown to save energy costs. A key potential bottleneck with an EMPC and MHE implementation is the on-line computational demand associated with solving the large scale dynamic optimization problems. Tracking a fast changing electricity price profile and utilizing it to build an energy savings plan requires strategies to avoid the computational delays. To obtain rapid solutions close to the optimal solution, Zavala and Biegler [22] proposed an advanced-step NMPC algorithm based on nonlinear programming (NLP) sensitivity. Real-time algorithms proposed in [23, 24] perform a single iteration of the control optimization problem by solving a quadratic programming (QP) problem constructed using the solution of the QP solved at the previous sampling instant. A continuation/generalized minimum residual (GMRES) based method is presented in [25] where a single Newton iteration is performed at each time step to get quick solutions of the optimal control problems. More detailed reviews on real-time algorithms for MHE and NMPC are presented in [26] and [27]. On the other hand, to obtain optimal solutions online quickly, various on-line initialization strategies are suggested in [26], including shift initialization and initialization based on parametric sensitivities.

In this chapter, we aim to develop a real-time energy management strategy for EAF operation. We begin by employing multi-rate MHE to reconstruct the state vector at any point in the batch duration. Although various state estimation tools exist [28, 29], MHE has become popular over the past decade [30] because of its constraint handling ability and the use of computationally efficient optimization algorithms. A parameter estimation based multi-rate MHE strategy for EAF operation was presented in an earlier contribution [31]. It used the sequential dynamic optimization approach and the case study showing the MHE tracking ability was for a short simulation horizon.

The MHE application was extended in [32] for the full batch time with the use of a simultaneous solution approach to reduce solution time for potential real-time application. However, the MHE in [31, 32] was not employed in a closed-loop control application. Although an economic model predictive control was implemented in [33] to deal with multi-rate nature of EAF measurements, it was based on a data-driven dynamic model as opposed to a nonlinear first-principles model as utilized in the present study. A non-time varying NMPC cost function was employed in the EAF application in [15], but perfect state information was assumed, and a sequential optimization approach applied. In the present work, we combine MHE and shrinking horizon EMPC with time varying cost coefficients into a single real-time energy management framework, utilizing a nonlinear first-principles based EAF model. We cast the NMPC and MHE optimization problems as NLP problems using the simultaneous approach to compute optimal solutions for the state estimates and control actions. Additionally, a novel initialization scheme is introduced for a combined MHE-NMPC implementation to obtain rapid solutions. Finally, the efficacy of the proposed energy demand-curbing strategy is demonstrated under RTD electricity pricing scenarios. We also compare the energy savings obtained with and without a price update.

The remainder of the chapter is structured as follows: Section 4.2 describes the first-principles based dynamic EAF model. In Section 4.3, we present the multi-rate MHE and shrinking horizon economics-based NMPC formulations, as well as the new initialization scheme. Section 4.4 discusses the case studies with results and discussion. Section 4.5 presents conclusions and identifies future research directions.

4.2 Electric arc furnace model

The current state of fundamental understanding about the EAF process remains incomplete due to its complexity and extreme operating conditions. The models built using computational fluid dynamics (CFD) [34] to capture details of only a section of furnace are well suited for design and engineering analysis, but are inappropriate

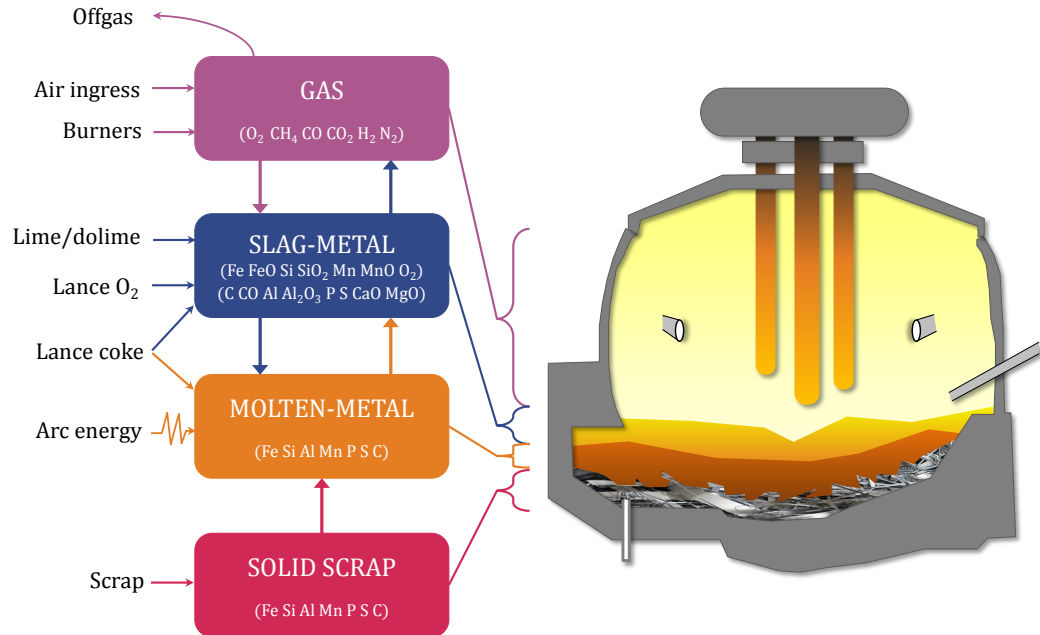


Figure 4.1: Schematic of the EAF model [39] employed showing inputs, outputs and material flow between the four zones.

for real-time control applications due to long simulation times [35]. Other models developed in the past to simulate an industrial EAF process using simplifying assumptions have focused on partitioning the furnace in multiple zones [36, 37, 38]. The heat and mass transfer taking place inside the zones and between the zones is then described using appropriate mathematical equations. The dynamic EAF model proposed in [39] considered 4 equilibrium zones with mass transport limitations (Fig. 4.1): gas, slag-metal interaction, molten steel and solid scrap zones. The *gas zone* contains all the gases filling up the free-board volume of furnace above the scrap steel. Burners are used to preheat the scrap before a high voltage is selected for the arc. The *slag-metal interaction zone* represents all the slag materials in addition to the upper part of molten metal that is in contact with the slag. The *molten steel zone* includes the metals in their liquid form once the scrap starts melting, excluding the portion already considered in the slag-metal interaction zone. The *solid scrap zone* comprises the scrap steel remaining in solid form. To explain the process phenomena in each zone, energy and material balances are considered. A major benefit of using

this approach is that it requires fewer parameters than a model based on reaction kinetics. In this paper we employ a modified version of the model developed in [39] to predict the composition and temperature of scrap steel, molten metal, slag and off-gas, as well as slag foam height and its effect on energy transfer from the arc. The model assumes that chemical equilibrium exists in the slag-metal interaction and the gas zones; it computes the chemical equilibrium in each zone by minimization of the Gibbs free energy. Empirical relationships describe the formation of slag foam due to carbon monoxide formation. Atom balances and fundamental mass transfer equations are applied to track the material in each zone and between the zones. The electric arc energy transfer, heat transfer via radiation, chemical reactions and convective heat transfer are taken into account by detailed relationships. MacRosty and Swartz [39] utilized industrial data in a parameter estimation technique based on the maximum likelihood function implemented within gPROMS/gEST [40] to estimate a set of model parameters. The first principles model of [39] was re-calibrated and modified in [41], with two changes incorporated to meet the demands of another industrial partner. First, a flat surface was assumed for solid scrap melting instead of a cone-frustum geometry, and second, the addition of JetBoxes used in the oxygen injection system of the furnace was included. The DAE system coded in the commercial modeling platform gPROMS [40] consisted of 40 differential and 1050 algebraic variables.

The nonlinearities contained in the radiation model of [41] were removed in [31, 32] through introduction of a new parameter which affects how energy from the arc power is divided between the furnace roof, walls, the solid scrap and the molten metal. The model parameters were re-tuned to obtain matching profiles for the plant and model data. Since metal oxides were found to be present in trace amounts in the molten metal zone, it was assumed that all the oxides are present in the slag-metal zone only. As a consequence, the corresponding states were eliminated, reducing number of differential states to 29 in the modified model. The gPROMS model is translated to an open-source Python based CasADi [42] framework for application of a simultaneous optimization strategy. State variables of the converted model that

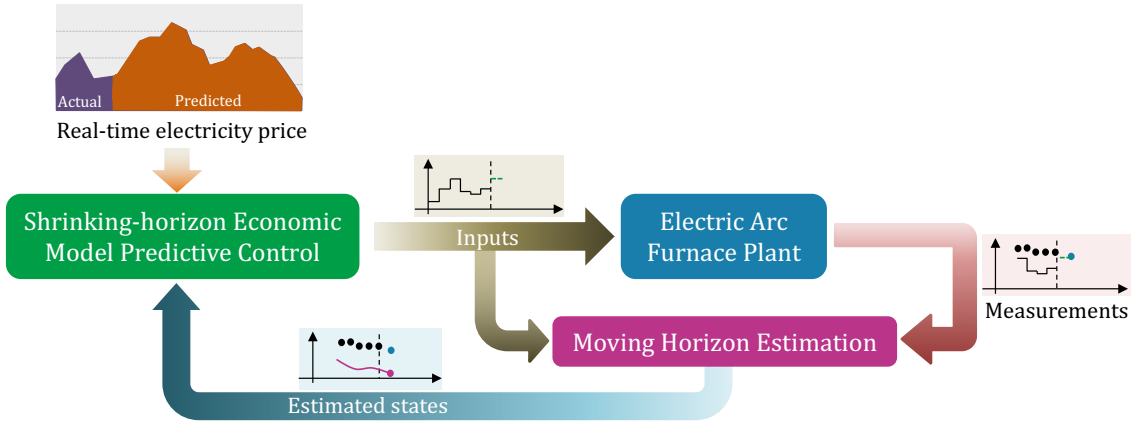


Figure 4.2: Real-time energy management control framework.

attain only small values ($\sim 1.0 \times 10^{-13}$) are removed and replaced with a constant.

Large-scale models pose computational challenges for real-time applications and necessary steps are needed to build a numerically well-behaved DAE system. Our implementation involves a model contraction technique for elimination of a subset of the algebraic variables and equations, using a functionality of CasADI. The CasADI function reformulates the model symbolically by transforming selected algebraic variables into dependent variables, which are determined by explicit expressions involving the differential and retained algebraic variables. The dynamic model employed for this study was consequently contracted to 28 differential and 121 algebraic variables.

4.3 Formulation and solution strategy

In this section, we describe the proposed real-time energy management strategy for the electric arc furnace operation. A key feature of the strategy involves a model-based real-time optimization implementation wherein an advanced control algorithm provides optimal inputs to the furnace as shown in Fig. 4.2. Given the real-time electricity price profile $c_{1i}(t)$ and the estimated states x_i obtained from the moving

horizon estimation, the shrinking horizon EMPC finds the optimal inputs \mathbf{u}_i . Only the inputs corresponding to the first control stage are injected to the plant. They are also stored for later use in defining the subsequent MHE problems. Once measurements \mathbf{y}_{i+1} are received by MHE, the next set of states is reconstructed. The cyclic strategy continues until the batch ends.

The recursive optimization procedure is computationally demanding. We employ the simultaneous full-discretization approach, in which the input trajectories are parameterized via piecewise constant functions, with an implicit Euler scheme used for the numerical solution of the DAE system. The DAE-constrained optimization problem is thus transformed to a general NLP (nonlinear programming) problem in an entirely algebraic form. Fast solutions of the sparse problem are obtained through the use of an interior-point solver and initialization of the primal and dual variables. The optimal control problems are efficiently initialized by finding good warm-start points using a novel scheme which primarily involves solving background problems in between the sampling time instants. In the subsequent subsections, we present a detailed description of the formulation and solution strategy.

4.3.1 Shrinking Horizon Economic Model Predictive Control

MPC formulations based on nonlinear dynamic plant models are typically used for highly nonlinear systems and/or processes that traverse a wide operating range; characteristics generally exhibited in batch operations. Since batch processes have a defined end point, a shrinking horizon formulation where both prediction and control horizons decrease as the controller advances along the batch time is practically desirable [43]. The shrinking horizon economic objective function used for the EAF maximizes the profit opportunity with respect to a single batch operation. Current and predicted energy price trajectories are stitched together to get time-dependent economic NMPC cost coefficients for electric arc power use. It would be ideal to

incorporate the model used by wholesale markets for price prediction in the economic NMPC framework since the forecasts are dependent on predicted demand. However, such a model is not easily available and also the expected increase in the NMPC problem dimension might make the on-line implementation infeasible. We assume the price determining mechanism to be independent from the EAF control framework. The price profile is updated every 5, 15 or 60 minutes depending on the time scale of energy transactions in the market and time when the batch process started. We further assume a deterministic optimization formulation where the forecast is perfectly known without any uncertainty. More sophisticated stochastic formulations where economic NMPC can differentiate between actual and predicted prices are also possible. Apart from the power input, the objective function is time-invariant with respect to the cost of material inputs.

Once the state estimates are obtained from multi-rate MHE (described in the next subsection) a shrinking horizon control problem, with t_f being the fixed end time of the batch, is constructed such that input bounds are satisfied. The DAE system (4.2) - (4.3) transformed into algebraic equations upon discretization of the state and control variables, appears as equality constraints. The economic NMPC problem at the current sampling time t_i is given as,

$$\begin{aligned} \max_{\mathbf{u}(t)} \quad & c_0 M_{steel}(t_f) - \left(\int_{t_i}^{t_f} c_{1i}(t) P dt + c_2 \int_{t_i}^{t_f} F_{CH_4,brnr} dt \right. \\ & \left. + c_3 \int_{t_i}^{t_f} (F_{O_2,Jetbox1} + F_{O_2,Jetbox2} + F_{O_2,Jetbox3}) dt \right) \end{aligned} \quad (4.1)$$

subject to

Model equations:

$$\dot{\mathbf{x}}(t) = \mathbf{f}(\mathbf{x}(t), \mathbf{z}(t), \mathbf{u}(t)) \quad (4.2)$$

$$\mathbf{0} = \mathbf{g}(\mathbf{x}(t), \mathbf{z}(t), \mathbf{u}(t)) \quad (4.3)$$

$$\mathbf{y}(t) = \mathbf{h}(\mathbf{x}(t), \mathbf{z}(t), \mathbf{u}(t)) \quad (4.4)$$

$$\mathbf{x}(t_i) = \mathbf{x}_{0i} \quad (4.5)$$

$$t \in [t_i, t_f] \quad (4.6)$$

Input constraints:

$$P^{\min}(t) \leq P \leq P^{\max}(t) \quad (4.7)$$

$$F_k^{\min}(t) \leq F_k \leq F_k^{\max}(t). \quad (4.8)$$

Here, P is the active arc power and the natural gas flow rate from the burner is $F_{CH_4,brnr}$. The flow rates of oxygen from the jetboxes 1,2, and 3 are denoted by $F_{O_2,Jetbox1}$, $F_{O_2,Jetbox2}$, and $F_{O_2,Jetbox3}$ respectively. The amount of molten steel that remains when the batch ends is indicated by M_{steel} . M_{steel} is a state variable. The unit cost associated with each of the control inputs are represented as c_k ($k = 0, 1, 2, 3$). The subscript i in c_1 is used to indicate the time index, thus distinguishing one cost profile from the next. The decision variables for the dynamic optimization problem $\mathbf{u}(t)$ comprise P , $F_{CH_4,brnr}$, $F_{O_2,Jetbox1}$, $F_{O_2,Jetbox2}$, and $F_{O_2,Jetbox3}$. $\mathbf{u}(t)$ is discretized to give piecewise constant controls. The four gas flow rates are denoted in (4.8) as F_k . The differential and algebraic states of the EAF model are denoted as \mathbf{x} and \mathbf{z} respectively, and the measured outputs as \mathbf{y} . \mathbf{f} and \mathbf{g} represent the differential and algebraic functions of the differential-algebraic equation EAF model in semi-explicit form, while \mathbf{h} is a function mapping \mathbf{x} and \mathbf{z} to the measurements \mathbf{y} . \mathbf{x}_{0i} denotes the initial condition of the state variables at t_i . The input constraints (4.7) and (4.8) provide bounds for each control stage. The added arc power and the gas flows are permitted to move between the upper (P^{\max}, F_k^{\max}) and lower bounds (P^{\min}, F_k^{\min}) so that the additions are within realistic limits. The optimal inputs corresponding to the first control stage are implemented on the plant.

4.3.2 Multi-rate Moving Horizon Estimation

The operation of the EAF is complex, and significant fluctuations occur due to materials being added at multiple time instants during the batch. As the first principles EAF

model represents an approximation of the real process phenomenon, plant-model mismatch is likely to exist. Unknown disturbances during the heat can also affect the estimation accuracy and control performance. The state estimation strategy described here handles the uncertainties by employing process noise terms. MHE is well suited for nonlinear constrained estimation because it solves a nonlinear dynamic optimization problem where user-defined constraints are handled directly [44, 45, 46]. The use of a fixed estimation horizon in MHE keeps the optimization problem tractable. The MHE implementation typically involves the application of state-of-the art NLP solvers to compute quick solutions in real-time [31, 47, 48, 49]. The estimation results depend on the availability of plant measurements. This issue arises for EAFs due to a limited number of measurements available for reconstruction of the state vector. Moreover, the measurements are usually taken at different sampling rates. Using all the measurements for estimation potentially improves the system observability which in turn decreases the estimation errors [50, 51]. Since MHE uses a past window of measurements it is straightforward to include measurements with variable sampling rate [31, 50, 51, 52, 53]. The multi-rate formulation described in our earlier work [31] is adopted in the present energy management strategy to take advantage of both the infrequent and frequent measurements.

We consider the EAF process positioned at time instant t_i where i represent the current sampling index, with a past history of measurements and control inputs available. The moving horizon measurement window is of length N control stages. The multi-rate MHE problem formulation considers measurements taken at multiple sampling rates. The infrequent measurements for the EAF are associated with the molten-metal and slag zones, while the frequent measurements correspond to the offgas composition, and the furnace roof and wall temperatures. We assume that the infrequent measurements are instantaneously available and are located at sampling time instants corresponding to the frequent measurements. We denote \mathbf{y}_k^F as the vector of only frequent measurements, and \mathbf{y}_k^{SF} as the vector containing both the frequent and infrequent measurements. The measurement structure in a moving horizon may be represented, for example, as $\mathbf{Y}_i = \{\mathbf{y}_{i-N}^F, \mathbf{y}_{i-N+1}^{SF}, \mathbf{y}_{i-N+2}^F, \dots, \mathbf{y}_{i-1}^{SF}, \mathbf{y}_i^F\}$; here

the measurement vector at time instant t_{i-N+1} comprises both the infrequent and frequent measurements whereas at sampling time t_{i-N} only frequent measurements are available. The sets of sampling times corresponding to the frequent, and combined frequent and infrequent measurements, are denoted as \mathbb{I}_F and \mathbb{I}_{SF} respectively. The example can be altered to accommodate different structures for \mathbf{Y}_i . The measurement sequence is updated at the next sampling time by including the new measurement set while dropping the earliest measurements. This restricts the growth of estimation problem size which also reduces the on-line computational burden. However, if the numerical complexity is not an issue then an expanding horizon least-squares estimation may be more appropriate for the batch process.

The multi-rate MHE optimization problem for a discrete-time nonlinear system observable for the state profile is given as:

$$\begin{aligned} \min_{\mathbf{x}_{i-N}, \mathbf{w}_k} & \sum_{k=i-N}^{i-1} \|\mathbf{w}_k\|_{Q^{-1}}^2 + \sum_{\substack{k=i-N \\ k \in \mathbb{I}_F}}^i \|\mathbf{v}_k^F\|_{(R^F)^{-1}}^2 \\ & + \sum_{\substack{k=i-N \\ k \in \mathbb{I}_{SF}}}^i \|\mathbf{v}_k^{SF}\|_{(R^{SF})^{-1}}^2 + \|\mathbf{x}_{i-N} - \hat{\mathbf{x}}_{i-N}\|_{S_i^{-1}}^2 \end{aligned} \quad (4.9)$$

$$\text{s.t. } \mathbf{x}_{k+1} = \mathbf{f}_k(\mathbf{x}_k, \mathbf{u}_k) + \mathbf{w}_k, \quad k = i-N, \dots, i-1 \quad (4.10)$$

$$\mathbf{y}_k^F = \mathbf{h}_k^F(\mathbf{x}_k) + \mathbf{v}_k^F, \quad k \in \mathbb{I}_F \quad (4.11)$$

$$\mathbf{y}_k^{SF} = \mathbf{h}_k^{SF}(\mathbf{x}_k) + \mathbf{v}_k^{SF}, \quad k \in \mathbb{I}_{SF} \quad (4.12)$$

$$\mathbf{x}^{LB} \leq \mathbf{x}_k \leq \mathbf{x}^{UB}, \quad (4.13)$$

$$\mathbf{w}^{LB} \leq \mathbf{w}_k \leq \mathbf{w}^{UB}. \quad (4.14)$$

Here, \mathbf{w}_k is included to represent the process noise (i.e. the model uncertainty). $\hat{\mathbf{x}}_{i-N}$ is the *a priori* estimate of the state at the starting point of the moving window. Given the states \mathbf{x}_k and the known inputs \mathbf{u}_k , $\mathbf{f}_k(\cdot)$ integrates the process model

forward over one sample time. The measurement functions $\mathbf{h}_k^F(\cdot)$ and $\mathbf{h}_k^{SF}(\cdot)$ map the state variables \mathbf{x}_k to the measurements \mathbf{y}_k^F and \mathbf{y}_k^{SF} respectively. The measurement noise terms corresponding to \mathbf{y}_k^F and \mathbf{y}_k^{SF} are represented respectively as \mathbf{v}_k^F and \mathbf{v}_k^{SF} . Equation (4.10) represents a discretized form of the DAE process model in which the algebraic states are considered as functions of the differential states and inputs through (4.3). The covariance matrices of appropriate dimensions for the model noise, measurement noise and for the arrival cost are represented here as Q , R^F , R^{SF} and S_i . The state constraints are provided by the lower bound \mathbf{x}^{LB} and the upper bound \mathbf{x}^{UB} . The model noise \mathbf{w}_k is allowed to move between lower and upper bounds of \mathbf{w}^{LB} and \mathbf{w}^{UB} respectively. The estimate of current states \mathbf{x}_i are obtained from the solution of optimization problem stated above.

The least-squares objective function of the multi-rate MHE scheme (4.9) comprises four terms. The first three terms are a weighted minimization of model and measurement errors over a moving time horizon of length N . The fourth term in (4.9) is the arrival cost that represents the measurement information not included in the moving window. The covariance S_i is generally updated when the next MHE problem is formulated, to S_{i+1} using the current solution. However, the covariance update is not necessary when the system is strongly observable [46]. An extended Kalman filter covariance propagation equation is commonly used [45],

$$S_{i+1} = Q + A_i [S_i - S_i C_i^T (R + C_i S_i C_i^T)^{-1} C_i S_i] A_i^{-1} \quad (4.15)$$

where A_i and C_i are matrices in the linearized model,

$$\begin{aligned} \mathbf{x}_{i+1} &= A_i \mathbf{x}_i + B_i \mathbf{u}_i \\ \mathbf{y}_i &= C_i \mathbf{x}_i + D_i \mathbf{u}_i. \end{aligned} \quad (4.16)$$

We have suppressed the superscripts ‘ F ’ and ‘ SF ’ for R and \mathbf{y} in (4.15) for ease of readability. However, appropriate dimensions for R and correct measurement functions ($\mathbf{h}_k^F(\cdot)$ or $\mathbf{h}_k^{SF}(\cdot)$) are to be considered when carrying out EKF update (4.15).

The solutions of the current MHE optimization problem (4.9) are represented as \mathbf{x}_{i-N}^* and \mathbf{w}_{i-N}^* . The covariance S_{i+1} can be computed using other filters as well, such as the unscented Kalman filter [54] and constrained particle filter [55]. Note that for time steps t_i with $i \leq N$, new measurements are added to the past history in consideration without dropping the oldest one, and also the initial state covariance is not changed.

4.3.3 Novel initialization scheme for MHE and NMPC

In both MHE and NMPC, subsequent problems are very similar with respect to the input data and problem structure. This important characteristic is utilized by researchers to generate good starting points for the optimization problems [26]. Although the initialization strategies used in the past have been able to reduce the computational time, it is still considered a major bottleneck for on-line control applications [56]. The prior works have focused more on effectively transferring selected and extended information from a previous solve to the next one. Strategies for obtaining fast on-line approximate solutions have been shown to work quite well even for complex models [57, 58]. Zavala and Biegler [27] utilized the time between sampling times to first solve a predicted NMPC problem and then used sensitivity information to update the predicted solution upon the availability of new measurements. One of the key components of these algorithms that make them so effective is the use of the time between two consecutive sampling instants. In the present work, the idea is utilized in a novel initialization scheme for a coupled MHE-NMPC implementation. The warm-start strategy proposed here generates initialization points very close to the optimal solution of MHE-NMPC. A forward model simulation is executed to obtain predicted measurements for solving predicted MHE-NMPC problems. The predicted MHE-NMPC solutions provide good warm-start points for primal and dual variables of the actual MHE-NMPC problems to be solved based on newly acquired measurements.

Suppose at time instant t_k , we have the following information: the current state

estimate \mathbf{x}_k and input \mathbf{u}_k . We have suppressed the superscripts used for representing slow and fast measurements for ease of readability. We refer to the time gap between consecutive sampling times of frequent measurements as ‘background’ time. We introduce an initialization scheme using the given information at time t_k for obtaining fast optimal solutions of MHE-NMPC problems:

In background mode, between t_k and t_{k+1} :

1. Use \mathbf{x}_k and \mathbf{u}_k to generate the predicted future measurements $\bar{\mathbf{y}}_{k+1}$ through a disturbance-free ($\mathbf{w}_k = 0$) model simulation $\bar{\mathbf{x}}_{k+1} = \mathbf{f}(\mathbf{x}_k, \mathbf{u}_k)$ and $\bar{\mathbf{y}}_{k+1} = \mathbf{h}(\bar{\mathbf{x}}_{k+1})$.
2. Construct and solve the predicted MHE problem using $\bar{\mathbf{y}}_{k+1}$ to get predicted state estimates $\tilde{\mathbf{x}}_{k+1}$. Retain the problem solution \tilde{s}_k^{mhe} (both primal and dual).
3. Define the predicted NMPC problem using $\tilde{\mathbf{x}}_{k+1}$ and the electricity price profile \tilde{c}_{1k} known at t_k . Solve the problem to obtain predicted input $\tilde{\mathbf{u}}_{k+1}$ and retain the solution \tilde{s}_k^{nmvc} (both primal and dual).

On-line, at t_{k+1} :

1. Receive the *true* measurements \mathbf{y}_{k+1} from the plant and solve the *true* MHE optimization problem by employing \tilde{s}_k^{mhe} as initial guesses to compute true state estimates \mathbf{x}_{k+1} .
2. Define the *true* NMPC problem using \mathbf{x}_{k+1} , and the electricity price profile $c_{1,k+1}$ known at t_{k+1} . Solve the *true* NMPC problem using \tilde{s}_k^{nmvc} as initial guesses to obtain the *true* input \mathbf{u}_{k+1} , and return to the background step.

The warm-start scheme can be used with any of the three dynamic optimization approaches: simultaneous, sequential, and multiple shooting (a detailed discussion on the three dynamic optimization approaches are provided in [59]); however, it is particularly useful for the simultaneous approach where initialization of the entire dynamic profiles is required. Depending on the closeness of the predicted and the *true*

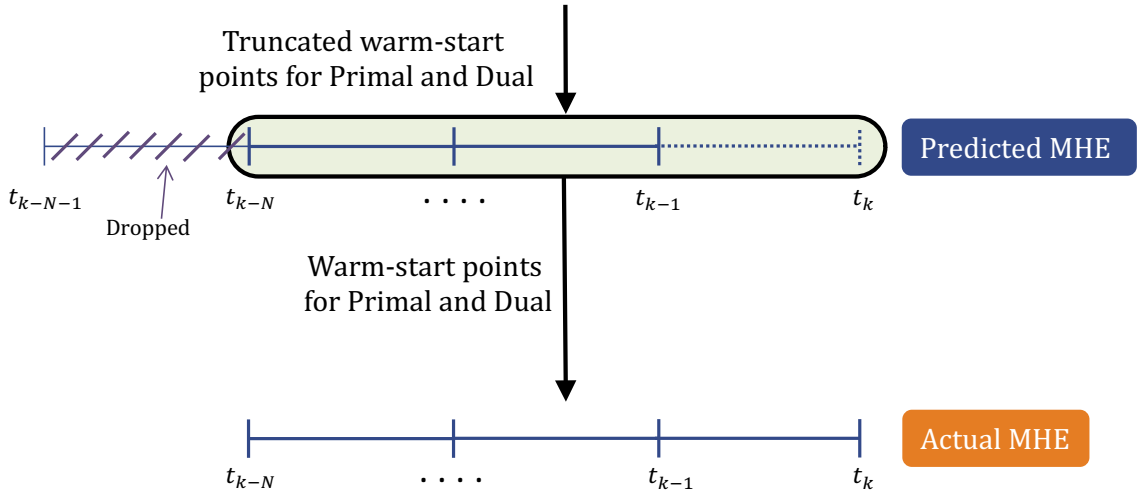


Figure 4.3: Initialization for Moving Horizon Estimation

values, the benefit of the scheme may vary. The initialization is particularly useful for MHE because good warm-start points are consequently available for both the primal and dual variables associated with the new sampling interval of the moving window (Fig. 4.3). Fig. 4.3 illustrates how warm-start points are passed from a predicted MHE solve to an actual MHE solve using the proposed initialization scheme.

4.3.4 Implementation

The energy management strategy is implemented for a discretized model using the Python front end of CasADi. The variable space of the EAF model written in gPROMS is first reduced in CasADi to get a reduced DAE system. Next, the dynamic optimization problems are solved by employing the simultaneous solution approach. We set 7 finite elements per control stage to carry out time discretization for MHE and NMPC. Using the simultaneous approach, the optimal control problems are expressed as large-scale sparse NLP problems, which are then solved with the interior-point solver IPOPT [60] using the linear solver MA27. We employ IDAS (part of the SUNDIALS [61] suite of solvers) for carrying out the plant and model simulations required for the forward integration and measurement generation. To warm-start

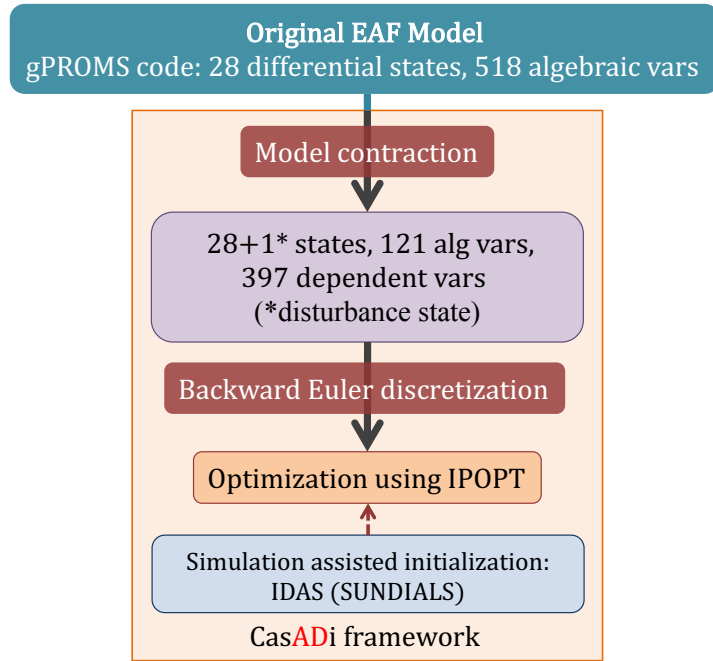


Figure 4.4: Dynamic optimization implementation framework.

the predicted MHE and NMPC problems, the primal and the dual information is transferred from their respective last *true* optimization solves. However, the MHE solution set is shortened by removing the first control stage values. The initial guesses for the primal values associated with the new terminal stage is obtained by a forward simulation. For the shrinking horizon NMPC, the variable values are dropped for the first time interval. The *true* MHE-NMPC problems are initialized with the primal and dual values of respective predicted solves. The implementation framework is illustrated in Fig. 4.4.

To include plant-model mismatch in our implementation, we decrease a power factor parameter k_p by 10% in the model used by MHE and NMPC. Due to the mismatch, the amount of electrical energy delivered to the solid scrap by the arc is decreased significantly within the MHE and NMPC models. The exact model equations affected by a perturbation in k_p is given in [41]. Since unmeasured disturbances can result in unsatisfactory MHE performance, we compensate the mismatch by augmenting the model states with an integrated disturbance state \mathbf{d}_k , assumed to be driven only by

white noise \mathbf{w}_{dk} . MHE is implemented by employing the augmented system

$$\begin{aligned}\mathbf{x}_{k+1} &= \mathbf{f}_k(\mathbf{x}_k, \mathbf{u}_k) + \mathbf{B}_d \mathbf{d}_k + \mathbf{w}_k, \\ \mathbf{y}_k^F &= \mathbf{h}_k^F(\mathbf{x}_k) + \mathbf{v}_k^F, \\ \mathbf{y}_k^{SF} &= \mathbf{h}_k^{SF}(\mathbf{x}_k) + \mathbf{v}_k^{SF}, \\ \mathbf{d}_{k+1} &= \mathbf{d}_k + \mathbf{w}_{dk},\end{aligned}\tag{4.17}$$

where \mathbf{B}_d adjusts the impact of disturbance state \mathbf{d}_k on the state equation. \mathbf{Q}_d represents the covariance of $\mathbf{w}_{dk} \sim \mathcal{N}(0, \mathbf{Q}_d)$. Disturbance models are discussed in greater depth in [51]. For the case studies presented in the next section, we have included the disturbance state in the differential equation corresponding to the state variable which represents the moles of manganese in the slag-metal zone. To implement this, we used $\mathbf{B}_d = e_i \in \mathbb{R}^{n \times 1}$ where i represents the state corresponding to the number of moles of manganese in the state vector of size n , and e_i is the i th unit vector. \mathbf{Q}_d is chosen as 0.2 for the case studies described in the next section.

4.4 Case studies

In this section we present four case studies to demonstrate potential benefits of a real-time implementation of the proposed energy management strategy. The studies correspond to changing electricity prices in a real-time dispatch market (RTD), with the price changing every hour. We also analyze the multi-rate MHE's ability to track the true states. Finally, we discuss the computational effort required to solve the MHE and NMPC dynamic optimization problems.

For testing the on-line energy management strategy, we utilize the first-principles EAF model comprising 28 differential and 121 algebraic states. The batch process is 60 minutes in duration, during which scrap metal is charged at time $t = 0$ and $t = 25$ minutes. The measurements for the process are available at different sampling rates, shown in Table 4.1. The frequent measurements are off-gas compositions and furnace

Table 4.1: Multi-rate measurement structure for the case study.

Time (min)	0 ... 42	43	44 ... 46	47	48 ... 60
Number of measured variables	6	13	6	8	6

Table 4.2: Measurement availability in the case study.

Measurement	Sampling Time	Variance
Off-gas compositions (CO, CO ₂ , O ₂ , H ₂) (dimensionless)	Every 1 min	0.01
T _{roof} , T _{wall} (K)	Every 1 min	3
Slag compositions (FeO, Al ₂ O ₃ , SiO ₂ , MgO, CaO) (dimensionless)	43rd min	0.1
Molten-metal temperature (K)	43rd & 47th min	5
Molten-metal carbon content (dimensionless)	43rd & 47th min	0.01

roof and wall temperatures with a sampling time of 1 minute. Slag chemistry data is available only at the 43rd minute of the heat duration. The molten metal temperature and carbon content are known at the 43rd and 47rd minute. The measurement data and the variance values are summarized in Table 4.2. With limited availability of frequent measurements, it is important to analyze the observability of the system before state estimation is carried out. This was assessed by computing the observability of the states of the linearized DAE model at each sampling time instant, using the state observability metric defined in [51]. It utilizes the singular value decomposition (SVD) of the observability matrix constructed from matrices A_i and C_i in the state space model (4.16). Since the lowest metric value obtained was 7.0×10^{-7} , the system is deemed to be fully observable. It is to be noted that the linearization procedure adopted here is not essential because the system observability can also be inferred by examining the IPOPT output [48]. The key step associated with this procedure involves extracting the reduced Hessian information from the IPOPT solution.

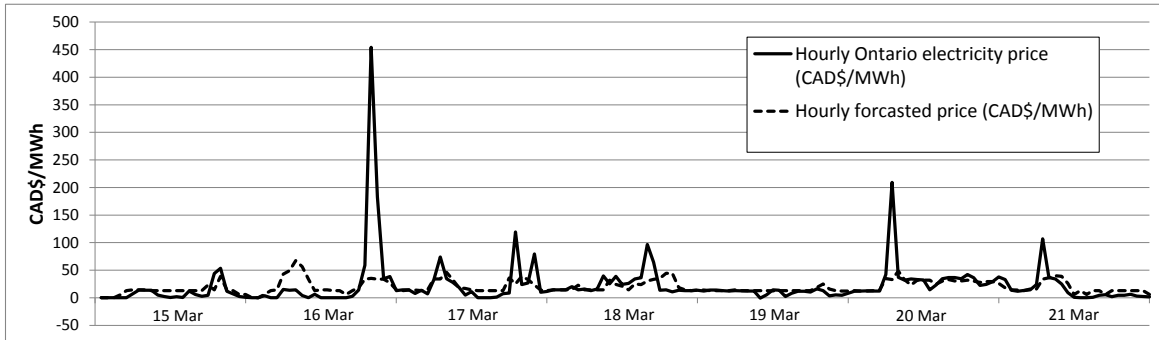


Figure 4.5: Hourly Ontario (Canada) electricity price (actual and predicted) for 15-21 March 2017.

4.4.1 Actual and predicted electricity prices

To make sure that the case studies are conducted using realistic pricing scenarios, we analyzed the actual and predicted hourly electricity prices in the province of Ontario (Canada) for 2016 and the first four months of 2017. Electricity price profiles are generally volatile and high spikes occur rather frequently. Fig. 4.5 shows the variation in electricity price over 15-21 March 2017. We can observe the price spikes and the inability of the forecast model employed by Ontario IESO (Independent Electricity System Operator) to predict these spikes. Upon studying the hourly price and the predictions for 2016, we observed that the predictions were 87.2% less than actual prices on average when the actual prices were greater than \$200/MWh. The actual prices exceeded \$200/MWh for 19 hourly price durations. The prices were between \$100/MWh and \$200/MWh in 42 hourly periods, and the average prediction difference was 55.4%. For the price range \$50 – \$100/MWh, the occurrence frequency was 173 (14.4 per month on average), with the average forecast error at 42%. The analysis is summarized in Fig. 4.6. The high magnitude of forecast error motivates us to study the economic impact of electricity price profile updates in the NMPC objective function. The following four case studies demonstrate the NMPC performance when different electricity price trajectories are encountered. The case

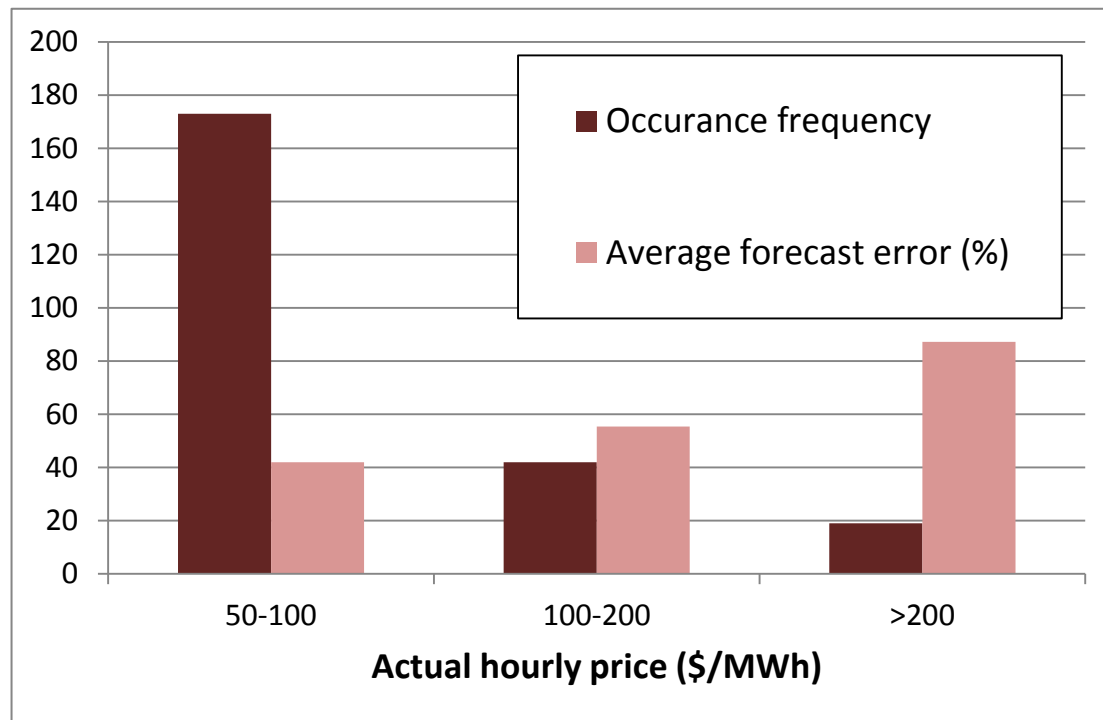


Figure 4.6: Price forecast error analysis for 2016 for the Ontario electricity wholesale market.

Table 4.3: Summary of the case studies comparing NMPC^{*nom*} with NMPC^{*up*}. Wherever % is shown, the values are with respect to NMPC^{*nom*}. The time of electricity price change is the time instant during the batch process of length 60 minutes.

Case No.	1	2	3	4
Time of electricity price change (min)	25	25	40	15
Electricity price before the change (\$/MWh)	308.24	30	308.24	308.24
Electricity price after the change (\$/MWh)	190.48	200	190.48	190.48
Predicted electricity price (\$/MWh)	10.96	15	10.96	10.96
Economic objective increase (%)	4.62	1.54	3.45	3.48
Decrease in electric power use (%)	23.06	8.49	17.34	17.9
Increase in other input use (%)	1.59	0.68	0.15	4.58
Reduction in peak electricity demand (%)	44.62	10.12	14.15	10.11

studies are summarized in Table 4.3.

4.4.2 Case study 1: Price peak decrease with price change at 25th min

Our first case study quantifies the economic performance of NMPC subject to an electricity price change at time $t = 25^{\text{th}}$ minute of the batch duration. The electricity price is \$308.24/MWh before the 25th min and \$190.48/MWh after the change. The price prediction for 25 to 60 min at time $t = 0$ min is \$10.96/MWh. The price variation corresponding to this case occurred in the Ontario market at 21:00-22:00 hours (7th April 2017), and is represented in Fig. 4.7a. The price profile is typical when the batch process is operated during the descent part of an electricity price peak. The price forecast error is expected to be high in such cases.

Here we are comparing two closed loop results, the first (NMPC^{*nom*}) where the price profile is not updated and the forecast price is continued to be used even after 25th minute, and the second (NMPC^{*up*}) where the price profile is updated at the 25th minute to reflect the actual price obtained from the wholesale market. We achieve a 4.62% increase in economic objective value when the price profile is updated. The

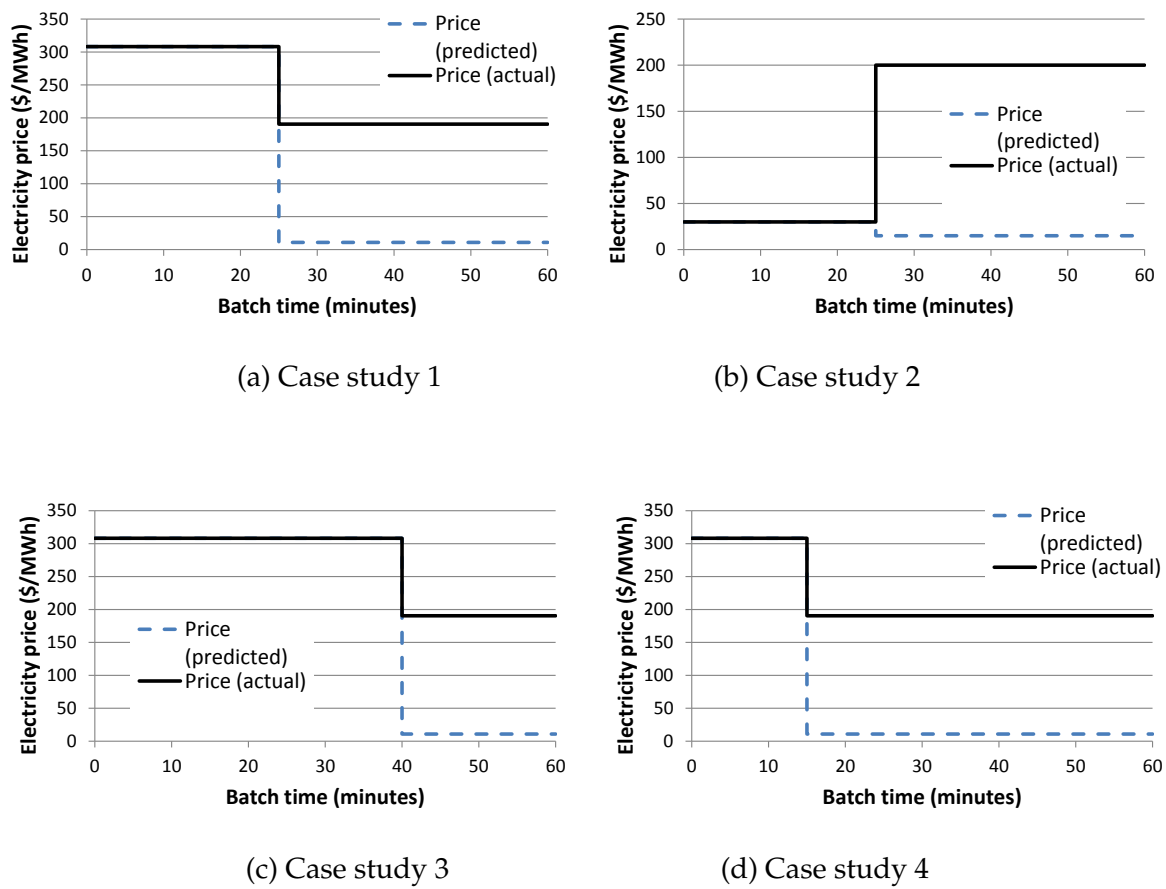


Figure 4.7: Electricity price profiles for the four case studies. The electricity price variation is for a 1 hour electricity price market.

economic objective increase is due to the fact that NMPC^{up} is able to see a higher price than the forecast for electricity post 25th min, and thus uses 23.06% less electrical energy and 1.59% more of the other inputs (CH₄ and O₂). The NMPC^{nom} sees a electricity price profile very different from the actual price post 25th min, and thus is not able to use the control inputs in a cost efficient manner. The normalized input profiles for both NMPC^{nom} and NMPC^{up} are given in Fig. 4.8. The input profiles are scaled for proprietary reasons. From the Fig. 4.8, it is apparent that NMPC^{nom} uses significantly higher electric arc power after 25th minute. Examining the other input trajectories, it can be seen that CH₄ input is not showing a major difference but O₂ consumption though the three jetboxes for NMPC^{up} is higher than that of NMPC^{nom}. Although we observe a large decrease in the electrical power use, the economic objective is not increased by that factor because less molten steel is produced when the total energy consumption is lower. Even though peak electricity demand minimization is not specifically formulated in the NMPC objective function, the peak demand for NMPC^{up} is 44.62% less than NMPC^{nom}. Peak shaving is an added advantage of using NMPC^{up} and is important for both the power grid and steel-industry sides. However, a more direct mathematical formulation to minimize peak demand is essential to study the economic trade-offs. The trajectories for off-gas measurements for the plant are shown in Fig. 4.9. We can notice that CO consumption is more for NMPC^{up}. NMPC^{up} works with the exact price profiles and is thus able to optimally identify CO as an energy source. It uses 0.16% less of CH₄ and instead generates energy through CO combustion. This is useful in economics and also, there is a decreased impact on the environment.

4.4.3 Case study 2: Price peak increase with price change at 25th min

Next, we investigate the effect of an electricity price profile with different characteristics. We again choose the price change time instant as the 25th minute of the batch

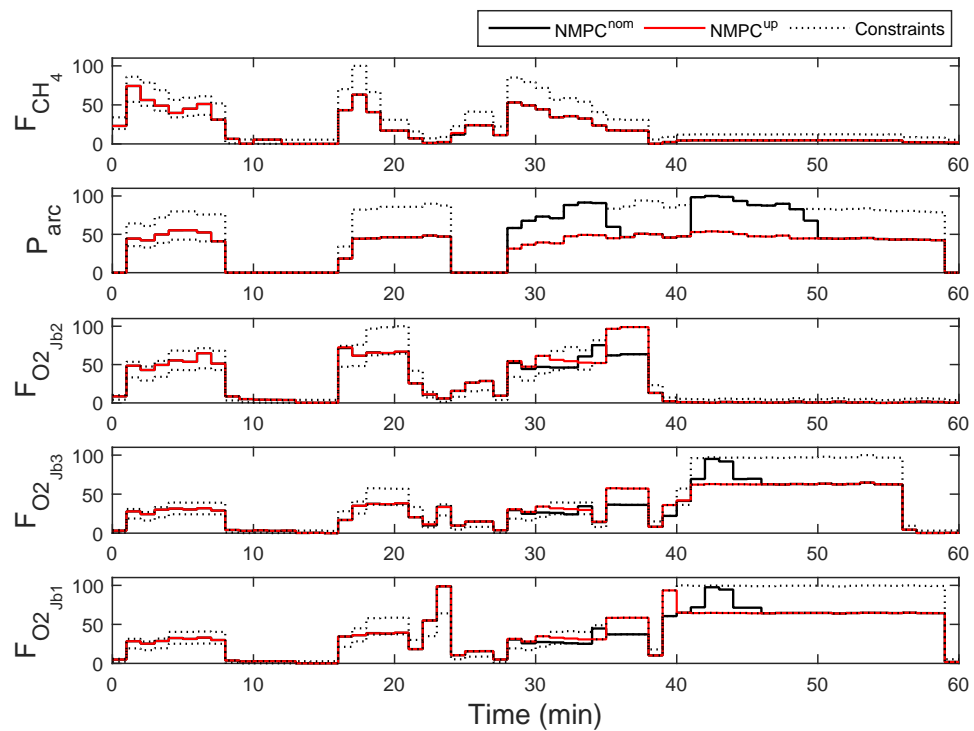


Figure 4.8: Case study 1: Input variable profiles.

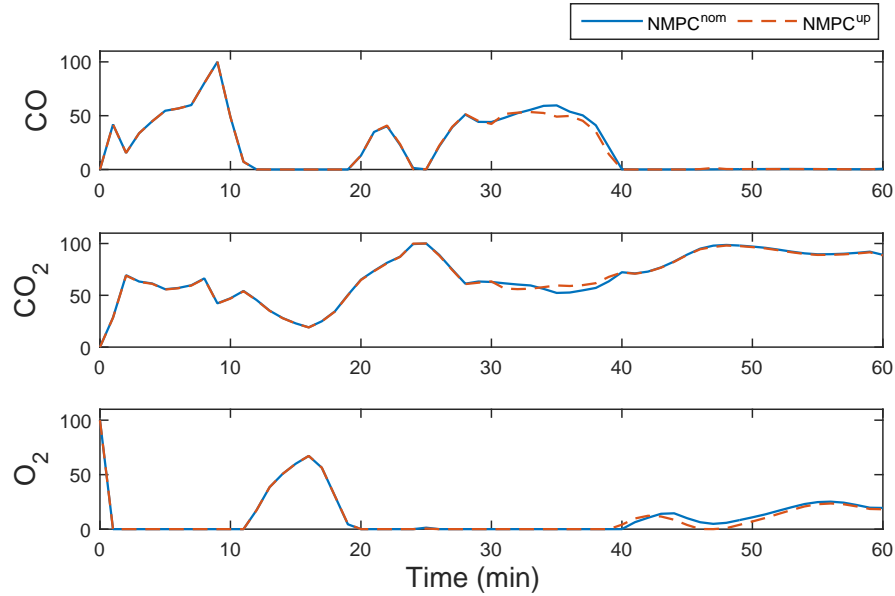


Figure 4.9: Case study 1: Off-gas profiles, scaled to within their maximum and minimum ranges.

duration (see Fig. 4.7b). The actual prices are \$30/MWh and \$200/MWh before and after the change respectively. The predicted price is \$15/MWh as the forecast model is not able to predict a sudden change in the price profile. In this case, NMPC^{up} gives us a 1.54% increase in economic objective value compared to NMPC^{nom}. The increase is lower compared to case study 1 mainly due to the batch operating under a lower actual electricity price (see Fig. 4.7b). This results in more scrap being melted earlier in the batch through increased arc power (see Fig. 4.7b), with less opportunity to reduce costs over the remainder of the batch. The electricity consumption for NMPC^{up} is 8.49% less and other inputs are utilized more by 0.68%. The input profiles are shown in Fig. 4.10. The peak electricity demand during the batch operation is reduced by 10.12% if NMPC^{up} is used instead of NMPC^{nom}.

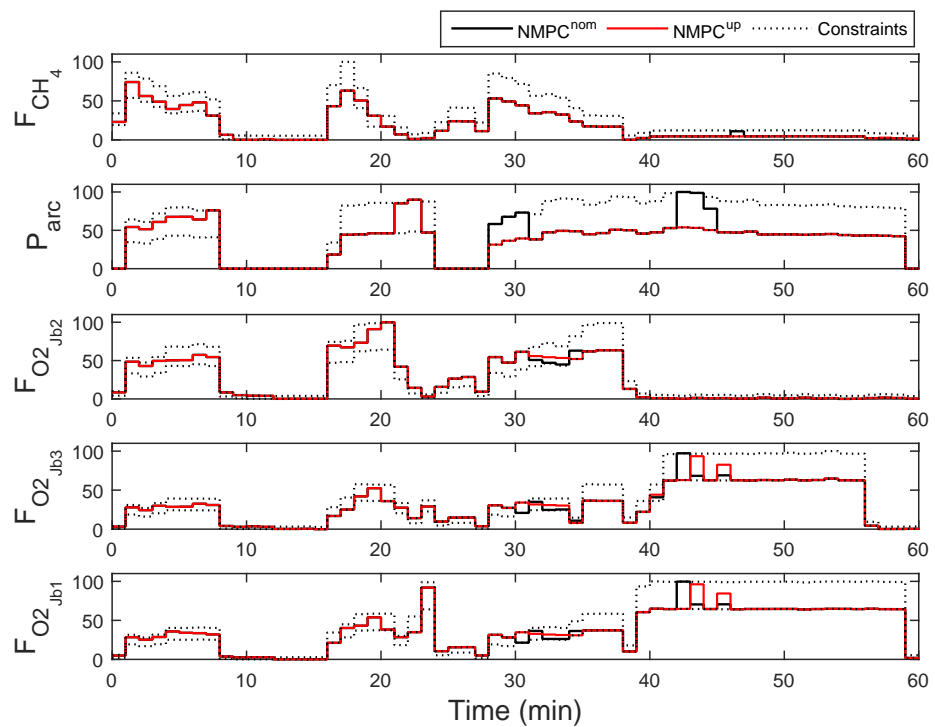


Figure 4.10: Case study 2: Input variable profiles.

4.4.4 Case study 3: Price decrease with a price change at 40th min

This case study uses the same electricity price data of case study 1 but a change in electricity price occurs at the 40th minute of the batch time (see Fig. 4.7c). We obtain a 3.45% increase in economic objective value when NMPC^{up} is employed instead of NMPC^{nom}. The economic objective value increase is less than case study 1 because the forecast error encountered by NMPC^{nom} is for a smaller section of the batch time span. NMPC^{up} utilizes 17.34% less electrical energy and 0.15% more of the other inputs. The peak electricity demand for NMPC^{up} is 14.15% less than that of NMPC^{nom}.

4.4.5 Case study 4: Price decrease with a price change at 15th min

The electricity price data of case study 1 is utilized in this case study, except a change in electricity price occurs at the 15th minute of the batch time (see Fig. 4.7d). NMPC^{up} continues to give a better economic objective value (3.48% increase) when compared with the NMPC^{nom} implementation. Although a greater economic objective value percent increase may be expected due to the earlier electricity price change, this is offset against the shorter duration of the initial high electricity price (\$308/MWh). This results in higher power usage by both schemes before the 25th minute (see Fig. 4.11) with more scrap being melted during this period and less opportunity for cost reduction for the remainder of the batch. NMPC^{up} consumes 17.9% less electric arc power and 4.58% more for the other inputs relative to NMPC^{nom}. The input profiles are shown in Fig. 4.11. The peak electricity demand point for NMPC^{up} is lowered by 10.11% in comparison to the maximum electric arc power utilization during the NMPC^{nom} implementation.

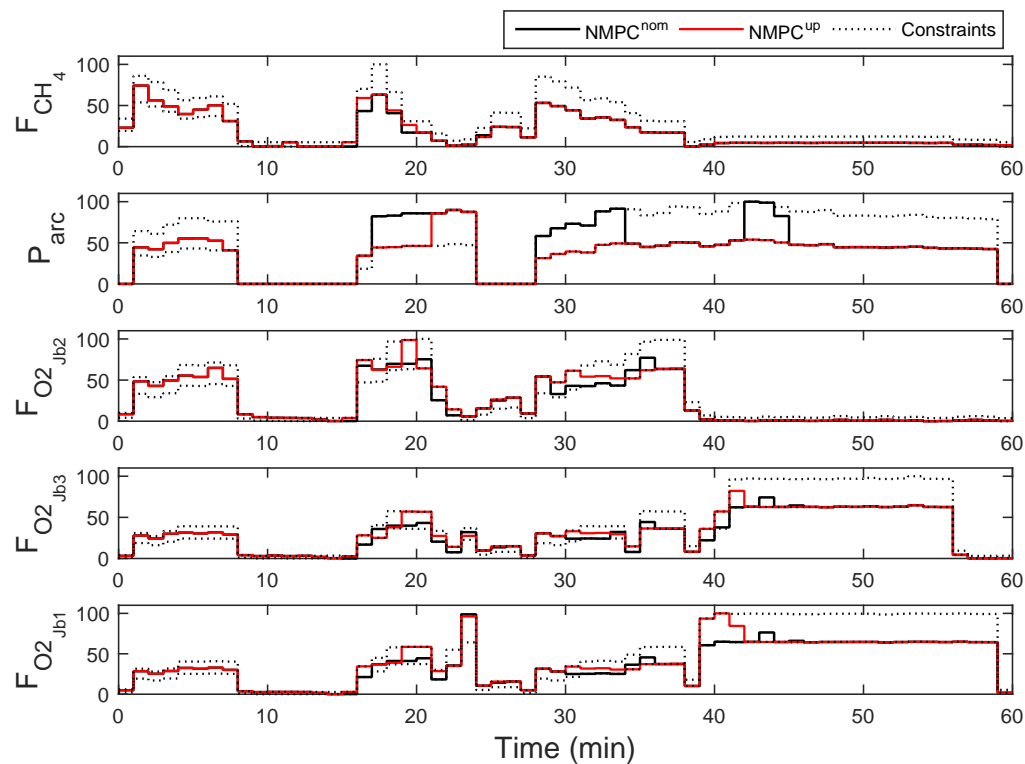


Figure 4.11: Case study 4: Input variable profiles.

4.4.6 Multi-rate MHE performance

We demonstrate the performance of multi-rate MHE in the presence of initial state discrepancy, plant-model mismatch and measurement noise. In all the case studies, the *true* initial conditions are perturbed by adding Gaussian noise with 1% relative variance. As discussed in Section 4.3.4, plant-model mismatch is artificially created by decreasing the power factor parameter k_p by 10%. Gaussian measurement noise is added to the *true* measurements according to their respective variances given in Table 4.2. The covariance matrix Q for model noise is selected based on a detailed analysis of multiple simulations. The moving horizon length is chosen to be 6 minutes. We also introduced upper and lower bounds for the differential states, the algebraic states, and the model noise variables. A subset of the *true* and estimated state variables is plotted with respect to time for case 1 in Fig. 4.12. We can observe that the multi-rate MHE is able to track the *true* states with good accuracy despite the multiple sources of error.

4.4.7 Computational results

An Intel Core i7-3770 processor with 4 CPU cores running Windows 7 at 3.40 GHz was used for all the numerical computations. The CPU times required to solve the multi-rate MHE problems for case study 1 (NMPC^{up}), using the proposed initialization (fMHE) and without using the scheme (nMHE), are shown in Fig. 4.13. The computational results for fNMPC (NMPC using the proposed initialization scheme) and nNMPC (NMPC without using the scheme) are presented in Fig. 4.14. We observe that the initialization scheme is able to reduce the computation time for both the MHE and NMPC significantly. The average CPU time required to solve the fMHE, nMHE, fNMPC and nNMPC problems are 0.7, 1.2, 1.9 and 10 seconds respectively. Thus, there is 76.8% decrease in total (MHE+NMPC) on-line CPU solve time when the proposed initialization scheme is used. Furthermore, computational times required for background MHE and NMPC solves are well within 1 minute.

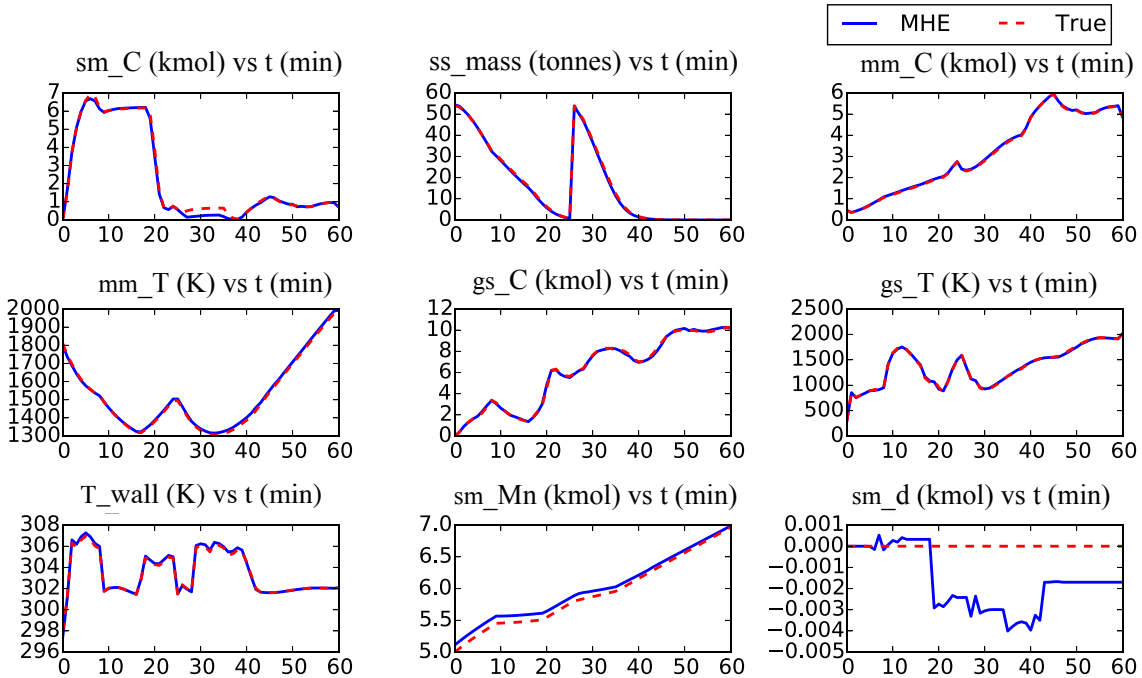


Figure 4.12: State estimates for case study 1 with respect to time (in minutes). sm_C: Carbon in slag-metal zone, ss_mass: Solid scrap mass, mm_C: Carbon in molten metal zone, mm_T: Temperature of molten metal, gs_C: Carbon in gas zone, gs_T: Temperature of gas, T_wall: Furnace wall temperature, sm_Mn: Manganese in slag-metal zone, sm_d: Disturbance state in slag-metal zone.

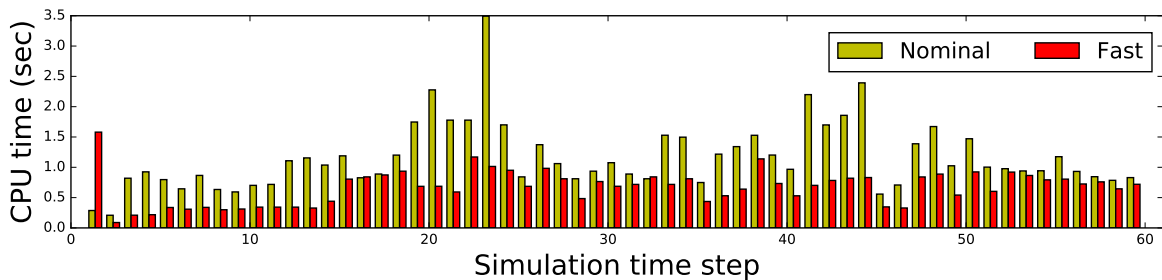


Figure 4.13: Solution times for MHE problems with horizons of $N = 6$ time steps. The solve time denoted by 'fast' represents computational time when the proposed initialization scheme is used. 'Nominal' represents the MHE solves carried out without the use of the proposed initialization scheme.

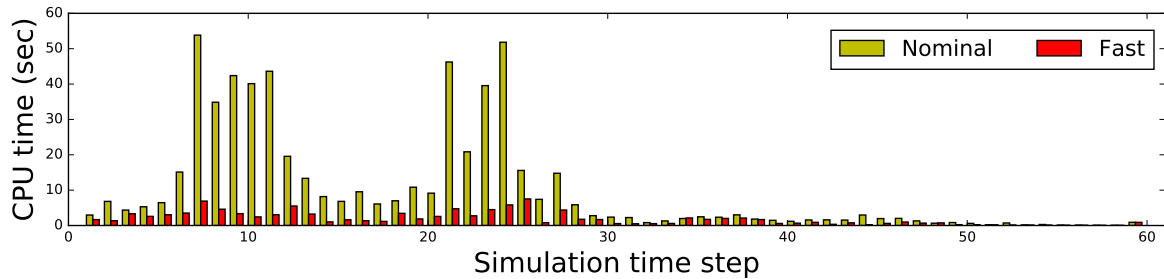


Figure 4.14: Solution times for shrinking horizon NMPC problems. The solve time denoted by ‘fast’ represents computational time when the proposed initialization scheme is used. ‘Nominal’ represents the NMPC solves carried out without the use of the proposed initialization scheme.

4.5 Conclusions and future work

In this work we developed a real-time energy management strategy for batch operation of electric arc furnaces. The strategy is efficient in reducing the energy requirements while effectively exploiting the changing electricity prices. The optimal inputs are computed with the use of a coupled MHE-NMPC application. Moreover, a novel initialization scheme is proposed to reduce the online solution times for the multi-rate MHE and shrinking horizon economics-based NMPC problems. The scheme uses the time between consecutive sampling times to generate warm start points for the upcoming on-line MHE-NMPC solves.

Our case studies focused on demonstrating NMPC economic performance in multiple scenarios of varying electricity prices. NMPC tackled the price variations by balancing the control inputs used to provide the electrical and chemical energy to the process. The challenging EAF process is operated within realistic limits by the economics-based NMPC. The strong convergence ability shown by the multi-rate MHE provided appropriate estimates to the NMPC. With modern power grids moving towards a smarter operation and generation, the proposed strategy can actively fit into and support this new energy utilization and consumption ecosystem. The case studies showed that the high energy intensive EAFs are capable of aiding the power grid by adjusting its operation in real-time through the use of advanced control tools NMPC

and MHE.

Immediate next steps are formulating an NMPC problem that can minimize the peak demand. We also aim to explore NMPC and MHE formulations for the variable batch length problem and incorporate them into an upper level scheduling layer. The integration of scheduling and control is envisaged to generate economic benefit due to better utilization of EAF operating resources. Furthermore, in-plant evaluation of the energy management strategy would be a useful step toward industrial adoption.

References

- [1] Steel Statistical Yearbook of World Steel Association. <http://www.worldsteel.org/steel-by-topic/statistics/steel-statistical-yearbook-.html>. 2016.
- [2] R. J. Fruehan. *The Making, Shaping, and Treating of Steel: Ironmaking volume*. Vol. 2. AISE Steel Foundation, 1999.
- [3] A. W. Dowling, R. Kumar, and V. M. Zavala. "A multi-scale optimization framework for electricity market participation". In: *Applied Energy* 190 (2017), pp. 147–164.
- [4] *Energy Management Brochure for businesses by IESO Ontario*. 2016. URL: www.ieso.ca/-/media/files/ieso/document-library/publications/the-bottom-line-on-energy-management.pdf?la=en.
- [5] Q. Wang, C. Zhang, Y. Ding, G. Xydis, J. Wang, and J. Østergaard. "Review of real-time electricity markets for integrating distributed energy resources and demand response". In: *Applied Energy* 138 (2015), pp. 695–706.
- [6] Q. Zhang and I. E. Grossmann. "Planning and scheduling for industrial demand side management: advances and challenges". In: *Alternative Energy Sources and Technologies*. Springer, 2016, pp. 383–414.
- [7] R. Pattison, C. R. Touretzky, T. Johansson, M. Baldea, and I. Harjunkoski. "Moving horizon scheduling of an air separation unit under fast-changing energy prices". In: *IFAC-PapersOnLine* 49.7 (2016), pp. 681–686.
- [8] S. Billings, F. Boland, and H Nicholson. "Electric arc furnace modelling and control". In: *Automatica* 15.2 (1979), pp. 137–148.
- [9] A. Morris and M. Sterling. "Identification and direct digital control of an electric arc furnace controller". In: *IEE Proceedings D (Control Theory and Applications)*. Vol. 128. 3. IET. 1981, pp. 123–128.
- [10] R. Nadira and P. B. Usoro. "Self-adjusting model algorithmic control of a three-phase electric arc furnace". In: *American Control Conference, 1988*. IEEE. 1988, pp. 227–232.

- [11] P. King and M. Nyman. "Modeling and control of an electric arc furnace using a feedforward artificial neural network". In: *Journal of Applied Physics* 80.3 (1996), pp. 1872–1877.
- [12] B. Boulet, G. Lalli, and M. Ajersch. "Modeling and control of an electric arc furnace". In: *American Control Conference (ACC)*. Vol. 4. IEEE. 2003, pp. 3060–3064.
- [13] D. Oosthuizen, I. Craig, and P. Pistorius. "Model predictive control of an electric arc furnace off-gas procedure combined with temperature control". In: *Africon*. Vol. 1. IEEE. 1999, pp. 415–420.
- [14] J. Bekker, I. Craig, and P. Pistorius. "Model predictive control of an electric arc furnace off-gas process". In: *Control Engineering Practice* 8.4 (2000), pp. 445–455.
- [15] R. D. M. MacRosty and C. L. E. Swartz. "Nonlinear predictive control of an electric arc furnace". In: *IFAC Proceedings Volumes* 40.11 (2007), pp. 285–290.
- [16] R. Amrit, J. B. Rawlings, and D. Angeli. "Economic optimization using model predictive control with a terminal cost". In: *Annual Reviews in Control* 35.2 (2011), pp. 178–186.
- [17] M. Ellis, H. Durand, and P. D. Christofides. "A tutorial review of economic model predictive control methods". In: *Journal of Process Control* 24.8 (2014), pp. 1156–1178.
- [18] M. Ellis and P. D. Christofides. "Economic model predictive control with time-varying objective function for nonlinear process systems". In: *AIChE Journal* 60.2 (2014), pp. 507–519.
- [19] D. Angeli, A. Casavola, and F. Tedesco. "Theoretical advances on Economic Model Predictive Control with time-varying costs". In: *Annual Reviews in Control* 41 (2016), pp. 218–224.
- [20] D. I. Mendoza-Serrano and D. J. Chmielewski. "Smart grid coordination in building HVAC systems: EMPC and the impact of forecasting". In: *Journal of Process Control* 24.8 (2014), pp. 1301–1310.

- [21] J. Feng, A. Brown, D. O'Brien, and D. J. Chmielewski. "Smart grid coordination of a chemical processing plant". In: *Chemical Engineering Science* 136 (2015), pp. 168–176.
- [22] V. M. Zavala and L. T. Biegler. "The advanced-step NMPC controller: Optimality, stability and robustness". In: *Automatica* 45.1 (2009), pp. 86–93.
- [23] M. Diehl, R. Findeisen, F. Allgöwer, H. G. Bock, and J. P. Schlöder. "Nominal stability of real-time iteration scheme for nonlinear model predictive control". In: *IEE Proceedings-Control Theory and Applications* 152.3 (2005), pp. 296–308.
- [24] D. DeHaan and M. Guay. "A new real-time approach for nonlinear model predictive control". In: *IFAC Proceedings Volumes* 38.1 (2005), pp. 1007–1012.
- [25] T. Ohtsuka. "A continuation/GMRES method for fast computation of nonlinear receding horizon control". In: *Automatica* 40.4 (2004), pp. 563–574.
- [26] M. Diehl, H. J. Ferreau, and N. Haverbeke. "Efficient numerical methods for nonlinear MPC and moving horizon estimation". In: *Nonlinear Model Predictive Control*. Springer, 2009, pp. 391–417.
- [27] L. Biegler, X Yang, and G. Fischer. "Advances in sensitivity-based nonlinear model predictive control and dynamic real-time optimization". In: *Journal of Process Control* 30 (2015), pp. 104–116.
- [28] D. Dochain. "State and parameter estimation in chemical and biochemical processes: a tutorial". In: *Journal of Process Control* 13.8 (2003), pp. 801–818.
- [29] V. A. Bavdekar, J. Prakash, S. C. Patwardhan, and S. L. Shah. "A moving window formulation for recursive Bayesian state estimation of systems with irregularly sampled and variable delays in measurements". In: *Industrial & Engineering Chemistry Research* 53.35 (2014), pp. 13750–13763.
- [30] F. Allgöwer, T. A. Badgwell, J. S. Qin, J. B. Rawlings, and S. J. Wright. "Nonlinear predictive control and moving horizon estimation - an introductory overview". In: *Advances in Control*. Springer, 1999, pp. 391–449.

- [31] S. Shyamal and C. L. E. Swartz. "A Multi-rate Moving Horizon Estimation Framework for Electric Arc Furnace Operation". In: *IFAC-PapersOnLine* 49.7 (2016), pp. 1175–1180.
- [32] S. Shyamal and C. L. E. Swartz. "Multi-Rate Moving Horizon Estimation for an Electric Arc Furnace Steelmaking Process". In: *2016 AIChE Annual Meeting* (2016).
- [33] M. M. Rashid, P. Mhaskar, and C. L. Swartz. "Multi-rate modeling and economic model predictive control of the electric arc furnace". In: *Journal of Process Control* 40 (2016), pp. 50–61.
- [34] Y. Li and R. J. Fruehan. "Computational fluid-dynamics simulation of postcombustion in the electric-arc furnace". In: *Metallurgical and Materials Transactions B* 34.3 (2003), pp. 333–343.
- [35] G. A. Irons. "Developments in electric arc furnace steelmaking". In: *AISTECH-Conference Proceedings-*. Vol. 1. Association for Iron & Steel Technology. 2005, p. 3.
- [36] S Matson and W. F. Ramirez. "Optimal operation of an electric arc furnace". In: *57 th Electric Furnace Conference*. 1999, pp. 719–730.
- [37] J. G. Bekker, I. K. Craig, and P. C. Pistorius. "Modeling and simulation of an electric arc furnace process". In: *ISIJ international* 39.1 (1999), pp. 23–32.
- [38] A. Fathi, Y. Saboohi, I. Škrjanc, and V. Logar. "Comprehensive Electric Arc Furnace Model for Simulation Purposes and Model-Based Control". In: *Steel Research International* 88.3 (2017), p. 1600083.
- [39] R. D. M. MacRosty and C. L. E. Swartz. "Dynamic modeling of an industrial electric arc furnace". In: *Industrial & Engineering Chemistry Research* 44 (2005), pp. 8067–8083.
- [40] Process Systems Enterprise Ltd. *gPROMS*, www.psenterprise.com/gproms, 1997–2015. 2015.

- [41] Y. Ghobara. "Modeling, Optimization and Estimation in Electric Arc Furnace (EAF) Operation". MA thesis. McMaster University, 2013, p. 8166.
- [42] J. Andersson. "A General-Purpose Software Framework for Dynamic Optimization". PhD thesis. Department of Electrical Engineering (ESAT/SCD) and Optimization in Engineering Center, Kasteelpark Arenberg 10, 3001-Heverlee, Belgium: Arenberg Doctoral School, KU Leuven, 2013.
- [43] Z. K. Nagy and R. D. Braatz. "Robust nonlinear model predictive control of batch processes". In: *AIChe Journal* 49.7 (2003), pp. 1776–1786.
- [44] D. G. Robertson and J. H. Lee. "On the use of constraints in least squares estimation and control". In: *Automatica* 38.7 (2002), pp. 1113–1123.
- [45] C. V. Rao, J. B. Rawlings, and D. Q. Mayne. "Constrained state estimation for nonlinear discrete-time systems: Stability and moving horizon approximations". In: *IEEE Transactions on Automatic Control* 48.2 (2003), pp. 246–258.
- [46] A. Alessandri, M. Baglietto, and G. Battistelli. "Moving-horizon state estimation for nonlinear discrete-time systems: New stability results and approximation schemes". In: *Automatica* 44.7 (2008), pp. 1753–1765.
- [47] A. Küpper, M. Diehl, J. P. Schlöder, H. G. Bock, and S. Engell. "Efficient moving horizon state and parameter estimation for SMB processes". In: *Journal of Process Control* 19.5 (2009), pp. 785–802.
- [48] V. M. Zavala and L. T. Biegler. "Optimization-based strategies for the operation of low-density polyethylene tubular reactors: Moving horizon estimation". In: *Computers & Chemical Engineering* 33.1 (2009), pp. 379–390.
- [49] F. Magnusson and J. Åkesson. "Dynamic optimization in JModelica.org". In: *Processes* 3.2 (2015), pp. 471–496.
- [50] R. López-Negrete and L. T. Biegler. "A moving horizon estimator for processes with multi-rate measurements: A nonlinear programming sensitivity approach". In: *Journal of Process Control* 22.4 (2012), pp. 677–688.

- [51] L. Ji and J. B. Rawlings. "Application of MHE to large-scale nonlinear processes with delayed lab measurements". In: *Computers & Chemical Engineering* 80 (2015), pp. 63–72.
- [52] S Kramer, R. Gesthuisen, and S Engell. "Fixed structure multirate state estimation". In: *American Control Conference (ACC)*. Vol. 7. IEEE. 2005, pp. 4613–4618.
- [53] S. Krämer and R. Gesthuisen. "Multirate state estimation using moving horizon estimation". In: *16th IFAC World Congress, IFAC Proceedings Volumes* 38.1 (2005), pp. 1–6.
- [54] C. C. Qu and J. Hahn. "Computation of arrival cost for moving horizon estimation via unscented Kalman filtering". In: *Journal of Process Control* 19.2 (2009), pp. 358–363.
- [55] R. Lopez-Negrete, S. C. Patwardhan, and L. T. Biegler. "Constrained particle filter approach to approximate the arrival cost in moving horizon estimation". In: *Journal of Process Control* 21.6 (2011), pp. 909–919.
- [56] J. B. Rawlings. "Moving horizon estimation". In: *Encyclopedia of Systems and Control* (2014), pp. 1–7.
- [57] R. Huang, V. M. Zavala, and L. T. Biegler. "Advanced step nonlinear model predictive control for air separation units". In: *Journal of Process Control* 19.4 (2009), pp. 678–685.
- [58] P. Kühl, M. Diehl, T. Kraus, J. P. Schlöder, and H. G. Bock. "A real-time algorithm for moving horizon state and parameter estimation". In: *Computers & Chemical Engineering* 35.1 (2011), pp. 71–83.
- [59] L. T. Biegler. *Nonlinear programming: concepts, algorithms, and applications to chemical processes*. SIAM, 2010.
- [60] A. Wächter and L. T. Biegler. "On the implementation of an interior-point filter line-search algorithm for large-scale nonlinear programming". In: *Mathematical Programming* 106.1 (2006), pp. 25–57.

- [61] A. C. Hindmarsh, P. N. Brown, K. E. Grant, S. L. Lee, R. Serban, D. E. Shumaker, and C. S. Woodward. “SUNDIALS: Suite of nonlinear and differential/algebraic equation solvers”. In: *ACM Transactions on Mathematical Software (TOMS)* 31.3 (2005), pp. 363–396.

Chapter 5

Real-time Dynamic Optimization-based Advisory System

5.1	Introduction	118
5.2	Electric arc furnace model	123
5.3	Dynamic optimization problem	125
5.4	Multi-tiered Optimization	129
5.5	Multi-rate Moving Horizon Estimation	135
5.6	Real-time Advisory System	141
5.7	Case studies	147
5.8	Conclusion	157
	References	157

The formulations and results in this chapter have been submitted, and will be presented in:

- [1] S. Shyamal and C.L.E. Swartz. "Real-Time Dynamic Optimization-based Advisory System for Electric Arc Furnace Operation". *Industrial and Engineering*

Chemistry (2018), submitted.

- [2] S. Shyamal and C.L.E. Swartz. "Operator-Triggered Advisory System for Electric Arc Furnace Process Optimization". *AIChE Annual Meeting* (2018). Pittsburgh, PA, USA.

Electric arc furnaces (EAFs) are widely applied in the steel industry for producing steel by melting scrap metal. This highly energy intensive steelmaking process is subject to limited automation, with decisions related to input amounts and timings taken by the operators. This leads to suboptimal EAF batch operation due to complex behaviors and relationships between variables that are inevitably not considered in the decision making. In this work, we introduce an advisory system that employs a first-principles EAF model to support the operator decision making in real time for economically optimal process operation. A dynamic optimization calculation can be triggered by the operator at any point in the batch, an action that can be repeated multiple times during the batch. The advisory system incorporates a multi-rate moving horizon estimator (MHE) that continually computes estimates of the process states utilizing current and past inputs and measurements. End-point constraints and potential extension of the batch duration are handled through a multi-tiered optimization algorithm. Our case studies demonstrate a major economic improvement when the dynamic optimization-based advisory system is used. We show that the online computational load is under 5 seconds on average when a proposed multi-tiered initialization scheme is used for solving the large-scale optimal control problems.

5.1 Introduction

Electric arc furnaces (EAFs) are widely used in the steel industry for production of steel by melting scrap steel collected from different sources, with approximately 25% of the world's steel production generated using EAFs [1]. Melting of steel is a highly energy intensive batch process, with the required energy provided in form of electrical and chemical energy. A single batch operation consumes approximately 400 kilowatt-hours/ton of steel produced [2]. The electrical energy is supplied through electric arcs to the scrap metal via multiple electrodes. The main sources of chemical energy are combustion of natural gas and oxygen injected through burners, and exothermic chemical reactions in a slag layer that floats above the molten metal. Also added to the EAF are carbon (both directly charged and lanced), fluxes comprising

lime and dolomite for formation of a reactive slag, and lanced oxygen. Key reactions taking place are formation of CO that contributes to a foamy slag that is useful for insulation of the furnace walls and roof from the arc, and oxidation of several elements in the bath. The high energy consumption by EAFs motivates the research and development of advanced control, estimation and optimization strategies for efficient and cost optimal operation. However, large fluctuations during the process, harsh operating conditions, and the limited availability of measurements pose challenges for real-time process optimization. EAFs are currently operated without the use of sophisticated optimization tools, with EAF operating decisions typically taken based on what has worked in the past. Given the relatively low level of automation in EAFs, fully automated dynamic real-time optimization is unlikely to be accepted by EAF operating personnel at present. However, there is an opportunity for designing an advisory system where the operators have a choice as to whether or not to implement the control moves calculated by economics-based real-time dynamic optimization. In this work, we introduce a real-time advisory system to enhance the EAF operation and generate savings through optimal utilization of inputs.

Early research works on EAF optimization focused on finding optimal operating decisions using a simplified model or a model describing only a subprocess/subsystem of the EAF. Woodside et al. utilized a 2 state model to formulate an optimal control problem to minimize EAF power usage [3]. Oosthuizen et al.[4] formulated and solved a set-point tracking model predictive control (MPC) problem which utilized a linear model. Bekker et al.[5] solved a MPC problem to track set-points of three variables for their EAF model . While a linear dynamic model may yield adequate performance for set-point tracking in EAF operations, they are less suitable for economic optimization due to model inaccuracy over the typically wide operating range. Matson and Ramirez developed a full-scale EAF model based on dynamic mass and energy balances, and used it to conduct dynamic optimization to minimize the FeO production, batch time and offgas CO content [6]. More recently, MacRosty and Swartz[7] developed a first-principles based differential-algebraic equation (DAE) model for an EAF,

and subsequently used it in a rigorous dynamic optimization framework[8]. They showed that dynamic optimization can be used to maximize profit by considering trade-offs between various inputs and processing time. A sequential approach was utilized in their work to solve the dynamic optimization problems. MacRosty and Swartz proposed an economics-based nonlinear MPC (NMPC) framework for EAF operation which utilized a comprehensive dynamic EAF model [9]. However, they assumed the availability of full system state and solved the dynamic optimization problem using a sequential solution approach. Rashid et al.[10, 11] formulated and solved an economic model predictive control (EMPC) problem for EAF operation, but instead of a rigorous first-principles model, they used data-driven models. Shyamal and Swartz[12] proposed an optimization-based decision support tool (DST) for EAF operation where MHE was coupled with a dynamic optimization implementation. The DST framework allowed the operators to execute the dynamic optimization when the need arises. The tracking ability of MHE was demonstrated only when the system is affected by measurement noise and plant-model mismatch; no initial state discrepancy was considered. Also recently, multi-rate MHE with NMPC was used to design a real-time energy management strategy for EAF operation [13]. In both the research works by Shyamal and Swartz[12, 13], the optimizer was allowed to manipulate only five inputs, and no strategy was provided to deal with potential infeasibilities associated with the end-point constraints. Our focus in this chapter is on the development of a framework for operator-triggered reoptimization, with the explicit handling of potential end-point infeasibilities through a multi-tiered optimization strategy.

For on-line reoptimization, state knowledge is necessary for initialization of the dynamic optimization problem. Although many tools such as the Extended Kalman Filter (EKF), Unscented Kalman Filter (UKF)[14], or particle filter are used by researchers for state estimation, moving horizon estimation (MHE) has become popular over the last decade due to its straightforward way of handling constraints [15, 16], use of a full-scale dynamic model in optimization and utilization of state-of-the-art

numerical optimization algorithms for fast solution times [17]. Significant effort is usually directed to solving the MHE problems quickly so as to avoid feedback delays. Since EAFs are characterized by availability of limited sensor measurements, it is difficult to obtain quality state estimates for an on-line implementation. Moreover, the measurements have different sampling rates and unknown disturbances often affect the process operation. There are limited research works available where state estimation is applied to an EAF. An EKF was employed by Billings and coworkers [18] for estimating states when the EAF process is in the refining stage. Since the model had only 4 states, it is insufficient to capture the detailed process complexity. Constrained multi-rate EKF has also been employed using a linearized state space model of the EAF[19]. An MHE optimization formulation for solution via a sequential approach was proposed by Shyamal and Swartz[20].

In this chapter, we propose a real-time dynamic optimization-based advisory system for EAF process operation. The advisory system utilizes a first-principles model to provide decision support to the operators by suggesting economics-based optimal input profiles. It uses multi-rate MHE to calculate state estimates at every sampling time; however, they are only sent to the multi-tiered optimizer if the operator calls for decision support. The operator triggered framework is very useful for the steel industry where a hybrid between open and closed-loop control has a good likelihood of acceptance, and is applicable to other batch and semi-batch processes as well. Our advisory system development builds on the earlier work of Shyamal and Swartz[12] but differs from it in several aspects. The framework proposed here includes a novel multi-tiered optimization algorithm to handle end-point constraints, five additional manipulated inputs are included which increases the dimension and complexity of the optimization problem on-line, model contraction that is implemented is described in detail, a multi-tiered initialization scheme is proposed for fast solution of the optimal control problems, and finally, our case studies relax the assumption of perfect initial state knowledge.

An integral component of the advisory system is the multi-tiered optimizer, which comprises three hierarchical optimization tiers to handle end-point constraint infeasibilities. A shrinking horizon formulation with an economics-based objective function is used for the optimization tiers. A key bottleneck in implementing real-time advanced control systems is the computational burden associated with solving the large-scale dynamic optimization problems on-line. For obtaining fast solutions to the MHE and the tiered-dynamic optimization problems, a simultaneous dynamic optimization approach is employed, in which the problem is transformed into a sparse nonlinear-programming (NLP) problem by discretizing the states and inputs [21]. The MHE-NMPC initialization scheme proposed in Shyamal and Swartz [13] is extended to develop a warm-start strategy for effective initialization of the dynamic optimization problems in the advisory system. The efficacy of the advisory system is evaluated for the EAF process using two case studies, through which four key factors are explored: (1) the impact of re-optimizations at different time points during the batch process operation, (2) handling of potential end-point constraint infeasibilities by increasing the degrees of freedom through stretching of the batch duration, (3) the convergence of MHE, and (4) computational feasibility of a real-time application. Our results show a major improvement in the profit obtained when the advisory system is invoked.

The remainder of the chapter is structured as follows. Section 5.2 provides a description of the EAF process model. Section 5.3 introduces the dynamic optimization problem and model contraction is discussed. Section 5.4 presents the multi-tired optimization algorithm for batch processes where the working of the three tiers is explained. We also show how the algorithm is tailored for the EAF process. The multi-rate MHE problem along with the arrival cost update formulation is discussed in Section 5.5. Section 5.6 describes the algorithmic implementation details of the real-time dynamic optimization-based advisory system. The description of the multi-tiered initialization scheme is also provided in this section. Section 5.7 presents the case studies for the electric arc steelmaking process, where the effectiveness of the

advisory system is demonstrated. Section 5.8 concludes the paper and identifies future research directions.

5.2 Electric arc furnace model

EAF operation is characterized by its complexity and the extreme conditions under which the process operates. A key challenge associated with modeling the EAF process is capturing sufficient detail to adequately track the economics and key states of the process, while yielding fast enough solutions for real-time application. Very detailed computational fluid dynamics (CFD) models are typically available only for a section of the furnace [22, 23]. Three-dimensional models are appropriate for yielding fast enough engineering and design studies but not suitable for real-time optimal control applications [24]. Models with reasonable simulation times are generally based on simplifying assumptions and typically divide the EAF into multiple zones [25, 5, 26]. Detailed physics-based mathematical equations are then employed to describe the heat and mass transfer occurring within and in-between the zones.

The dynamic first-principles based EAF model used in this paper is based on that proposed by MacRosty and Swartz[7], which considers four zones, namely, gas, slag-metal, molten-metal and solid scrap zones, as depicted in Fig. 5.1. The *gas zone* represents the gases which fill up the furnace volume above the solid scrap metal. The *slag-metal interaction* zone considers the liquid slag materials and the part of the molten-metal layer which remains in contact with the slag. The *molten-metal* zone considers metals in their molten form once scrap begins to melt. It excludes the part of liquid mass already considered in the *slag-metal* zone. The *solid scrap* zone consists of the non-melted scrap mass in solid form. The process phenomena happening in the each of the four zones are modeled through the mass and energy balances. A key advantage of the equilibrium-based modeling is that we need to deal with fewer parameters compared to a kinetics-based approach. The multi-zone system [7] assumes chemical equilibrium in *slag-metal* and *gas* zones. The equilibrium is

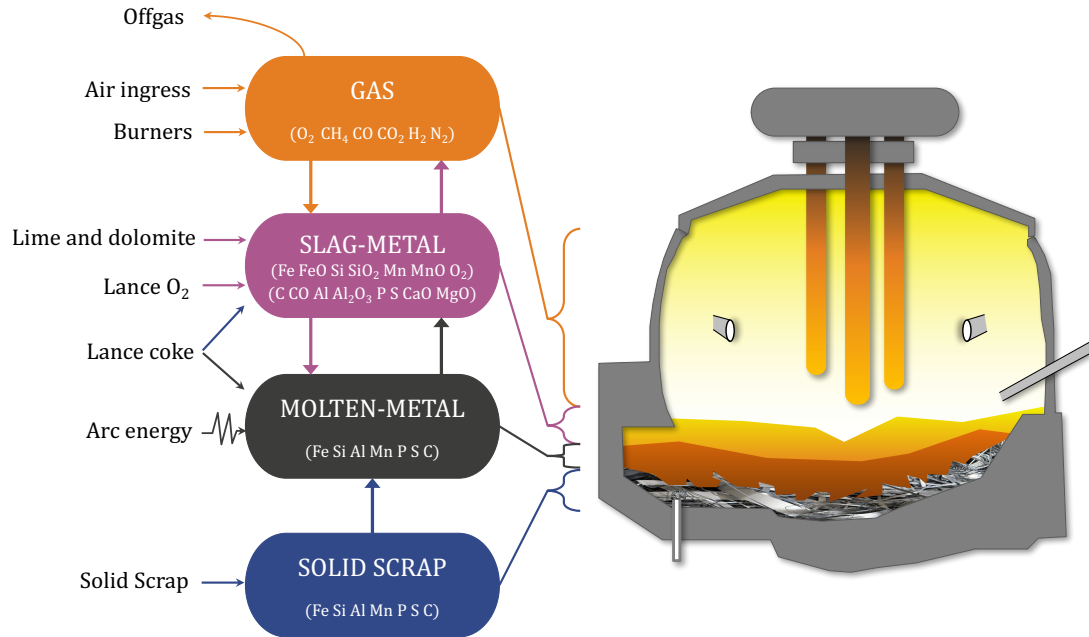


Figure 5.1: Schematic of the EAF model [7, 13] used in the study showing the 4 zones and associated inputs, outputs and material flows.

determined by incorporating equations for minimization of Gibbs free energy. The model also considers slag foaming, which is caused by evolution of carbon monoxide, through empirical relationships. The materials are tracked within and between each zone through mass transfer equations and elemental balances. Detailed mathematical relationships take in to account of the heat transfer from the arc, chemical reactions, convective and radiative heat transfers. Model parameters were estimated in gPROMS/gEST[27] by employing the maximum likelihood function and using real plant data sets. The EAF model was modified by Ghobara [19] to include models for three JetBoxes which provide oxygen and also a flat geometry was assumed instead of a cone-frustum for scrap melting. The commercial modeling tool gPROMS was used to model the DAE system which consisted of 40 differential and 1050 algebraic states.

The highly nonlinear radiation model which accounted for the radiative heat transfer in the EAF was removed in [20] and replaced with a parameter which partitions the arc energy between molten-metal, scrap metal, furnace roof and walls. Parameters

were re-estimated to obtain matching profiles with the plant data. Also, since *molten-metal* zone contains negligible amounts of metal oxides, it was assumed that all the metal oxides are contained in the *slag-metal* zone. The state variables associated with metal oxides in the *molten-metal* zone were removed. The modified model contained 29 differential states. The gPROMS model [20] was translated to a Python-based CasADI [28] framework for carrying out optimization using the simultaneous approach [12, 13]. Also, a state variable which attained negligible values ($\sim 1.0 \times 10^{-13}$) was removed and replaced with a parameter. In this work we employ the EAF model used in [12, 13] to do a detailed analysis using three case studies. The DAE model has 28 differential and 518 algebraic variables. The model further went through a model contraction procedure[12, 13] described in Section 5.3. In the next section we describe the general dynamic optimization problem and the proposed multi-tiered optimization strategy to tackle the end-point constraints.

5.3 Dynamic optimization problem

In this section, we describe the general form of dynamic optimization problem we solve in this work.

5.3.1 Model formulation

A wide class of first principles-based models can be represented as a differential-algebraic equation (DAE) system, written in semi-explicit form as

$$\dot{\mathbf{x}}(t) = \mathbf{f}'_d(\mathbf{x}(t), \mathbf{z}'(t), \mathbf{u}(t), \mathbf{p}) \quad (5.1a)$$

$$\mathbf{0} = \mathbf{f}'_a(\mathbf{x}(t), \mathbf{z}'(t), \mathbf{u}(t), \mathbf{p}) \quad (5.1b)$$

$$\mathbf{y}(t) = \mathbf{h}(\mathbf{x}(t), \mathbf{z}'(t)) \quad (5.1c)$$

$$\mathbf{x}(t_i) = \mathbf{x}_{0i} \quad (5.1d)$$

$$t \in [t_i, t_f] \quad (5.1e)$$

where \mathbf{x} represents the set of differential state variables and \mathbf{z}' the set of algebraic variables, the process is described through equations \mathbf{f}'_d and \mathbf{f}'_a . The inputs for the system are represented by \mathbf{u} , and the system parameters are denoted by \mathbf{p} . The equations \mathbf{h} describe the mapping of the differential and algebraic states to system outputs \mathbf{y} . The system evolves from given initial time t_i to final time t_f for given initial states \mathbf{x}_{0i} .

The inputs are typically parameterized, with piecewise constant or piecewise linear function being common choices. The high dimension of DAEs arising in the modeling of large-scale process systems has prompted the development of model reduction techniques [29, 30]. Here, we describe model contraction which preserves the integrity of the original DAE system, but reduces the search space through elimination of variables through the equality constraints, and is a step that is available in solver platforms such as CasADI.

5.3.2 Model contraction

We describe model contraction as a procedure to eliminate a subset of algebraic variables by converting them into dependent variables \mathbf{d} . Such an elimination process will also remove an equal number of algebraic equations[31]. The contracted model is given as,

$$\dot{\mathbf{x}}(t) = \mathbf{f}_d(\mathbf{x}(t), \mathbf{z}(t), \mathbf{u}(t), \mathbf{p}) \quad (5.2a)$$

$$\mathbf{0} = \mathbf{f}_a(\mathbf{x}(t), \mathbf{z}(t), \mathbf{u}(t), \mathbf{p}) \quad (5.2b)$$

$$\mathbf{d}(t) = \mathbf{f}_e(\mathbf{x}(t), \mathbf{z}(t), \mathbf{u}(t), \mathbf{p}) \quad (5.2c)$$

$$\mathbf{y}(t) = \mathbf{h}(\mathbf{x}(t), \mathbf{z}(t), \mathbf{d}(t)) \quad (5.2d)$$

$$\mathbf{x}(t_i) = \mathbf{x}_{0i} \quad (5.2e)$$

$$t \in [t_i, t_f], \quad (5.2f)$$

where, \mathbf{d} is a subset of \mathbf{z}' , and \mathbf{z} are the remaining algebraic variables. It is to be noted that the above model contraction preserves the model fidelity; however, the model sparsity is sacrificed to obtain a more compact DAE model than the original one. A useful outcome of this procedure is that equations (5.2c) describing the evolution of \mathbf{d} can be considered external to the model with \mathbf{d} is post-calculated. Although we represent the new differential equation function as \mathbf{f}_d , dimension of \mathbf{f}_d is equal to dimension of \mathbf{f}'_d . If \mathbf{d} appears in constraints or the objective function, then the explicit expression \mathbf{f}_e is used instead. Such a substitution is potentially needed when formulating a dynamic optimization or an MHE problem.

We have implemented model contraction using the CasADi framework [28]. The reformulation is achieved by calling the in-built function ‘eliminate_alg()’ on the DAE system (described using the in-built ‘DaeBuilder class’ of CasADi). The function symbolically reformulates the DAE system and directly provides the contracted DAE system. However, the elimination process is transparent to the user. Symbolic transformation methods are described in detail in Magnusson[31].

Remark: Model contraction is also implemented in the software package, JModelica [32]. gPROMS [27] implements a similar internal restructuring referred to as called ‘model pruning’ for obtaining a minimum-sized model for simulation and optimization tasks. However, for implementation of model contraction from the ground up, the user guides of CasADi and JModelica (and the references given there) are useful resources.

5.3.3 Optimization formulation

Given the current states \mathbf{x}_i provided by a state estimation strategy at time t_i , the dynamic optimization problem takes the following general form

$$\max_{\mathbf{u}(t), t \in [t_i, t_f]} \quad \Phi(t_f) := \int_{t_i}^{t_f} \psi(\mathbf{x}(t), \mathbf{z}(t), \mathbf{u}(t), \mathbf{p}) dt \quad (5.3a)$$

$$\text{subject to } \dot{\mathbf{x}}(t) = \mathbf{f}_d(\mathbf{x}(t), \mathbf{z}(t), \mathbf{u}(t), \mathbf{p}), \quad (5.3b)$$

$$\mathbf{0} = \mathbf{f}_a(\mathbf{x}(t), \mathbf{z}(t), \mathbf{u}(t), \mathbf{p}), \quad (5.3c)$$

$$\mathbf{u}^L \leq \mathbf{u}(t) \leq \mathbf{u}^U, \quad (5.3d)$$

$$\mathbf{x}^L \leq \mathbf{x}(t) \leq \mathbf{x}^U, \quad \forall t \in [t_i, t_f] \quad (5.3e)$$

$$\mathbf{x}_f^L \leq \mathbf{x}(t_f) \leq \mathbf{x}_f^U, \quad (5.3f)$$

$$\mathbf{z}^L \leq \mathbf{z}(t) \leq \mathbf{z}^U, \quad (5.3g)$$

$$\mathbf{x}(t_i) = \mathbf{x}_i, \quad (5.3h)$$

where Φ represents the objective function. We aim to find the optimal inputs \mathbf{u} so as to maximize Φ while satisfying the model equations 5.3b and (5.3c), and constraints on inputs (5.3d), algebraic variables (5.3g) and differential state variables (5.3e), (5.3f). The superscripts L and U represent the lower and upper bounds respectively. This general representation admits various types of objective function such as an economics-based objective function, set-point tracking MPC objective function, and so forth.

A key bottleneck in solving the above dynamic optimization problem in batch control applications is the end-point constraint (5.3f). This is typically hard to satisfy since it is possible that with a given \mathbf{x}_i , no set of inputs can help steer the states to the region $[\mathbf{x}_f^L, \mathbf{x}_f^U]$ within a fixed time horizon $[t_i, t_f]$. An immediate consequence can be optimization solvers flagging an infeasibility output solve message leading to an overall halt of an advanced control procedure. This is highly undesirable from a practical implementation standpoint, and an effective strategy is needed to generate useful optimization results even when faced with such situations. One way to tackle the problem is to include the final time t_f in the decision variable space for the optimization problem [33], which for a fixed number of control variables stretches/contracts control intervals to find the optimal t_f [34]. Apart from an increase in the problem complexity, a couple of key issues arise. First, accuracy of numerical discretization will decrease if control intervals are stretched. Although an adaptive discretization

scheme can be employed, the problem complexity will increase substantially. Second, there will be a mismatch in the sampling times and control intervals, which will pose implementation challenges. Thus, development of a resilient real-time strategy is necessary when a simply removing the end-point constraint is not acceptable. Having described the general dynamic optimization problem, in the next subsection we propose a multi-tiered optimization strategy for dynamic optimization with end-point constraints.

5.4 Multi-tiered Optimization

In this section, we present a strategy for handling a dynamic optimization problem with end-point constraints through multi-tiered optimization. The strategy incorporates three sequential dynamic optimization tiers where the second and third tier come into effect when the previous tier fails to give a solution. It is particularly useful for end-point constraints for which the likelihood of feasibility increases with batch time, such as residual solid scrap or content of carbon in the molten steel in electric arc steelmaking. An important characteristics of the strategy is that for problems in which the end-point constraints limit problem feasibility, application of the tiered optimization approach terminates with a feasible solution to a modified problem, that is generally also acceptable from an industrial application perspective. We describe each of the three tiers in the subsequent subsections.

5.4.1 Tier 1: Direct optimization

In this tier, we directly attempt to solve the original dynamic optimization problem given in (5.3a)-(5.3h). Any of the three dynamic optimization approaches viz. sequential, simultaneous and multiple-shooting can be employed to solve the problem. However, the NLP solvers used in the three approaches are allowed to carry out the optimization up to a maximum number of iterations max_{iter} . In order for the

solver optimization procedure to terminate within reasonable time. The max_{iter} is a tunable parameter and a suitable value can be chosen depending on the problem size and computational time needed for each solver iteration. If the solver declares optimality upon termination, then we do not move to the next tier. However, if the solver terminates due to infeasibility or maximum number of iterations begin reached, then we proceed to Tier 2.

5.4.2 Tier 2: Feasibility through horizon extension

In Tier 2, we reformulate the original dynamic optimization problem of Tier 1 to enhance the likelihood of achieving feasibility. The time horizon $t \in [t_i, t_f]$ considered in Tier 1 is extended in integral steps. The extended problem for N_e integer time steps extension is given as

$$\max_{\mathbf{u}(t), t \in [t_i, t_f + N_e \Delta T]} \Phi(t_f + N_e \Delta T) := \int_{t_i}^{t_f + N_e \Delta T} \psi(\mathbf{x}(t), \mathbf{z}(t), \mathbf{u}(t), \mathbf{p}) dt \quad (5.4a)$$

subject to Extended set of equations :

$$(5.3b) - (5.3d), (5.3g), (5.3h), \quad (5.4b)$$

$$\mathbf{x}^L \leq \mathbf{x}(t) \leq \mathbf{x}^U, \quad \forall t \in [t_i, t_f + N_e \Delta T] \quad (5.4c)$$

$$\mathbf{x}_f^L \leq \mathbf{x}(t) \leq \mathbf{x}_f^U, \quad t = t_f + N_e \Delta T. \quad (5.4d)$$

This extension provides additional inputs for manipulation by dynamic optimization. These additional degrees of freedom provide a straightforward way to enhance the achievement of feasibility for systems where end-point constraints are more likely to be satisfied when batch length is extended. We describe a serial and a parallel implementation for Tier 2:

- **Serial implementation:** First, a 1 time step extension problem ($N_e = 1$) is formulated and solved. If it remains infeasible or the maximum number of iterations is reached, then a second problem where $N_e = 2$ is solved. This sequence of problem is continued up to a specified limited number of time step

extensions N_{ext} . If a feasible solution is not achieved within the iteration limit at the maximum extended batch length, we proceed to Tier 3; otherwise we stop in Tier 2 and report the solution obtained with the associated extension (number of time steps: $N_{e_{min}}$ value) required to achieve feasibility.

- **Parallel implementation:** We formulate and solve N_{ext} extended problems in parallel. This effectively uses available parallel computational architecture. Solver exit messages for all the N_{ext} solves are collected and then if none of them is solved to full optimality, we proceed to Tier 3. If one or more problems are solved, then we choose the extension $N_{e_{min}}$ associated with the solve with the minimum extension value.

Both the implementations attempt to find the minimum integral extension required to achieve feasibility. It is to be noted that the two implementations are attempting to solve a mixed-integer dynamic optimization (MIDO)[35, 36] problem via explicit enumeration. If feasibility is not achieved, then we move to the final Tier 3 which is described below.

5.4.3 Tier 3: End-point constraint relaxation

In this tier, we reformulate the extended problem of Tier 2 by softening[37] the end-point constraint at $t_f + N_{ext}\Delta T$ using slack variable ϵ . The reformulated problem is given as

$$\max_{\mathbf{u}(t), t \in [t_i, t_f + N_{ext}\Delta T]} \Phi(t_f + N_{ext}\Delta T) := \int_{t_i}^{t_f + N_{ext}\Delta T} \psi(\mathbf{x}(t), \mathbf{z}(t), \mathbf{u}(t), \mathbf{p}) dt + \|\boldsymbol{\epsilon}\|_{D-1}^2 \quad (5.5a)$$

$$\text{subject to } (5.4b), (5.4c) \quad (5.5b)$$

Softened end-point constraint:

$$\mathbf{x}_{t_f + N_{ext}\Delta T}^L - \boldsymbol{\epsilon} \leq \mathbf{x}(t_f + N_{ext}\Delta T) \leq \mathbf{x}_{t_f + N_{ext}\Delta T}^U + \boldsymbol{\epsilon} \quad (5.5c)$$

$$\boldsymbol{\epsilon} \geq \mathbf{0}, \quad (5.5d)$$

where the modified objective function contains the additional least squares penalty term for the slack variables. The weighting for each of the slack variables in the penalty term is given by diagonal matrix D . The soft constraint (5.5c) accommodates any infeasibility caused due to end-point constraint violation at $t_f + N_{ext}\Delta T$.

This relaxed problem will be feasible if feasibility is limited by end-point constraints, and we stop at Tier 3. The use of three tiers is designed to arrive at a reasonable solution to the original problem in circumstances where the original problem is not feasible; with the solutions thus obtained implemented on the plant. The working of the three tiers is summarized in Fig. 5.2. A hierarchical or multi-tiered approach for prioritizing objectives in dynamic optimizations was proposed in Swartz[38], and a tiered approach was also employed by Chong and Swartz[39, 40, 41, 42] to design frameworks for optimal operation of plants during shutdowns. The optimization tiers aiming to these studies are used to handle prioritized objectives with consideration of feasibility. The present tiered algorithm, however, has no conflicting optimization objectives, and is used to resolve infeasibilities caused due to end-point constraints. In the next subsection we describe the specific application of the multi-tiered optimization to EAF operation.

5.4.4 EAF Implementation

We aim to maximize the economics of the EAF batch process by solving a dynamic optimization problem based on the first-principles EAF model. The optimization is tackled through the multi-tiered optimization strategy before the decision support is provided to the operator. The first tier, *direct optimization*, solves a shrinking horizon dynamic optimization problem with an economic objective and a constraint on the end point solid scrap mass m_{ss} . The second and third tiers come into effect if infeasibility is detected in Tier 1. The second tier attempts to achieve feasibility through horizon extension, whereas the third tier solves a relaxed problem.

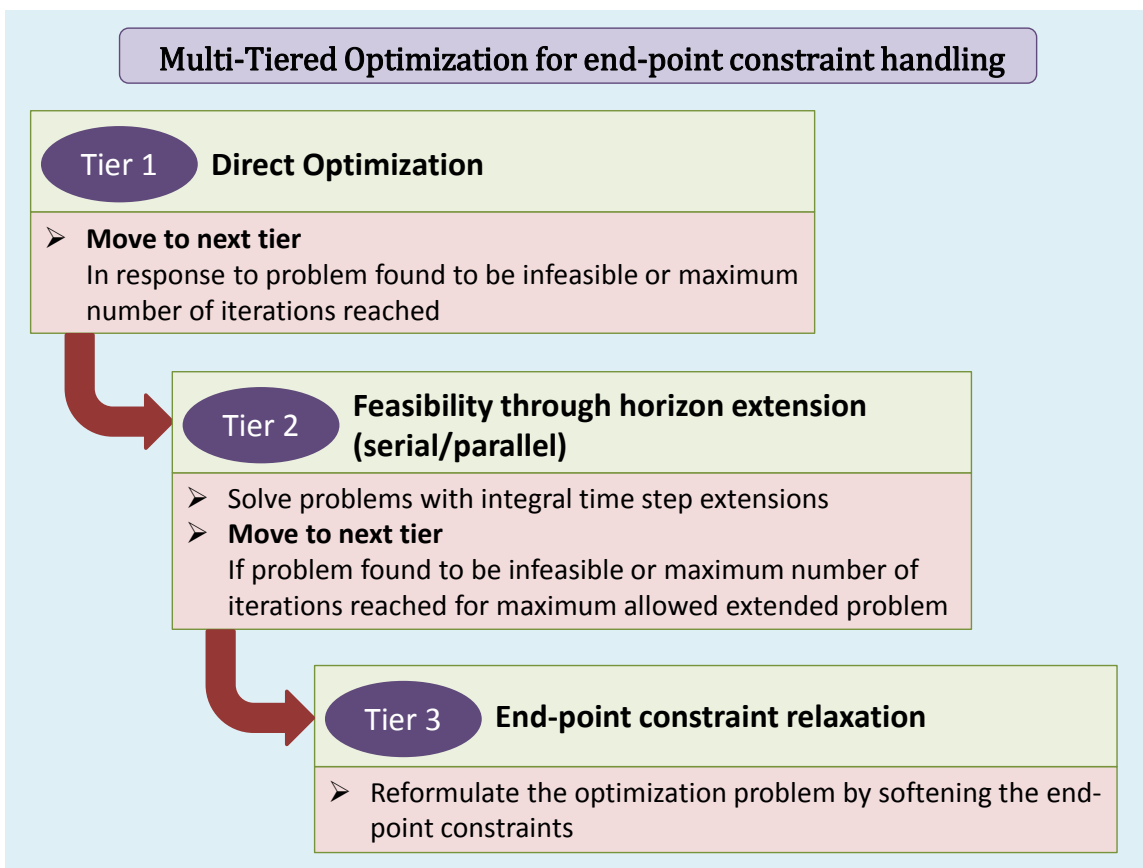


Figure 5.2: Multi-tiered optimization strategy.

Tier 1: Direct Optimization

In the first tier, we aim to maximize economics subject to the EAF model (5.2) in order to find the optimal input trajectories. The objective function for the EAF is to maximize profit at the end of the EAF batch, which is given as

$$\begin{aligned} \Phi(t_f) := & c_0 M_{steel}(t_f) - \left(c_1 \int_{t_i}^{t_f} P dt + c_2 \int_{t_i}^{t_f} F_{CH_4,brnr} dt + c_3 \int_{t_i}^{t_f} F_{C_lance} dt \right. \\ & + c_4 \int_{t_i}^{t_f} F_{C_charge} dt + c_5 \int_{t_i}^{t_f} (F_{O_2,Jetbox1} + F_{O_2,Jetbox2} + F_{O_2,Jetbox3}) dt \\ & \left. + c_6 \int_{t_i}^{t_f} F_{CaO} dt + c_7 \int_{t_i}^{t_f} F_{Dolomite} dt + c_8 \int_{t_i}^{t_f} F_{1stCharge} dt + c_9 \int_{t_i}^{t_f} F_{2ndCharge} dt \right), \end{aligned} \quad (5.6)$$

where M_{steel} is the state variable for the amount of molten steel and its corresponding selling price is denoted by c_0 . M_{steel} produced at t_f is the major source of revenue and profit is calculated by subtracting from it the total cost incurred for all the inputs applied throughout the duration of the batch. The ten utilized inputs are: electric arc power P , flow of burner natural gas $F_{CH_4,brnr}$, lancing carbon F_{C_lance} , charged carbon F_{C_charge} , flow of oxygen from three JetBoxes ($F_{O_2,Jetbox1}, F_{O_2,Jetbox2}, F_{O_2,Jetbox3}$), lime F_{CaO} , dolomite $F_{Dolomite}$ and second scrap charge $F_{2ndCharge}$. We discretize the integral in (5.6) with no loss in accuracy due to piecewise constant input trajectories.

The input constraints are given as

$$P^{min}(t) \leq P(t) \leq P^{max}(t) \quad (5.7a)$$

$$F^{min}(t) \leq F \leq F^{max}(t), \quad (5.7b)$$

where superscripts min and max denotes the lower and upper limits respectively. The input constraint have been implemented to ensure that we obtain the optimal input

sequence in the realistic operating range of the furnace. Path constraints

$$T_{wall} \leq T^{max}, \quad (5.8)$$

$$T_{roof} \leq T^{max}, \quad (5.9)$$

ensure that the furnace wall (T_{wall}) and roof temperatures (T_{roof}) are below the maximum allowed temperature T^{max} . Additionally, we have end-point constraints

$$m_{ss}(t_f) \leq \delta_{ss}, \quad (5.10)$$

$$y_{carbon}(t_f) \leq Y_c^{max}, \quad (5.11)$$

for the optimization problem. Equation 5.10 ensures that all the scrap left is essentially melted by the end of the batch, where $m_{ss}(t_f)$ represent the amount of solid scrap left at final time t_f , and δ_{ss} is the specified tolerance. Equation 5.11 ensures that the carbon content of the steel $y_{carbon}(t_f)$ at t_f is within the specified level Y_c^{max} . This end-point constraint can potentially lead to infeasibility which is tackled using the tiers 2 and 3. The second and third tiers are applied with respect to the limiting end-point constraint (5.10), as described in sections 5.4.2 and 5.4.3.

5.5 Multi-rate Moving Horizon Estimation

For carrying out an operator-triggered multi-tiered optimization at any time step t_i , it is important to reconstruct the states \mathbf{x}_i using the available measurements up to the current time. MHE reconstructs the state by solving a dynamic optimization problem subject to the model and other specified constraints [16]. Since MHE solves a dynamic optimization problem to determine the state estimates, efficient nonlinear programming (NLP) solvers [43, 44, 45, 20] can be used to arrive at the solutions quickly. MHE uses a past fixed-sized moving window of measurements to keep the problem size reasonable. However, when problem size is not a major concern, then an expanding horizon least-squares estimation can be used to avoid loss of

information due to a moving horizon [46]. The respective problem constitutes full information least-squares estimation where all measurements up to the current time are considered in the formulation [16]. It is to be noted that the use of a past history of measurements by MHE provides a straightforward way to use measurements with different sampling rates[47, 48, 49, 50, 20]. The use of all the available measurements potentially leads to an increase in the system observability and also a reduction in estimation errors [49, 50]. The next subsections describes the model used in the MHE formulation, the least-squares problem and the arrival cost calculation.

5.5.1 Model for State Estimation

We consider the process formulated as a stochastic DAE system

$$\dot{\mathbf{x}}(t) = \mathbf{f}_d(\mathbf{x}(t), \mathbf{z}(t), \mathbf{u}(t), \mathbf{p}) + \mathbf{w}_t(t) \quad (5.12a)$$

$$\mathbf{0} = \mathbf{f}_a(\mathbf{x}(t), \mathbf{z}(t), \mathbf{u}(t), \mathbf{p}) \quad (5.12b)$$

$$\mathbf{d}(t) = \mathbf{f}_e(\mathbf{x}(t), \mathbf{z}(t), \mathbf{u}(t), \mathbf{p}) \quad (5.12c)$$

$$\mathbf{y}(t) = \mathbf{h}(\mathbf{x}(t), \mathbf{z}(t), \mathbf{d}(t)) + \mathbf{v}_t(t) \quad (5.12d)$$

where \mathbf{w}_t represents the errors in the differential equations constituting process noise, and is useful for accounting for disturbances and model mismatch. Equation (5.12d) denotes the measurement equation where \mathbf{v}_t accounts for measurement noise. Typically both \mathbf{w}_t and \mathbf{v}_t are modeled as a normally distributed uncorrelated sequence of random variables.

Discretization of the above DAE system is carried out during optimization for subsequent computations. Since discretization is performed according to the optimization strategy employed (simultaneous, multiple shooting), we therefore consider here the conceptual discretization of the DAE system to state the constrained least-squares MHE formulation [51]. We also assume that inputs \mathbf{u} are only manipulated at discrete time points k . The subscript k is now introduced here to distinguish variable values

at discrete time points from continuous values. Thus, using (5.12a) and (5.12b), and removing \mathbf{p} for ease of representation, we obtain

$$\mathbf{x}_{k+1} = \mathbf{x}_k + \int_{t_k}^{t_{k+1}} \mathbf{f}_d(\mathbf{x}(t), \mathbf{u}_k) dt + \int_{t_k}^{t_{k+1}} \mathbf{w}_t(t) dt, \quad (5.13)$$

which is represented as

$$\mathbf{x}_{k+1} = \mathbf{F}_d(\mathbf{x}_k, \mathbf{u}_k) + \mathbf{w}_k. \quad (5.14)$$

We also obtain the discrete time measurement equation as

$$\mathbf{y}_k = \mathbf{h}(\mathbf{x}_k) + \mathbf{v}_k. \quad (5.15)$$

We note here that (5.14) represents a closed form solution of the DAE system which is not always possible to obtain. Here it is viewed conceptually, with the algebraic and dependent variables/equations considered to be eliminated. Here, $t_k = k\Delta T$, where ΔT is the sampling period.

5.5.2 Constrained Least-Squares Formulation

We consider the process at a given time instant t_i with a past history of measurements and inputs available up to t_i . An MHE window of fixed N sampling times is assumed. Here, we write the MHE formulation for a multi-rate measurement structure. The key assumptions are that the time points of slow (infrequent) measurements coincide with those of the fast (frequent) ones, and there are no delays associated with availability of measurements. The vector of fast measurements are denoted is \mathbf{y}_k^F , while \mathbf{y}_k^{SF} represents a measurement vector containing both the slow and fast measurements. So, a measurement structure for MHE can be represented, for example, as $\{\mathbf{y}_{i-N}^{SF}, \mathbf{y}_{i-N+1}^F, \mathbf{y}_{i-N+2}^{SF}, \dots, \mathbf{y}_{i-1}^F, \mathbf{y}_i^{SF}\}$. In the example, at time instants $[t_{i-N}, t_{i-N+2}, t_i]$ both the slow and fast measurements are available, whereas only fast measurements are available at time instants $[t_{i-N+1}, t_{i-1}]$. The measurement structure

of the example can easily be modified to accommodate different multi-rate sampling. As we proceed in time, new measurements are added to the structure, and the earliest ones dropped.

The multi-rate MHE problem for a discrete-time system is given as

$$\begin{aligned} \min_{\mathbf{x}_{i-N}, \mathbf{w}_k} & \sum_{k=i-N}^{i-1} \|\mathbf{w}_k\|_Q^{-1} + \sum_{\substack{k=i-N \\ k \in \mathbb{I}_F}}^i \|\mathbf{v}_k^F\|_{(R^F)^{-1}}^2 \\ & + \sum_{\substack{k=i-N \\ k \in \mathbb{I}_{SF}}}^i \|\mathbf{v}_k^{SF}\|_{(R^{SF})^{-1}}^2 + \|\mathbf{x}_{i-N} - \hat{\mathbf{x}}_{i-N}\|_{S_i^{-1}}^2 \end{aligned} \quad (5.16)$$

$$\text{s.t. } \mathbf{x}_{k+1} = \mathbf{F}_d(\mathbf{x}_k, \mathbf{u}_k) + \mathbf{w}_k, \quad k = i-N, \dots, i-1 \quad (5.17a)$$

$$\mathbf{y}_k^F = \mathbf{h}_k^F(\mathbf{x}_k) + \mathbf{v}_k^F, \quad k \in \mathbb{I}_F \quad (5.17b)$$

$$\mathbf{y}_k^{SF} = \mathbf{h}_k^{SF}(\mathbf{x}_k) + \mathbf{v}_k^{SF}, \quad k \in \mathbb{I}_{SF} \quad (5.17c)$$

$$\mathbf{x}^{LB} \leq \mathbf{x}_k \leq \mathbf{x}^{UB}, \quad (5.17d)$$

$$\mathbf{w}^{LB} \leq \mathbf{w}_k \leq \mathbf{w}^{UB}, \quad (5.17e)$$

where \mathbb{I}_F and \mathbb{I}_{SF} represent the sets of sampling times where only fast measurements (super script F) and both slow and fast measurements (superscript SF) are available respectively. $\hat{\mathbf{x}}_{i-N}$ denotes the *a priori* estimate of the state variable value at the earliest time point in the moving horizon. We represent two separate measurements functions \mathbf{h}_k^F and \mathbf{h}_k^{SF} to map the states \mathbf{x}_k to the sensor measurements \mathbf{y}_k^F and \mathbf{y}_k^{SF} respectively. Similarly, \mathbf{v}_k^F and \mathbf{v}_k^{SF} represent the associated measurement noise. Equations (5.17d) and (5.17e) provides the lower $[\mathbf{x}^{LB}, \mathbf{w}^{LB}]$ and upper bounds $[\mathbf{x}^{UB}, \mathbf{w}^{UB}]$ on the state variables \mathbf{x} and model noise \mathbf{w} respectively. The covariance matrices associated with the model noise, measurement noise (for F and SF) and initial state error is denoted here as Q , R^F , R^{SF} and S_i respectively. The state estimates \mathbf{x}_i at t_i is obtained by solving the least squares problem.

It can be observed that the MHE least squares objective function is composed of four terms where the first three are used to minimize weighted model and measurement errors. The fourth term, arrival cost or cost to arrive, minimizes the initial state discrepancy. The cost to arrive term is important because we are dropping measurements due to the moving nature of MHE. The initial state error covariance is also generally updated every time step thus the subscript i is used for S matrix. However, the update is not entirely necessary when the system is strongly observable [52]. Zavala [53] showed that a single parameter penalizing the arrival cost is sufficient to achieve convergence. In the next subsection, we describe the EKF covariance update formula [16] which is commonly used for updating the initial state covariance matrix.

5.5.3 Arrival Cost Update

To update the arrival cost covariance matrix S using the EKF update formula we need a discrete time model linearized at every sampling time. We first consider the continuous time stochastic DAE model (5.12). Linearizing (5.12) around a given time t_k gives (suppressing \mathbf{p} for ease of readability)

$$\dot{\mathbf{x}}(t) = P_k \mathbf{x}(t) + J_k \mathbf{z}(t) + K_k \mathbf{u}(t) + \mathbf{w}_t(t) \quad (5.18a)$$

$$\mathbf{0} = G_k \mathbf{x}(t) + H_k \mathbf{z}(t) + L_k \mathbf{u}(t), \quad (5.18b)$$

$$\mathbf{d}(t) = O_k \mathbf{x}(t) + T_k \mathbf{z}(t) + V_k \mathbf{u}(t), \quad (5.18c)$$

$$\mathbf{y}(t) = E_k \mathbf{x}(t) + F_k \mathbf{z}(t) + M_k \mathbf{d}(t) + \mathbf{v}_t(t). \quad (5.18d)$$

Here, matrices $P_k, J_k, K_k, G_k, H_k, L_k, O_k, T_k, V_k, E_k, F_k$ and M_k are generally obtained by computing respective Jacobian values at the linearized point [54]. Although, now a discretization can be carried out by an appropriate integration of the continuous system through a zero-order hold on $\mathbf{u}(t)$, this transformation involves computing the matrix exponential. For large-scale systems where the system matrices are prone to be ill-conditioned, we employ an alternate way of transformation which uses the Explicit

Euler scheme for discretization. Although the approach is less accurate, we can completely avoid the complications associated with calculating matrix exponentials. Using the Explicit Euler scheme, we obtain the discretized form as

$$\frac{\mathbf{x}_{k+1} - \mathbf{x}_k}{\delta_1} = P_k \mathbf{x}_k + J_k \mathbf{z}_k + K_k \mathbf{u}_k + \mathbf{w}_k, \quad (5.19a)$$

$$\mathbf{0} = G_k \mathbf{x}_k + H_k \mathbf{z}_k + L_k \mathbf{u}_k, \quad (5.19b)$$

$$\mathbf{d}_k = O_k \mathbf{x}_k + T_k \mathbf{z}_k + V_k \mathbf{u}_k, \quad (5.19c)$$

$$\mathbf{y}_k = E_k \mathbf{x}_k + F_k \mathbf{z}_k + M_k \mathbf{d}_k + \mathbf{v}_k, \quad (5.19d)$$

where δ_1 denotes the Explicit Euler step size. Now, we use (5.19b) to eliminate \mathbf{z}_k from (5.19a), (5.19c) and (5.19d). Further, using (5.19c) to substitute \mathbf{d}_k in (5.19d) and rearranging terms gives the discretized state space model to be used for EKF updates,

$$\mathbf{x}_{k+1} = \delta_1 (P_k - J_k H_k^{-1} G_k + I) \mathbf{x}_k + \delta_1 (K_k - J_k H_k^{-1} L_k) \mathbf{u}_k + \mathbf{w}_k \quad (5.20a)$$

$$\begin{aligned} \mathbf{y}_k = & (E_k - F_k H_k^{-1} G_k - M_k T_k H_k^{-1} G_k + M_k O_k) \mathbf{x}_k \\ & + (M_k V_k - F_k H_k^{-1} L_k - M_k T_k H_k^{-1} L_k) \mathbf{u}_k + \mathbf{v}_k \end{aligned}$$

where I is an identity matrix of dimension equal to number of states. Replacing, $[\delta_1 (P_k - J_k H_k^{-1} G_k + I)]$, $[\delta_1 (K_k - J_k H_k^{-1} L_k)]$, $[(E_k - F_k H_k^{-1} G_k - M_k T_k H_k^{-1} G_k + M_k O_k)]$ and $[(M_k V_k - F_k H_k^{-1} L_k - M_k T_k H_k^{-1} L_k)]$ with A_k , B_k , C_k and D_k respectively, we thus have the time-varying discrete state space model in standard form as

$$\begin{aligned} \mathbf{x}_{k+1} = & A_k \mathbf{x}_k + B_k \mathbf{u}_k + \mathbf{w}_k \\ \mathbf{y}_k = & C_k \mathbf{x}_k + D_k \mathbf{u}_k + \mathbf{v}_k. \end{aligned} \quad (5.21)$$

For the above system at a given time, an EKF covariance propagation equation is given as [16],

$$S_{k+1} = Q + A_k [S_k - S_k C_k^T (R + C_k S_k C_k^T)^{-1} C_k S_k] A_k^{-1}. \quad (5.22)$$

Although, the superscripts ‘SF’ and ‘F’ have been suppressed in (5.22) for R and C , and in (5.21), appropriate dimensions according to the multi-rate measurement structure need to be considered. It is to be noted that other filters such as the constrained particle filter [55] and unscented KF [56] can also be employed to update S_i . The update is not carried for batch process with sampling times t_i ($i \leq N$), since measurements are not yet dropped.

5.5.4 Disturbance handling

To tackle unmeasured disturbances with nonzero mean and plant-model mismatch, the model states are augmented with disturbance states \mathbf{x}_k^d to construct a modified system for MHE

$$\mathbf{x}_{k+1} = \mathbf{F}_d(\mathbf{x}_k, \mathbf{u}_k) + \mathbf{B}_d \mathbf{x}_k^d + \mathbf{w}_k, \quad (5.23a)$$

$$\mathbf{y}_k^F = \mathbf{h}_k^F(\mathbf{x}_k) + \mathbf{v}_k^F, \quad (5.23b)$$

$$\mathbf{y}_k^{SF} = \mathbf{h}_k^{SF}(\mathbf{x}_k) + \mathbf{v}_k^{SF}, \quad (5.23c)$$

$$\mathbf{x}_{k+1}^d = \mathbf{x}_k^d + \mathbf{w}_{dk}, \quad (5.23d)$$

where \mathbf{x}_k^d is driven by a new set of white noise variables $\mathbf{w}_{dk} \sim \mathcal{N}(0, \mathbf{Q}_d)$. A well chosen \mathbf{B}_d ensures that the corresponding state equations have the right impact due to the movement of the disturbance states \mathbf{x}_k^d . More detail on the disturbance model and its effect are discussed in Ji and Rawlings[50].

5.6 Real-time Advisory System

EAFs are currently operated with limited automation, and operators make decisions related to input quantities to be added as well as their respective timings during the batch. Our development is focused on improving this suboptimal operation where more informed decisions can be made based on a full scale first principles EAF model.

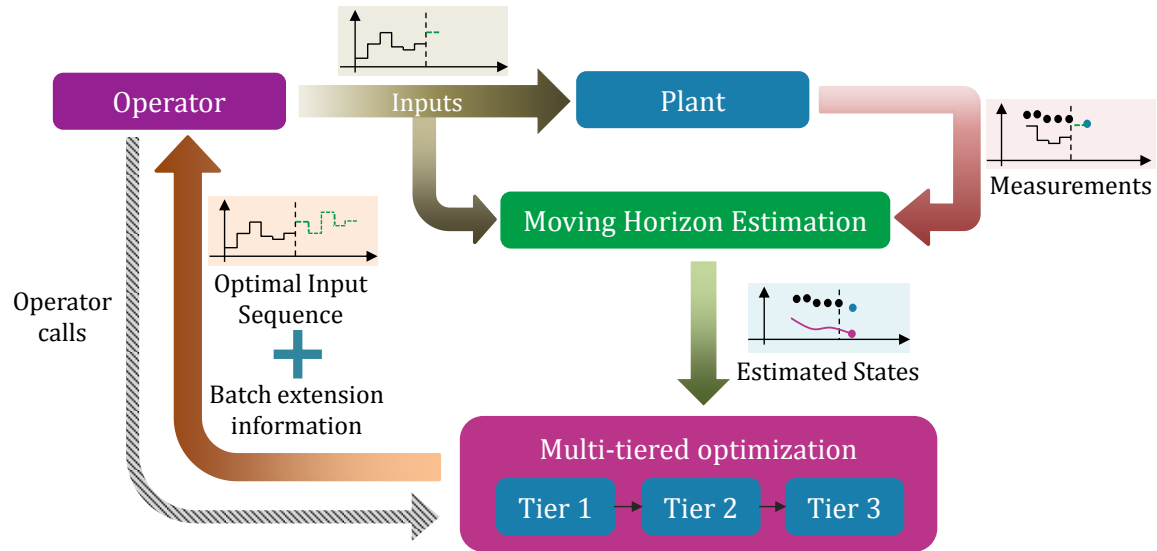


Figure 5.3: Real-time advisory system.

Implementing a large-scale model for decision support is challenging owing to the formulation and implementation complexities. In this section we will describe the advisory system in detail, as well as the mathematics operating in the background.

5.6.1 Algorithm operation

The main objective of the real-time advisory system is to provide an input sequence as decision support to the EAF operators when needed (see Fig. 5.3). The need is tied to the operators calling for support and this is the only manual decision component involved in the working of the advisory system. This flexibility is well suited for actual industrial practice where multiple external factors are important to operate a process. A key component of the advisory system is multi-rate MHE which runs in parallel with the EAF. The state estimates are subsequently provided to a multi-tiered optimizer to calculate the optimal input sequence to maximize the profit. The shrinking horizon optimizer is called upon only when the operator triggers the advisory system. Shrinking horizon problems are characterized by a fixed end point time while the current time (where each optimization is solved) only moves. Although a large

problem is expected at the start times, problem size decreases linearly as we march along the time. The advisory system uses a multi-tiered initialization scheme in combination with state-of-the-art NLP solvers to obtain fast solutions to the dynamic optimization problems.

The operator may choose to implement the input recommendation provided by the advisory system up-to a certain time in the batch by implementing only the initial subset of the suggested input moves and then trigger the advisory system again at a later time. Since the input sequence computed by the system is based on a rigorous optimization involving a high fidelity first-principles model, it takes complex relationships related to the physical phenomenon in to account when determining the optimal way to meet the economic objective. Since EAF batch operation is characterized by frequent fluctuations due to various additions and difficult operating conditions, an advisory tool must be capable of handling disturbances. Our advisory system directly targets economics by effectively solving optimal control problems in real-time. The tiered optimization scheme is also capable of providing information related to lengthening of batch if required, so that operators are aware of the predicted impact and can take remedial action at an early stage. This is more likely to happen if optimization is triggered late in the batch, or implementation of optimal decisions is delayed.

5.6.2 Multi-tiered initialization strategy

For decision support to be available to the operators in real-time, solving the optimization problems of the tiers and MHE problem quickly is really important. Since, subsequent MHE and optimization problems have similar structures, it is useful to use the past solves effectively to generate good warm start points for the current solves. Warm-start strategies have been successfully employed by multiple researchers to solve MHE and NMPC problem on-line [57, 58, 59, 60]. Zavala and Biegler introduced an advanced-step NMPC and fast MHE strategy for getting quick approximate

solutions to the online optimal control problems based on NLP sensitivity [60, 61]. Real-time algorithms have been proposed where solution of the quadratic programming (QP) problem obtained at the previous sampling time is used to construct and carry out a single iteration of the controller optimization [62, 63]. A comprehensive review on the real-time algorithms for solving MHE and NMPC problems is presented in Diehl et al. [57] and Biegler et al. [60]. For obtaining quick optimal solutions to online MHE-NMPC problems, various initialization strategies such as initialization based on parametric sensitivities and shift initialization can be employed[57]. In a recent work, Shyamal and Swartz [13] proposed a novel initialization scheme to solve on-line MHE-NMPC problems quickly to optimality by effectively using the time between sample times. Here, we adapt the scheme for our advisory system application. We solve predicted optimization problems in the background and then use the solutions for warm-starting the actual problems. The proposed multi-tiered initialization strategy generates warm-start points for both the primal and dual variables.

We consider the current time instant (on-line time) as t_i where the state estimates \mathbf{x}_k and the inputs applied to the plant \mathbf{u}_k are available. The time available to us before the next sampling time t_{i+1} is referred to here as background time. The superscripts for slow and fast measurements are suppressed here for ease of readability. Now, we introduce the multi-tiered initialization strategy for the real-time advisory system:

In background, between t_k and t_{k+1} :

- **Tier 1:** While keeping \mathbf{w}_k as 0, carry out a disturbance-free forward model simulation $\bar{\mathbf{x}}_{k+1} = \mathbf{f}(\mathbf{x}_k, \mathbf{u}_k)$ using \mathbf{x}_k and \mathbf{u}_k . Obtain the predicted measurement $\bar{\mathbf{y}}_{k+1} = \mathbf{h}(\bar{\mathbf{x}}_{k+1})$ and pass it to Tier 2.
- **Tier 2:** Use $\bar{\mathbf{y}}_{k+1}$ to construct a predicted MHE problem. Solve it and obtain the predicted state estimates $\tilde{\mathbf{x}}_{k+1}$ to be passed to Tier 3. Also, store the optimal primal and dual values \tilde{s}_k^{mhe} .

- **Tier 3:** Use $\tilde{\mathbf{x}}_{k+1}$ to construct and solve optimization problems in the multi-tiered optimization strategy. Store the solutions obtained from 1/2/3 optimization tiers as $\tilde{s}_k^{opt1}/\tilde{s}_k^{opt2}/\tilde{s}_k^{opt3}$ (both primal and dual).

On-line, at t_{k+1} :

- **Tier 1:** Obtain the current plant measurements \mathbf{y}_{k+1} and construct the actual MHE problem. Use \tilde{s}_k^{mhe} to warm start the problem; solve it to get the actual current state estimates \mathbf{x}_{k+1} and pass it to Tier 2.
If operator triggers the advisory system, go to Tier 2; otherwise return to the background step.
- **Tier 2:** Construct and solve optimization problems associated with the multi-tiered optimization strategy by using $\tilde{s}_k^{opt1}/\tilde{s}_k^{opt2}/\tilde{s}_k^{opt3}$ for initialization. Obtain the optimal input sequence $\{\mathbf{u}_{k+1}, \dots, \mathbf{u}_{t_f}\}$ and send it to the operator. Return to the background step.

While the effectiveness of the multi-tiered strategy would in general depend on how close the predicted and actual problems are, we have obtained substantial reductions in solve times with this approach for all the case studies considered. Also, the strategy can effectively implemented for any of the three dynamic optimization approaches viz. single shooting, multiple shooting and simultaneous (details of the approaches in Biegler [33]. The multi-tiered initialization helps to generate fast solutions of the optimization problems in the tiers of the multi-tiered optimization strategy.

5.6.3 Implementation

Model contraction is first used in CasADi to remove 397 algebraic variables from the original DAE model containing 28 differential and 518 algebraic variables. The eliminated algebraic variables becomes the dependent variables defined by explicit functions of only the differential state and remaining algebraic variables. The advisory

system is implemented for a discretized model using the Python front end of CasADi. We use the Implicit Euler scheme with 7 time steps per minute (the sampling time for EAF system is 1 minute) for discretization. A simultaneous approach, which is useful for real-time applications such as advisory systems, is employed here for solving the optimization problems [64, 13]. The infinite dimensional optimization problem is thus converted to a sparse large-scale NLP problem. We employ interior-point solver IPOPT [65] (with MA27 as the linear solver) to solve the NLP. We have also used IDAS (part of SUNDIALS suite of solvers [66]) for carrying out forward simulations for generating measurements.

For the multi-tiered optimization algorithm, the \max_{iter} parameter is set to 100. For Tier 2 of the optimization, the maximum allowed extension was chosen as 3. This is reasonable since it is not desirable to extend a EAF batch by a substantial amount in usual scenarios. To warm start the predicted MHE and optimization problems in the multi-tiered initialization strategy, we used the most recent respective solves to initialize the problems. For initializing the predicted MHE, the last MHE solution is taken after removing the primal and dual value associated with the first control stage. We then add the guesses for the primal variables values for the new control stage using a forward simulation. The predicted shrinking horizon optimization problems are initialized by taking the primal and dual variable values from the last solve and dropping the variables values associated with the first control interval.

Plant-model mismatch was incorporated by decreasing a power factor parameter k_p by 10% in the model employed by the multi-tiered optimization and MHE. This reduction in the k_p value leads to a significant reduction in the electrical energy transferred to the scrap Q_{arc} by the arc power P_r . The exact model equation effected by this mismatch is [7] $Q_{arc} = k_p P_r$. Another disturbance is introduced through a step increase of parameter k_{dm} in the plant during the batch operation. This change significantly reduces the melting rate of solid scrap, \dot{M}_{melt} , in the plant since the melt

rate is modeled using the following equation

$$\dot{M}_{melt} = \frac{Q_{ss}(T_{ss}/T_{melt})}{\left[\Delta H_{f,Fe} + \int_{T_{ss}}^{T_{melt}} C_{p,Fe} dt\right] k_{dm}}, \quad (5.24)$$

where T_{ss} and T_{melt} represent the solid-scrap temperature and melting point temperature of scrap. Q_{ss} denotes heat of fusion of Fe while $C_{p,Fe}$ is the heat capacity of Fe. k_{dm} accounts for any variation in the solid-scrap composition and its bulk density. To mitigate the effects of the mismatch and the disturbance, two disturbance states are introduced for the state variables representing the solid scrap mass and the moles of managenese in the *slag-metal* zone. This is implemented by using \mathbf{B}_d as $e_i \in \mathbb{R}^{n \times 1}$ where i denotes state variable number for the solid scrap mass and the moles of managenese in the state variable vector of size n , and e_i represents the i th unit vector. We chose \mathbf{Q}_d as 0.015 and 0.2 for disturbance states of the solid scrap mass and the moles of managenese respectively.

5.7 Case studies

In this section we present three case studies to demonstrate potential benefits of a real-time implementation of the proposed advisory system. The studies correspond to scenarios where we study the effect of advisory system executions on economics and how the system deals with disturbances and infeasibilities. We also analyze the multi-rate MHE's ability to track the true states. Finally, we discuss the computational effort required to solve the MHE and shrinking horizon dynamic optimization problems.

5.7.1 Problem Setup

We implement the advisory system using the first principles EAF model comprising of 28 state variables and 512 algebraic variables. The model contraction using CasADI reduced the algebraic variables to 121 while yielding 391 dependent variables. The

Table 5.1: Multi-rate measurement structure for the EAF process.

Time (min)	0 ... 42	43	44 ... 46	47	48 ... 60
Number of measured variables	6	13	6	8	6

Table 5.2: Measurement availability for the EAF process.

Measurement	Sampling Time	Variance
Off-gas compositions (CO, CO ₂ , O ₂ , H ₂) (dimensionless)	Every 1 min	0.01
T _{roof} , T _{wall} (K)	Every 1 min	3
Slag compositions (FeO, Al ₂ O ₃ , SiO ₂ , MgO, CaO) (dimensionless)	43rd min	0.1
Molten-metal temperature (K)	43rd & 47th min	5
Molten-metal carbon content (dimensionless)	43rd & 47th min	0.01

EAF operation considered here is a 60 minute batch process with 10 manipulated inputs. The process starts with the first scrap charged at time $t = 0$ minute and second scrap charged at 25th minute. Although, the scrap charging times are considered to be fixed for the case studies, the charging times itself can also be optimized.

The measurements are available with different sampling rates described in Table 5.1. There are 6 fast measurements, comprising the off-gas compositions and the furnace roof and wall temperatures, that are available every 1 minute. Slag chemistry information in the form of 5 measurements is available at the 43rd minute of the batch duration. Molten metal carbon content and temperature are measured at 43rd and 47th minute. Since these slow measurements give valuable information about the process, a multi-rate MHE design is essential for optimal performance of the state estimator. The measurements with their corresponding sampling time points and variances are listed in Table 5.2. The MHE performance is demonstrated when the initial conditions are unknown and there is plant-model mismatch as well as measurement noise.

Carrying out an observability analysis is important before proceeding with implementing MHE. This is particularly useful for systems where limited measurements are available. The DAE model is first linearized at each sampling time and then the observability metric value checked[50] at the corresponding time points. The observability matrix for the system constructed and a Singular Value Decomposition (SVD) carried out to give the singular values. The linearized model is then transformed to observability canonical form which yields the transformed z -space corresponding to the original x -space of the linearized model. The observability metric value for each state is then computed by projecting it on to the z -space with the weight assigned to it being the associated singular value. Very low values of the observability metric imply an unobservable or a weakly observable system. The lowest observability metric value identified for our system is 7.0×10^{-7} which implies that the system is fully observable. It is to be noted that instead of carrying out the linearization procedure, output from the IPOPT solver can be examined directly to determine the system observability [44].

It is possible that implementation of either of the three solutions obtained from the three tiers cannot actually ensure that the state variable value $\mathbf{x}_{plant}(t_{f_{tier}})$ at the final time is within specified bounds. This is due to disturbances effecting the plant. In order to associate a cost to the amount of scrap left while calculating the economic objective value, we extend the simulation when estimated states $\mathbf{x}_{est}(t_{f_{tier}})$ at $t_{f_{tier}}$ are not within the specified upper and lower bounds. It is to be noted here that an estimate of the current states is useful to operators even without the optimization calculation being triggered. We assume that the last implemented input moves are reimplemented to the plant in order to melt the remaining scrap. The reimplementation is carried out until the state estimates are within their bounds. We also place an upper limit $N_{extra} = 10$ on these re-implementations to ensure that the extended implementation terminates within a reasonable period.

5.7.2 Case Study Descriptions and Results

In the next set of subsection we describe the two case studies conducted to test the real-time advisory system. First case study demonstrates the economic benefit of carrying out an increased number of re-optimizations through calling the advisory system more often. The first case study shows the effectiveness of the advisory system when plant is effected by a major disturbance. The second case study explores the use of three tiers.

Case study 1: Economic benefit of real-time advisory system execution

In this case we compare three scenarios: when the optimization in the advisory system is activated once, twice and thrice times by the EAF operators. Since, there is flexibility in the advisory system for operators to execute it when decision support is required, this case illustrates the scenarios where the number of executions can differ. This case study emulates a situation where plant is effected by major disturbances while the batch process is evolving in time. To create such a situation the parameter k_{dm} was chosen because it has a major impact on the implementation of the solution on the plant. The parameter k_{dm} , described earlier, was increased in the plant by 5% at 28th minute. This step increase leads to a significant decrease in the rate of scrap melting from 28th minute onwards during the batch. An immediate impact is that more solid scrap will be left at 60th minute and a batch extension will be required. Besides the disturbance, we also considered plant-model mismatch, unknown initial states and measurement noises for both the case studies.

In scenario 2 and 3, optimization is first carried out at 0th minute and the calculated moves are implemented only until the 30th minute. At the 30th minute, a reoptimization is done for both scenarios 2 and 3. The new calculated inputs are

Table 5.3: Results for Case study 2.

	Scenario 1	Scenario 2	Scenario 3
Times at which advisory system was called (min)	0	0, 30	0, 30, 40
Number of re-optimizations	0	1	2
Economic objective function value (\$)	9350	9654	9777
Scrap left at 60th minutes	18.27	17.23	16.21
Further extension of batch done for comparison (minutes)	6	4	4
Actual scrap left at extended time (kg)	7.78	7.22	7.16

subsequently implemented until the end of the batch for scenario 2. However, for scenario 3, another reoptimization is carried out at 40th minute.

For all the three scenarios, MHE is running in the background to provide the state estimates when needed. The end-point constraint is implemented for solid scrap mass (m_{ss}) at 60th minute. There is no lower bound for $m_{ss}(t = 60 \text{ min})$, and the final scrap remaining is specified to be less than 8 kg out of 118.35 tonnes scrap charged. The input bounds for $[F_{CaO}, F_{C_lance}, F_{2ndCharge}, F_{Dolomite}, F_{C_charge}, F_{CH_4,brnr}]$ are $\pm 20\%$ compared to the nominal value. Lower bound values for P and $[F_{O_2,Jetbox1}, F_{O_2,Jetbox2}, F_{O_2,Jetbox2}]$ are considered as 10% and 40% of the nominal values respectively. Upper bound values for P and $[F_{O_2,Jetbox1}, F_{O_2,Jetbox2}, F_{O_2,Jetbox2}]$ are specified as +130% and +120% of the nominal values.

The three scenarios are compared in Table 5.3. For this case study, the multi-tiered optimization algorithm always stopped at tier 1 only. We observe that for scenario 2 we get 3.25% increase in profit compared to scenario 1. Also, scenario 3 has a 1.27% higher economic objective value compared to scenario 2. This increase percent will potentially lead to a major increase in annual steelmaking profit. Thus, the case study demonstrated that more frequent reoptimizations can lead to substantial increase in profit. In limit of reoptimizations carried out at every 1 minute, the implementation

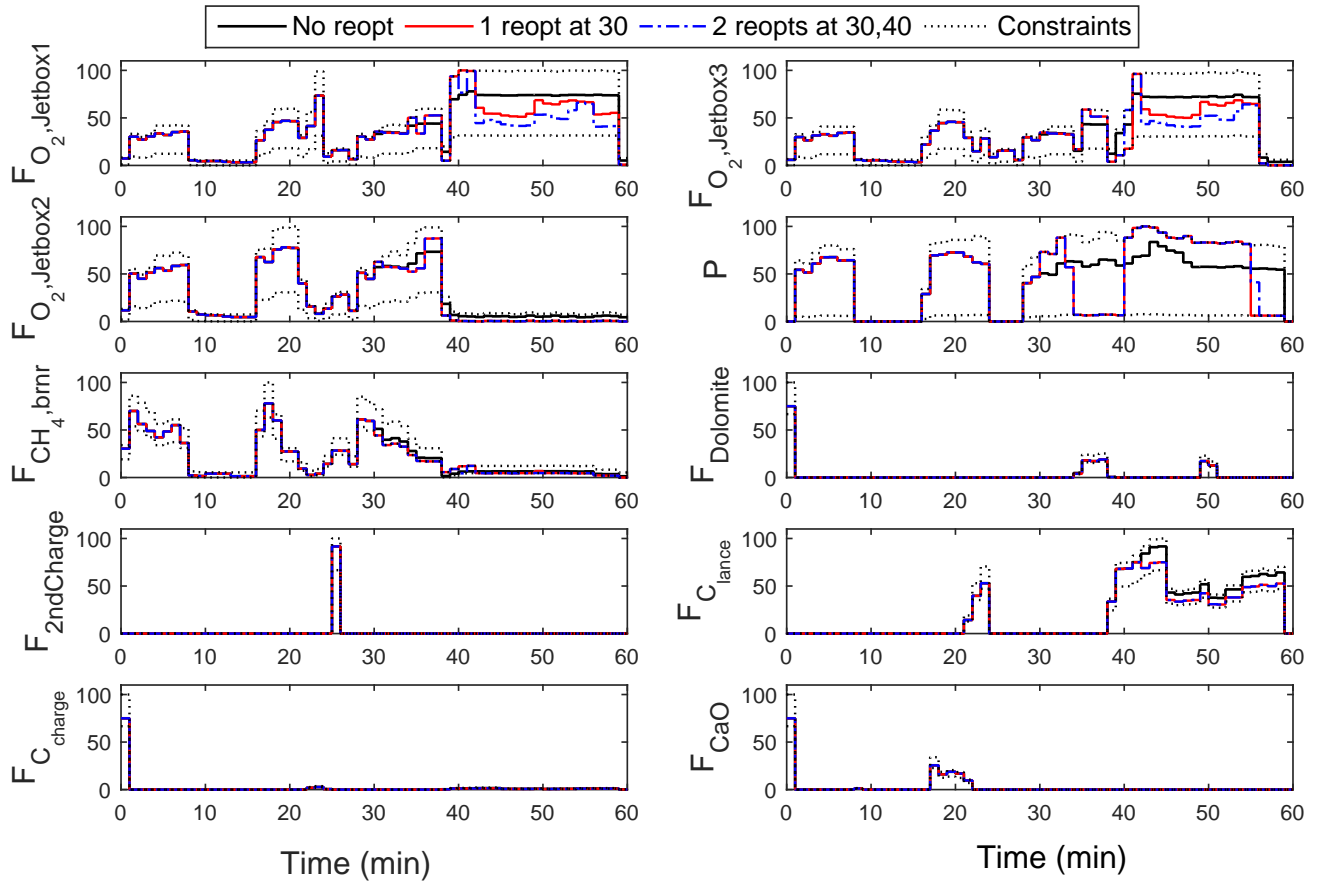


Figure 5.4: Input profiles for case study 1.

naturally extends to nonlinear model predictive control (NMPC). Fig. 5.4 shows how the calculated inputs differ for the three scenarios. We observe that scenario 2 and 3 are using considerably less oxygen and electric arc power post 30 minutes during the batch operation, leading to a substantial decrease in operating cost. Scenario 3 has lower oxygen usage but slightly more of electric arc power usage compared to scenario 2.

From Table 5.3, we observe that scrap left at 60th minute is less when more re-optimizations are carried out. We used extended simulation for comparison because the scrap left at 60th min was more than 8 kg for all the three scenarios. Since the rate of melting is decreased at 28th minute due to the disturbance, if we keep im-

plementing input moves calculated at 0th min as in scenario 1, the batch potentially needs to be extended by 6 minutes in order to make sure the scrap left is less than 8 kg. However, for scenario 2 and 3 only a 4 minute extension is required since MHE is able to deduce that a major disturbance has happened and this crucial information is supplied to the triggered reoptimizations carried out at the 30th and [30,40]th minutes respectively. This case demonstrates that re-optimizations are important in two ways: increasing economic profit and avoiding batch extension while tackling disturbances. The extension in batch length can sometimes lead to a delayed start of subsequent batches and also delays in downstream processes. Although we have not taken these costs in account within this paper, these cost increases can lead to further reduction of the final profit.

Case study 2: Feasibility through multi-tiered optimization strategy

In this case study, we carry out a single reoptimization at the 45th minute of the batch process. A disturbance is introduced through a step increase of k_{dm} by 12.3% at 38th minute during the batch operation. We also lowered the upper and lower bounds of the electric power input to 10% and 78% of the nominal values respectively. This combined change led to Tier 1 solving up to the maximum iteration limit of 100 without finding an optimal solution. Then, Tier 2 came into action and three extended dynamic optimization problems were solved serially for each of the integral extensions up to 3 time steps. We kept the upper limit of extensions in Tier 2 as 3 time steps. Since all the three problems reached maximum iterations, the advisory system moved to Tier 3 to solve a relaxed problem by softening the end point constraint on final solid scrap mass. In this case study, we set the tuning parameters V_{max} to 1 and D as 0.01. The end-point upper bound on remaining solid scrap at final time is 8 kg. The profit obtained is 9632.7 which is 3% more compared to the scenario where no reoptimization is carried out. Since a relaxed extended optimization problem is

solved at the 45th minute, 31 kg of solid scrap was left at 63rd minute. We carried out extended implementation of 10 time steps at 63rd minute because solid scrap left at the time is more than 8 kg. After the 10 steps of extended implementation, the final scrap mass left is 18.2 kg. This case demonstrates that the tiered algorithm is able to compute reasonable solution even when the original optimization problems fails to solve.

5.7.3 Moving Horizon Estimation Results

In this section we discuss the performance of multi-rate MHE. For all the three case studies, Gaussian noise of 1% relative variance was added to the true initial conditions of the state variables. Measurements were perturbed by adding Gaussian noise of relative variances according to the values given in Table 5.2. The covariance matrix Q for the model uncertainty was chosen based on multiple trial simulations. We also implemented upper and lower bounds for the state, the algebraic and the model noise variables. A moving horizon length of 6 was selected for all the case studies. Fig.5.5 represents a subset of the true states and the estimated states for case study 2. We also show how the absolute value of estimation error given by $|x_{true} - x_{estimated}|$ varies with respect to time. We notice that MHE is able to track the true states despite of the plant-model mismatch, initial state discrepancy, unknown disturbance and measurement noise. We observe that the estimation error increased around the 40-50th minute due to the disturbance being introduced in the plant. However, MHE handles this and decreases the estimation error post 45th min. Furthermore, the total time horizon of state profiles is 73 minutes which includes the 13 minute extension due to the tiered optimization algorithm and extended implementation.

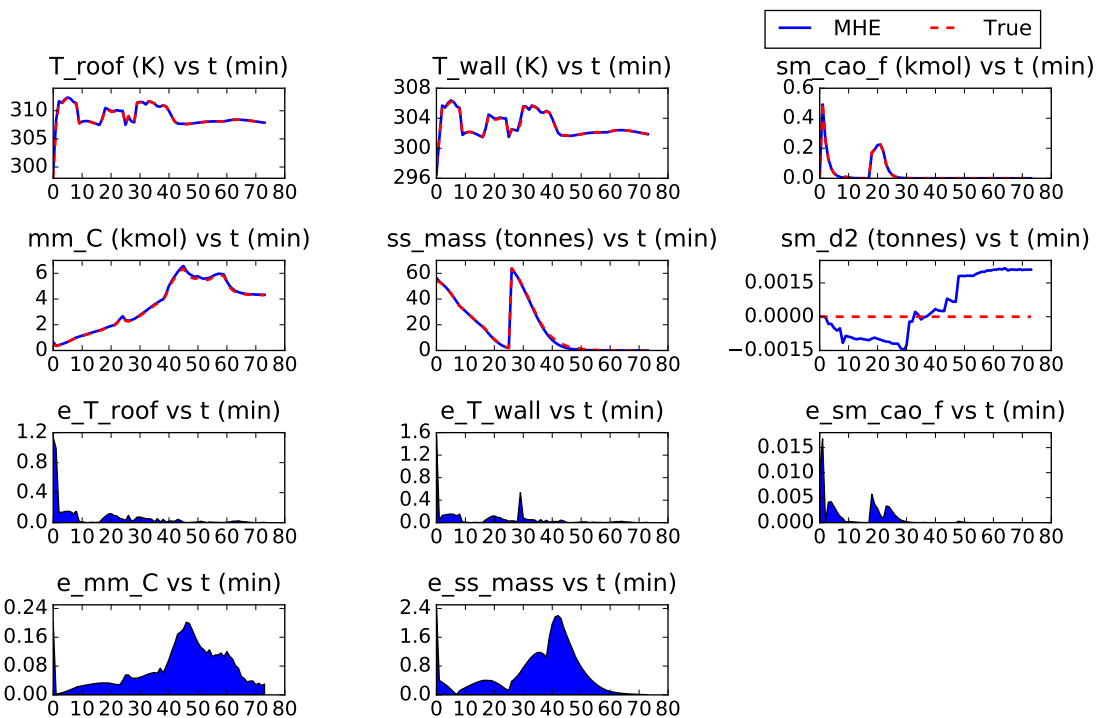


Figure 5.5: State estimate profiles and corresponding estimation error (variable name appended with 'e_') varying with respect to time (in minutes) for case study 3. T_{roof} (temperature of furnace roof), T_{wall} (temperature of furnace wall), sm_cao_f (floating carbon content in slag-metal zone), mm_C (Moles of Carbon in molten-metal zone), ss_mass (mass of solid scrap) and sm_d2 (Disturbance state for ss_mass).

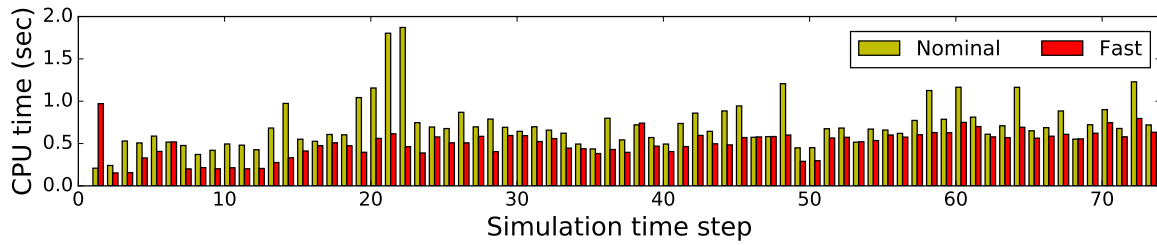


Figure 5.6: Solution times for multi-rate MHE problems (horizon length is 6 minutes) for case study 3. ‘Fast’ represents solution times when the multi-tiered initialization scheme is used. ‘Nominal’ denotes solutions times when the proposed initialization scheme is not utilized.

Table 5.4: Solution times for the multi-tiered dynamic optimization problems of case study 3.

Time points where multi-tiered optimizer is called	0th minute		45th minute			
	1	1	2	2	3	
Activated tier number	1	1	2	2	3	
Solution time (CPU seconds) without the use of multi-tiered initialization	25.7	6.8	6.6	7.3	7.1	2.1
Solution time (CPU seconds) with the use of multi-tiered initialization	2.1	1.1	0.9	1.2	1.1	0.6

5.7.4 Computational Results

We have employed an Intel Core i7-3770 processor (with 4 CPU cores) running Windows 7 at 3.4 GHz for all numerical computations. The CPU times required for solving the multi-rate MHE problems, with (fMHE) and without (nMHE) the use of the proposed multi-tiered initialization scheme, for case study 3 are shown in Fig. 5.6. The average solution times for fMHE and nMHE are 0.49 and 0.71 seconds respectively. So, there is 31% decrease in MHE solve time due to the use of the multi-tiered warm-start strategy. The solution times for the multi-tiered dynamic optimization problems of case study 3 are given in Table 5.4. The advantage of using the multi-tiered initialization scheme is apparent. The solution times for the advisory system used in case study 1 and 2 were on average below 5 seconds. Furthermore, the solution time for the predicted problems solved in the multi-tiered initialization strategy for all the three case studies were well below 1 minute.

5.8 Conclusion

In this work we introduced a real-time dynamic optimization-based advisory system for EAF batch operation. The advisory system combines the multi-tiered dynamic optimization with MHE to provide online decision support to the EAF plant operators. The three tiers of the optimizer effectively handle the endpoint constraints. At any point during the batch operation, the optimizer can be triggered by the operators. The initial conditions for the optimization problem are obtained from multi-rate MHE which runs in parallel. We also proposed a multi-tiered initialization scheme for obtaining fast solutions from the advisory system.

Our case studies for the electric arc steelmaking process showed the economic benefit of using the real-time advisory system. We demonstrated the usefulness of reoptimizations in operating the challenging process optimally. The strong convergence of MHE directly influenced the optimizer results and provided a firm basis for activating the tiered optimization algorithm. We showed that the advisory system is capable of providing decision support to the operators in real-time without significant delays.

For the next steps, we aim to formulate the optimization problem to find the optimal batch length. We would like to explore the possibility of contraction in total time duration of batch operation. As a future work, we intend to investigate alternate objective function formulations where environmental effects such as emissions are also considered. Also, in-plant evaluation of the real-time advisory system constitutes an important step for industrial usage.

References

- [1] Steel Statistical Yearbook of World Steel Association. <http://www.worldsteel.org/steel-by-topic/statistics/steel-statistical-yearbook-.html>. 2016.
- [2] R. J. Fruehan. *The Making, Shaping, and Treating of Steel: Ironmaking volume*. Vol. 2. AISE Steel Foundation, 1999.
- [3] C Woodside, B Pagurek, J. Pauksens, and A Ogale. "Singular arcs occurring in optimal electric steel refining". In: *IEEE transactions on automatic control* 15.5 (1970), pp. 549–556.
- [4] D. Oosthuizen, I. Craig, and P. Pistorius. "Model predictive control of an electric arc furnace off-gas procedure combined with temperature control". In: *Africon*. Vol. 1. IEEE. 1999, pp. 415–420.
- [5] J. G. Bekker, I. K. Craig, and P. C. Pistorius. "Modeling and simulation of an electric arc furnace process". In: *ISIJ international* 39.1 (1999), pp. 23–32.
- [6] S Matson and W. F. Ramirez. "Optimal operation of an electric arc furnace". In: *57 th Electric Furnace Conference*. 1999, pp. 719–730.
- [7] R. D. MacRosty and C. L. E. Swartz. "Dynamic modeling of an industrial electric arc furnace". In: *Industrial & engineering chemistry research* 44.21 (2005), pp. 8067–8083.
- [8] R. D. MacRosty and C. L. E. Swartz. "Dynamic optimization of electric arc furnace operation". In: *AIChE journal* 53.3 (2007), pp. 640–653.
- [9] R. D. M. MacRosty and C. L. E. Swartz. "Nonlinear predictive control of an electric arc furnace". In: *IFAC Proceedings Volumes* 40.11 (2007), pp. 285–290.
- [10] M. M. Rashid, P. Mhaskar, and C. L. Swartz. "Multi-rate modeling and economic model predictive control of the electric arc furnace". In: *Journal of Process Control* 40 (2016), pp. 50–61.
- [11] M. M. Rashid, P. Mhaskar, and C. L. E. Swartz. "Handling multi-rate and missing data in variable duration economic model predictive control of batch processes". In: *AIChE Journal* 63.7 (2017), pp. 2705–2718.

- [12] S. Shyamal and C. L. E. Swartz. "Optimization-based Online Decision Support Tool for Electric Arc Furnace Operation". In: *IFAC-PapersOnLine* 50.1 (2017), pp. 10784–10789.
- [13] S. Shyamal and C. L. E. Swartz. "Real-time energy management for electric arc furnace operation". In: *Journal of Process Control* <https://doi.org/10.1016/j.jprocont.2018.03.002> (2018).
- [14] C. C. Qu and J. Hahn. "Process monitoring and parameter estimation via unscented Kalman filtering". In: *Journal of Loss Prevention in the Process Industries* 22.6 (2009), pp. 703–709.
- [15] D. G. Robertson and J. H. Lee. "On the use of constraints in least squares estimation and control". In: *Automatica* 38.7 (2002), pp. 1113–1123.
- [16] C. V. Rao, J. B. Rawlings, and D. Q. Mayne. "Constrained state estimation for nonlinear discrete-time systems: Stability and moving horizon approximations". In: *IEEE Transactions on Automatic Control* 48.2 (2003), pp. 246–258.
- [17] F. Allgöwer, T. A. Badgwell, J. S. Qin, J. B. Rawlings, and S. J. Wright. "Nonlinear predictive control and moving horizon estimation - an introductory overview". In: *Advances in Control*. Springer, 1999, pp. 391–449.
- [18] S. Billings, F. Boland, and H. Nicholson. "Electric arc furnace modelling and control". In: *Automatica* 15.2 (1979), pp. 137–148.
- [19] E. M. Y. Ghobara. "Modeling, Optimization and Estimation in Electric Arc Furnace (EAF) Operation". PhD thesis. 2013.
- [20] S. Shyamal and C. L. E. Swartz. "A Multi-rate Moving Horizon Estimation Framework for Electric Arc Furnace Operation". In: *IFAC-PapersOnLine* 49.7 (2016), pp. 1175–1180.
- [21] L. T. Biegler. "New directions for nonlinear process optimization". In: *Current Opinion in Chemical Engineering* 21 (2018), pp. 32–40.

- [22] Y. Li and R. J. Fruehan. "Computational fluid-dynamics simulation of postcombustion in the electric-arc furnace". In: *Metallurgical and Materials Transactions B* 34.3 (2003), pp. 333–343.
- [23] X. Tang, M. Kirschen, M. Abel, and H. Pfeifer. "Modelling of EAF Off-Gas Post Combustion in Dedusting Systems using CFD Methods". In: *steel research international* 74.4 (2003), pp. 201–210.
- [24] G. A. Irons. "Developments in electric arc furnace steelmaking". In: *AISTECH-Conference Proceedings-*. Vol. 1. Association for Iron & Steel Technology. 2005, p. 3.
- [25] S Matson and W. F. Ramirez. "Optimal operation of an electric arc furnace". In: *57 th Electric Furnace Conference*. 1999, pp. 719–730.
- [26] A. Fathi, Y. Saboohi, I. Škrjanc, and V. Logar. "Comprehensive Electric Arc Furnace Model for Simulation Purposes and Model-Based Control". In: *Steel Research International* 88.3 (2017), p. 1600083.
- [27] Process Systems Enterprise Ltd. *gPROMS*, www.psenterprise.com/gproms, 1997-2015. 2015.
- [28] J. Andersson. "A General-Purpose Software Framework for Dynamic Optimization". PhD thesis. Department of Electrical Engineering (ESAT/SCD) and Optimization in Engineering Center, Kasteelpark Arenberg 10, 3001-Heverlee, Belgium: Arenberg Doctoral School, KU Leuven, 2013.
- [29] Y. Cao, C. L. Swartz, J. Flores-Cerrillo, and J. Ma. "Dynamic modeling and collocation-based model reduction of cryogenic air separation units". In: *AIChE Journal* 62.5 (2016), pp. 1602–1615.
- [30] J. Hahn and T. F. Edgar. "Balancing approach to minimal realization and model reduction of stable nonlinear systems". In: *Industrial & engineering chemistry research* 41.9 (2002), pp. 2204–2212.
- [31] F. Magnusson. "Numerical and symbolic methods for dynamic optimization". In: (2016).

- [32] J. Åkesson, K.-E. Årzén, M. Gäfvert, T. Bergdahl, and H. Tummescheit. "Modeling and optimization with Optimica and JModelica.org - Languages and tools for solving large-scale dynamic optimization problems". In: *Computers & Chemical Engineering* 34.11 (2010), pp. 1737–1749.
- [33] L. T. Biegler. *Nonlinear programming: concepts, algorithms, and applications to chemical processes*. SIAM, 2010.
- [34] B. Chachuat, A. B. Singer, and P. I. Barton. "Global mixed-integer dynamic optimization". In: *AIChE Journal* 51.8 (2005), pp. 2235–2253.
- [35] V. Sakizlis, J. D. Perkins, and E. N. Pistikopoulos. "Recent advances in optimization-based simultaneous process and control design". In: *Computers & Chemical Engineering* 28.10 (2004), pp. 2069–2086.
- [36] A. Flores-Tlacuahuac and L. T. Biegler. "Simultaneous mixed-integer dynamic optimization for integrated design and control". In: *Computers & chemical engineering* 31.5-6 (2007), pp. 588–600.
- [37] J. M. Maciejowski. *Predictive control: with constraints*. Pearson education, 2002.
- [38] C. L. E. Swartz. "An algorithm for hierarchical supervisory control". In: *Computers & chemical engineering* 19.11 (1995), pp. 1173–1180.
- [39] Z. Chong and C. L. E. Swartz. "Optimal operation of process plants under partial shutdown conditions". In: *AIChE Journal* 59.11 (2013), pp. 4151–4168.
- [40] Z. Chong and C. L. E. Swartz. "Optimal response under partial plant shutdown with discontinuous dynamic models". In: *Computers & Chemical Engineering* 86 (2016), pp. 120–135.
- [41] Z. Chong and C. L. E. Swartz. "Discontinuous Modeling Formulations for the Optimal Control of Partial Shutdowns". In: *IFAC Proceedings Volumes* 44.1 (2011), pp. 3659–3664.
- [42] Z. Chong and C. L. E. Swartz. "Model-based control of multi-unit systems under partial shutdown conditions". In: *American Control Conference, 2009. ACC'09*. IEEE. 2009, pp. 160–165.

- [43] A. Küpper, M. Diehl, J. P. Schlöder, H. G. Bock, and S. Engell. "Efficient moving horizon state and parameter estimation for SMB processes". In: *Journal of Process Control* 19.5 (2009), pp. 785–802.
- [44] V. M. Zavala and L. T. Biegler. "Optimization-based strategies for the operation of low-density polyethylene tubular reactors: Moving horizon estimation". In: *Computers & Chemical Engineering* 33.1 (2009), pp. 379–390.
- [45] F. Magnusson and J. Åkesson. "Dynamic optimization in JModelica.org". In: *Processes* 3.2 (2015), pp. 471–496.
- [46] H. Jang, J. H. Lee, and L. T. Biegler. "A robust NMPC scheme for semi-batch polymerization reactors". In: *IFAC-PapersOnLine* 49.7 (2016), pp. 37–42.
- [47] S Kramer, R. Gesthuisen, and S Engell. "Fixed structure multirate state estimation". In: *American Control Conference (ACC)*. Vol. 7. IEEE. 2005, pp. 4613–4618.
- [48] S. Krämer and R. Gesthuisen. "Multirate state estimation using moving horizon estimation". In: *16th IFAC World Congress, IFAC Proceedings Volumes* 38.1 (2005), pp. 1–6.
- [49] R. López-Negrete and L. T. Biegler. "A moving horizon estimator for processes with multi-rate measurements: A nonlinear programming sensitivity approach". In: *Journal of Process Control* 22.4 (2012), pp. 677–688.
- [50] L. Ji and J. B. Rawlings. "Application of MHE to large-scale nonlinear processes with delayed lab measurements". In: *Computers & Chemical Engineering* 80 (2015), pp. 63–72.
- [51] C. V. Rao and J. B. Rawlings. "Constrained process monitoring: Moving-horizon approach". In: *AIChE journal* 48.1 (2002), pp. 97–109.
- [52] A. Alessandri, M. Baglietto, and G. Battistelli. "Moving-horizon state estimation for nonlinear discrete-time systems: New stability results and approximation schemes". In: *Automatica* 44.7 (2008), pp. 1753–1765.

- [53] V. M. Zavala. "Stability analysis of an approximate scheme for moving horizon estimation". In: *Computers & Chemical Engineering* 34.10 (2010), pp. 1662–1670.
- [54] D. Simon. *Optimal state estimation: Kalman, H infinity, and nonlinear approaches*. John Wiley & Sons, 2006.
- [55] R. Lopez-Negrete, S. C. Patwardhan, and L. T. Biegler. "Constrained particle filter approach to approximate the arrival cost in moving horizon estimation". In: *Journal of Process Control* 21.6 (2011), pp. 909–919.
- [56] C. C. Qu and J. Hahn. "Computation of arrival cost for moving horizon estimation via unscented Kalman filtering". In: *Journal of Process Control* 19.2 (2009), pp. 358–363.
- [57] M. Diehl, H. J. Ferreau, and N. Haverbeke. "Efficient numerical methods for nonlinear MPC and moving horizon estimation". In: *Nonlinear Model Predictive Control*. Springer, 2009, pp. 391–417.
- [58] R. Huang, V. M. Zavala, and L. T. Biegler. "Advanced step nonlinear model predictive control for air separation units". In: *Journal of Process Control* 19.4 (2009), pp. 678–685.
- [59] P. Kühl, M. Diehl, T. Kraus, J. P. Schlöder, and H. G. Bock. "A real-time algorithm for moving horizon state and parameter estimation". In: *Computers & Chemical Engineering* 35.1 (2011), pp. 71–83.
- [60] L. Biegler, X Yang, and G. Fischer. "Advances in sensitivity-based nonlinear model predictive control and dynamic real-time optimization". In: *Journal of Process Control* 30 (2015), pp. 104–116.
- [61] V. M. Zavala, C. D. Laird, and L. T. Biegler. "A fast moving horizon estimation algorithm based on nonlinear programming sensitivity". In: *Journal of Process Control* 18.9 (2008), pp. 876–884.
- [62] M. Diehl, R. Findeisen, F. Allgöwer, H. G. Bock, and J. P. Schlöder. "Nominal stability of real-time iteration scheme for nonlinear model predictive control". In: *IEE Proceedings-Control Theory and Applications* 152.3 (2005), pp. 296–308.

- [63] D. DeHaan and M. Guay. "A new real-time approach for nonlinear model predictive control". In: *IFAC Proceedings Volumes* 38.1 (2005), pp. 1007–1012.
- [64] S. Shyamal and C. L. E. Swartz. "Multi-Rate Moving Horizon Estimation for an Electric Arc Furnace Steelmaking Process". In: *2016 AIChE Annual Meeting* (2016).
- [65] A. Wächter and L. T. Biegler. "On the implementation of an interior-point filter line-search algorithm for large-scale nonlinear programming". In: *Mathematical Programming* 106.1 (2006), pp. 25–57.
- [66] A. C. Hindmarsh, P. N. Brown, K. E. Grant, S. L. Lee, R. Serban, D. E. Shumaker, and C. S. Woodward. "SUNDIALS: Suite of nonlinear and differential/algebraic equation solvers". In: *ACM Transactions on Mathematical Software (TOMS)* 31.3 (2005), pp. 363–396.

Chapter 6

Conclusion

6.1 Summary and Key Contributions	165
6.2 Recommendations for Future Work	168

This chapter summarizes the key contributions from this research, and highlights recommendations for future research avenues.

6.1 Summary and Key Contributions

The key contributions of this work are as follows:

In Chapter 2, a dynamic model of the EAF process developed by MacRosty and Swartz [1] is reformulated and used within an optimization framework to determine the optimal input trajectories. We investigated the simultaneous solution approach for optimizing the EAF operation. We showed that the model-based optimization is able to determine the optimal power use when the electricity cost is high or low.

Computational time for optimization with the sequential method was compared with a simultaneous approach and reduced to enhance the on-line implementation of the model. Further, we presented the simulation and optimization web interfaces developed in collaboration with McMaster Steel Research Centre (SRC) for SRC industrial members.

In Chapter 3, we developed a rigorous framework to do multi-rate MHE for the EAF process. We proposed a novel parameter estimation-based framework for solving multi-rate MHE problem using the sequential dynamic optimization approach. The strategy involves approximation of process noise terms with a continuous function. The estimator showed strong performance in tracking the internal states of the EAF model, in the presence of plant-model mismatch, improving from poor initial guesses of the states. We also presented two frameworks to implement MHE online using the sequential and the simultaneous approaches. We then introduced a novel initialization method for the MHE problem based on a background solve to improve solution time. The performance of the MHE under different conditions and using different optimization strategies was illustrated through application to a case study. Next, we introduced an online decision support tool (DST) for EAF operation. A multi-rate MHE was coupled with an economics-based optimizer to reconstruct the states and provide optimal decisions to the operators. A case study was presented to demonstrate the increase in profit through the use of the DST.

In Chapter 4, we developed a real-time energy management strategy for batch operation of electric arc furnaces. The strategy is efficient in reducing the energy requirements while effectively exploiting the changing electricity prices. The optimal inputs are computed with the use of a coupled MHE-NMPC application. Moreover, a novel initialization scheme is proposed to reduce the online solution times for the multi-rate MHE and shrinking horizon economics-based NMPC problems. The scheme uses the time between consecutive sampling times to generate warm start points for the upcoming on-line MHE-NMPC solves. Our case studies focused on demonstrating

NMPC economic performance in multiple scenarios of varying electricity prices. NMPC tackled the price variations by balancing the control inputs used to provide the electrical and chemical energy to the process. The challenging EAF process is operated within realistic limits by the economics-based NMPC. The strong convergence ability shown by the multi-rate MHE provided appropriate estimates to the NMPC. With modern power grids moving towards a smarter operation and generation, the proposed strategy can actively fit into and support this new energy utilization and consumption ecosystem. The case studies showed that the highly energy intensive EAFs are capable of aiding the power grid by adjusting their operation in real-time through the use of advanced control tools NMPC and MHE.

In Chapter 5, we introduced a real-time advisory system which computes economically optimal input trajectories based on a first-principles model. The advisory system development combined the novel multi-tiered dynamic optimization algorithm with multi-rate MHE to provide online decision support to the EAF operators. The three tiers of the optimizer effectively handled the endpoint constraints by achieving feasibility through a priority based calculation sequence. The optimizer is called upon only when the operator triggers the advisory system. The initial conditions for the optimization problem are obtained from the multi-rate MHE which runs in parallel with the plant. We also proposed a multi-tiered initialization scheme for obtaining a fast solution from the advisory system. Our case studies for the electric arc steel-making process showed the economic benefit of using the real-time advisory system. Optimal inputs provided by the advisory system made sure that the challenging process is operated economically while respecting constraints. The advisory system implementation showed that it can fill the gap in current EAF advanced control applications. The real-time advisory system algorithm is applicable to other batch and semi-batch processes as well.

6.2 Recommendations for Future Work

Several broad candidate areas for further exploration are identified. They are:

- A useful next step would be formulation of an NMPC problem that can minimize the peak electricity demand.
- It will be useful to explore NMPC and MHE formulations for the variable batch length problem and incorporate them into an upper level scheduling layer. The integration of scheduling and control is envisaged to generate economic benefit due to better utilization of EAF operating resources.
- In-plant evaluation of the energy management strategy would be a useful step toward industrial adoption.
- It is useful to formulate the optimization problem to find the optimal batch length (not just extension of batch duration due to infeasibility).
- Incorporating a lower-level control, such as manipulation of electrode height, in the dynamic optimization formulation would be a useful avenue to study.
- An interesting research direction is to explore the effects of increased frequency of slow measurements and quantifying the quality of the state estimates and process economics thus obtained.